AXON REGENERATION FOLLOWING PERIPHERAL NERVE LESION IS DRIVEN BY COFILIN MEDIATED ACTIN TURNOVER

Dissertation

zur Erlangung des Doktorgrades (Dr. rer. nat.)
an der
Mathematisch-Naturwissenschaftlichen Fakultät
der
Rheinischen Friedrich-Wilhelms-Universität Bonn

vorgelegt von
Claudia Juliane Laskowski
aus Leipzig

Bonn, Februar 2016

Angefertigt mit Genehmigung der Mathematisch-Naturwissenschaftlichen
Fakultät der Rheinischen Friedrich-Wilhelms-Universität

Erstgutachter: Prof. Dr. Frank Bradke
Zweitgutachter: Prof. Dr. Michael Hoch
Tag der Promotion: 23. Juni 2016
Erscheinungsjahr: 2016

Ehrenwörtliche Versicherung:

Ich versichere hiermit ehrenwörtlich, dass ich die Dissertation mit dem Titel "Axon regeneration following peripheral nerve lesion is driven by cofilin mediated actin turnover" selbständig und ohne unerlaubte Hilfe angefertigt habe. Ich habe mich dabei keiner anderen als der von mir ausdrücklich bezeichneten Hilfen und Quellen bedient.

Erklärung:

Hiermit erkläre ich, dass ich mich nicht anderweitig einer Doktorprüfung ohne Erfolg unterzogen habe. Die Dissertation wurde in ihrer jetzigen oder ähnlichen Form bei keiner anderen Hochschule eingereicht und hat noch keinen sonstigen Prüfungszwecken gedient.

Bonn, den 18. Februar 2016

Claudia Juliane Laskowski

Die vorliegende Arbeit wurde in der Arbeitsgruppe "Axonales Wachstum und Regeneration" von Prof. Dr. Frank Bradke am Max-Planck-Institut für Neurobiologie in Martinsried und am Deutschen Zentrum für Neurodegenerative Erkrankungen (DZNE) e.V. in Bonn angefertigt.

TABLE OF CONTENTS

ABBREVIATIONS

AAV	Adeno associated virus
ABP	Actin binding protein
AC	ADF/cofilin
AC1 KO	ADF and cofilin 1 knockout
AC1C2 KO	ADF, cofilin 1 and cofilin 2 knockout
AC2 KO	ADF and cofilin 2 knockout
ADF	Actin depolymerizing factor
ADP	Adenosine diphosphate
AIP1	Actin-interacting protein 1
AIS	Axon initial segment
AKT	Protein kinase B
Ala	Alanine
AP	Action potential
Arg1	Arginase 1
Arp 2/3	Actin related protein 2/3
Asp	Aspartate
ATF3	cAMP-dependent transcription factor 3
ATP	Adenosine triphosphate
BBB	Blood brain barrier
bGH	Bovine growth hormone
BSA	Bovine serum albumine
C1 KO	Cofilin 1 knockout
C1C2 KO	Cofilin 1 and cofilin 2 knockout
C2 KO	Cofilin 2 knockout
cAMP	Cyclic adenosine monophosphate
CAP	Cyclase-associated protein
CAP-23	Cortical cytoskeleton associated protein 23
C-domain	Central domain
ChABC	Chondroitinase ABC
CIN	Chronophin
CLASP	CLIP-associated proteins

CLIP	Cytoplasmatic linker proteins
cm	Centimeter
CMV	Cytomegalovirus
CNS	Central nervous system
CNTF	Ciliary neurotrophic factor
Cre	Cre recombinase
CREB	cAMP response element-binding protein
CSF	Cerebrospinal fluid
CSPG	Chondroitin sulfate proteoglycans
CytoD	Cytochalasin D
DAPI	4',6-diamidino-2-phenylindole
DC	Dorsal column
DCL	Dorsal column lesion
DCX	Doublecortin
DMEM	Dulbecco's Modified Eagle's Medium
DMSO	Dimethylsulfoxide
DNA	Deoxyribonucleic acid
dNTP	Deoxynucleoside triphosphate
DREZ	Dorsal root entry zone
DRG	Dorsal root ganglia
EB-3	End-binding protein 3
ECL	Enhanced chemoluminescence
ECM	Extracellular matrix
EDTA	Ethylenediaminetetraacetic acid
eGFP	Enhanced green fluorescent protein
EGTA	Ethylene glycol tetraacetic acid
EM	Electron microscopy
Ena/VASP	Ena/Vasodilator-stimulated phosphoprotein
Erk	Extracellular-signal-regulated kinases
EtOH	Ethanol
F-actin	Filamentous actin
FBS	Fetal bovine serum
G-actin	Globular actin
GAG	Glycosaminoglycan

GAP-43	Growth associated protein 43
GAPDH	Glyceraldehyde-3-phosphate dehydrogenase
GC	Growth cone
GDP	Guanosine diphosphate
GFAP	Glial fibrillary acidic protein
GM	Grey matter
gp130	Glycoprotein 130
GTP	Guanosine triphosphate
HBSS	Hanks' Balanced Salt Solution
HCl	Hydrochloric acid
HDAC5	Histone deacetylase 5
HS	Horse serum
ICC	Immunocytochemistry
IHC	Immunohistochemistry
IL-6	Interleukin 6
Jasp	Jasplakinolide
kDA	Kilo Dalton
KLF	Kruppel-like factor
L4/5	Lumbar level 4/5
LB	Lysogeny broth
LIF	Leukemia inhibitory factor
LIMK	Lin-11, Isl-1, and Mec-3
LINGO-1	Leucine rich repeat and immunoglobin-like domain-containing protein 1
LS	Lesion site
m	Meter
mA	Milliampere
MAG	Myelin-associated glycoprotein
MAI	Myelin associated inhibitors
MAP	Microtubule associated protein
µg	Microgram
µm	Micrometer
min	Minute
mm	Millimeter

ms	Millisecond
MT	Microtubule
mTOR	Mammalian target of rapamycin
NA	Numerical aperture
NaCl	Sodium chloride
NaOH	Sodium hydroxide
NB	Neurobasal medium
NGF	Nerve growth factor
NgR	Nogo receptor
NGS	Normal goat serum
NLS	Nuclear localization signal
nm	Nanometer
nM	Nanomolar
No./#	Number
Nogo-A	Neurite outgrowth inhibitor A
NPY	Neuropeptide Y
NT	Neurotransmitter
NT3	Neurotrophic factor 3
OMgp	Oligodendrocyte myelin glycoprotein
p75NTR	Protein 75 neurotrophin receptor
PAGE	Polyacrylamide gel electrophoresis
PAK	Protein 21 activated kinase
PBS	Phosphate buffered saline
pCof	Phosphorylated cofilin
PCR	Polymerase chain reaction
PDE4	Phosphodiesterase 4
PDK 1/2	Phosphatidylinositol-dependent kinase 1/2
P-domain	Peripheral domain
PFA	Paraformaldehyde
pH	Potentia hydrogenii
Phe	Phenylalanine
PHEM	Pipes Hepes EGTA $MgCl_2$
P_i	Inorganic phosphate
PI	Proteasome inhibitor

PI3K	Phosphoinositide 3-kinase
PIP_2	Phosphatidylinositol (4,5) bisphosphate
PIP_3	Phosphatidylinositol (3,4,5) trisphosphate
PKCμ	Protein kinase C μ
PLL	Poly-L-lysine
PNL	Peripheral nerve lesion
PNS	Peripheral nervous system
psi	Pound-force per square inch
PTEN	Phosphatase and tensin homolog
PVDF	Polyvinylidene difluoride
RAG	Regeneration associated gene
RFP	Red fluorescent protein
RGC	Retinal ganglion cell
RhoA	Ras homolog gene family member A
RIPA	Radioimmunoprecipitation assay
ROCK	Rho kinase
rpm	Rounds per minute
RT	Room temperature
RTK	Receptor tyrosine kinase
SCI	Spinal cord injury
SDS	Sodium dodecyl sulfate
sec	Seconds
SEM	Standard error of the mean
Ser	Serine
SMAD1	Mothers against decapentaplegic homolog 1
SPRR1A	Small proline-rich repeat protein 1A
SSH1	Slingshot homolog 1
STAT3	Signal transducer and activator of transcription 3
+TIP	Plus-end tracking protein
T12	Thoracic level 12
TAE	Tris-acetate-EDTA buffer
TB	Terrific broth
TBS	Tris-buffered saline
tCof	Total cofilin

TESK	Testicular kinase
TF	Transcription factor
TGF	Transforming growth factor
Trk	Tyrosine receptor kinase
TSC	Tuberous sclerosis protein
Tyr	Tyrosine
T-Zone	Transition zone
U	Units
V	Volt
VIP	Vasointestinal peptide
WB	Western blot
WM	White matter
WPRE	Woodchuck hepatitis virus posttranscriptional regulatory element
WT	Wild-type

1 SUMMARY

While axons of the adult peripheral nervous system (PNS) maintain the ability to regenerate, axons of the central nervous system (CNS) fail to regrow upon injury. Subsequently, trauma to the spinal cord leads to irreversible loss of function below the site of injury. Primary sensory neurons constitute a classical exception. A lesion to the peripheral axons of dorsal root ganglia (DRG) neurons is able to reinitiate the intrinsic competence for axonal growth and to trigger regeneration in their central axons. This phenomenon called "conditioning" demonstrated decades ago that axon regeneration is possible in the CNS. However, the understanding of the underlying mechanisms is still fragmentary. My data show direct correlations between changes of the actin and microtubule cytoskeleton and the observed increase in axonal growth following a conditioning lesion. The morphology and the mode of elongation of DRG growth cones are significantly altered. Most importantly, I report that high actin dynamics and turnover are necessary for axon regeneration. My data indicate that a single family of actin regulatory proteins, actin depolymerizing protein (ADF)/cofilin (AC), drives the conditioning regenerative response. In fact, genetic ablation of all 3 isoforms of the AC family, ADF, cofilin 1 and cofilin 2 leads to a complete loss of the conditioning effect both in cell culture and *in vivo*. Blockade of F-actin retrograde flow and protrusion dynamics accounted for this failure in axon growth and regeneration. In particular, I found that the actin severing activity of AC proteins is essential for axon growth and regeneration. To assess whether AC activity is not only necessary but also sufficient for axon growth, AC isoforms were overexpressed individually in DRG neurons. *In vitro*, overexpression of cofilin 1, but not ADF and cofilin 2 enhanced axon outgrowth on both permissive and inhibitory substrates. In conclusion, my data reveal that actin remodeling contributes to mediating the conditioning effect in adult DRG neurons. Moreover, AC mediated actin turnover facilitates axon growth and regeneration by recapitulating processes that occur during neurite initiation in development.

2 INTRODUCTION

Perception, cognition, behavior and locomotion all rely on the proper functioning of the nervous system. It seems, however, that the maintenance of the complex neuronal circuitry needed for these elaborate functions, has developed at the expense of the regenerative ability of neurons. In simpler nervous systems of invertebrates and primitive vertebrates, axons can regenerate in both the peripheral nervous system (PNS) and central nervous system (CNS) (reviewed in Gaze, 1970, Lurie and Selzer, 1991, Wanner et al., 1995, Wu et al., 2007). In the course of evolution though, the ability to regenerate was lost in the mammalian CNS. Consequently, trauma to the brain or spinal cord leads to permanent disconnection and loss of function. Despite the urgency to develop effective treatments, the knowledge of the cellular and molecular events underlying axonal damage and regeneration is limited. This thesis investigates the mechanisms that facilitate regeneration in dorsal root ganglion neurons after a conditioning peripheral nerve lesion, a well-suited model to study the intrinsic growth ability of neurons. In the future, understanding of the basic molecular events underlying the "conditioning phenomenon" will help to develop strategies to promote regeneration and functional recovery after traumatic spinal cord injury (SCI). The first sections of the introduction describe the mechanisms of axon growth, the failure of regeneration after SCI and the conditioning lesion paradigm. The subsequent sections are dedicated to the neuronal cytoskeleton with special emphasis on the actin cytoskeleton and the ADF/cofilin family of actin-regulatory proteins.

2.1 Axon growth and regeneration in the nervous system

The nervous system developed to facilitate communication between different parts of the body and to precisely coordinate voluntary and involuntary actions in animals. In vertebrates the nervous system consists of two main parts, the CNS and the PNS. The CNS comprises the brain and spinal cord. The PNS consists mainly of nerves and ganglia outside of the CNS and its main function is to relay information from the CNS to the limbs and organs, and vice versa. At the cellular level, the nervous system is composed of diverse specialized cells, including

neurons. Neurons typically have a single cell body, several dendrites and one axon that allow them to receive and transmit signals (**Figure 2.1**). They propagate these signals in the form of electrochemical waves (also called action potentials) that travel along the axons, resulting in the release of neurotransmitters at the interface between neuronal cells: the synapses.

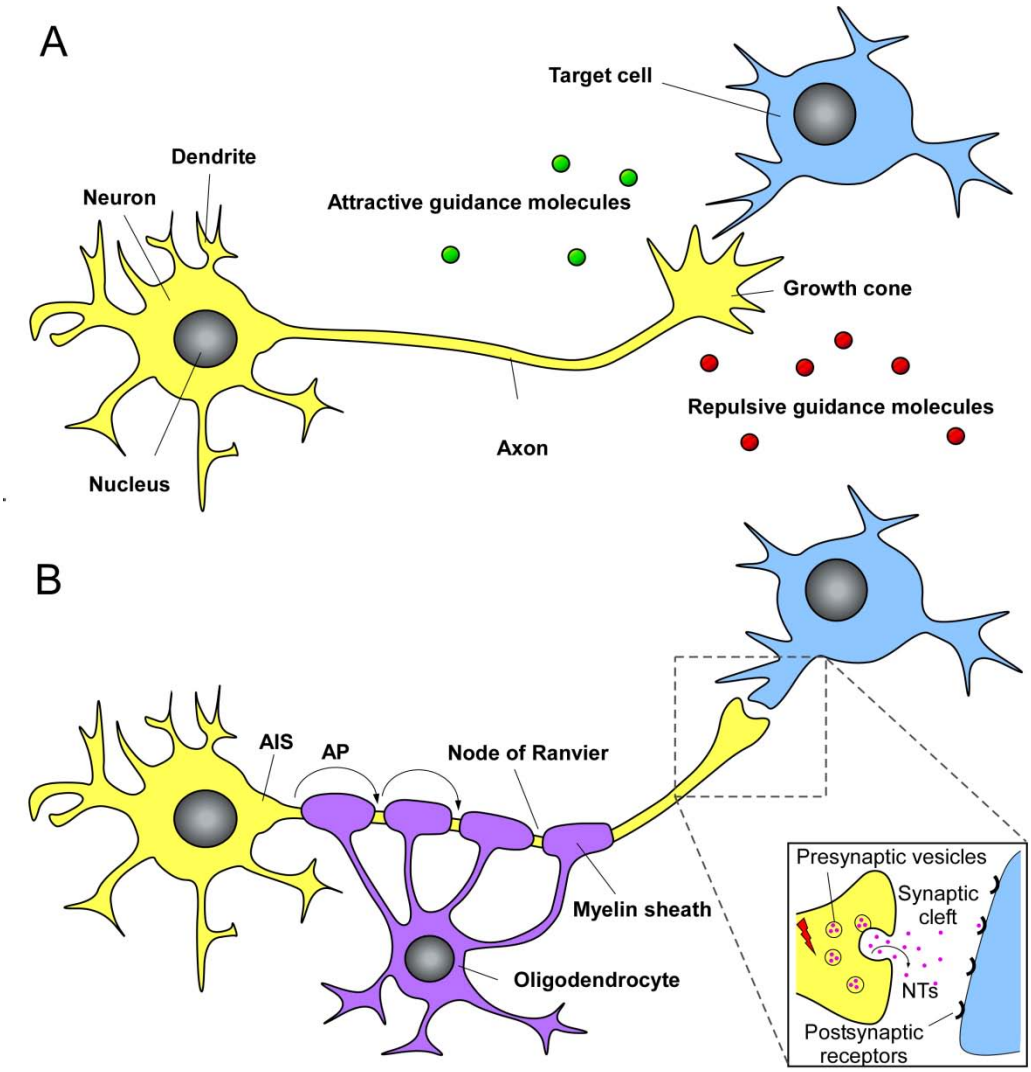

Figure 2.1. Establishment of a neuronal network. A) During development neurons extend their neurites through a complex extracellular environment with the help of growth cones, the "sensory and motor organs" at the neurite tip. The growth cone senses repulsive and attractive guidance cues and eventually steers the axon to its appropriate target. B) Subsequently, a synaptic contact is established with the target cell. Action potentials (APs) are generated and conducted from the axon initial segment (AIS) down to the axon terminals, eventually leading to the release of neurotransmitters (NTs) from synaptic vesicles in the presynaptic cell into the synaptic cleft. The NTs are bound by receptors in the postsynaptic membrane and lead to the generation of postsynaptic potentials.

In addition to neurons, other specialized cells including glia are contained in the nervous system. They provide structural and metabolic support to neurons in

healthy nervous system tissue, but also play a critical role upon traumatic spinal cord injury (as discussed in the following chapter "Spinal cord injury – the higher, the worse"). Neurons and glia form complex functional neuronal networks that are essential for perception, cognition and locomotion. But how are these complex networks established?

During development all neurons of the nervous system extend their axons through a complex and frequently changing environment and are guided by repulsive and attractive molecular cues, including netrins, slits, semaphorins, and ephrins (Bashaw and Klein, 2010, Raper and Mason, 2010). The growth cone, "the sensory and motor organ" at the tip of the axon senses the guidance cues and steers towards or away from them (**Figure 2.1**) in order to reach its target. Unlike other tissues that largely expand through mitosis and differentiation, the elongation of axons after having reached their targets is unique: nerve fibers are subjected to stretch as adjoining tissues enlarge and move away from each other during development (Loverde and Pfister, 2015). As a consequence of this tension, the fibers elongate, reaching up to 1 m in length and 1 µm in thickness, making neurons the largest cells in the body by both volume and surface area (Goldberg, 2003). To enable such substantial axonal growth, membrane, cytoplasmic proteins and cytoskeletal elements are required to be produced in the correct amounts. Moreover, the proteins need to be transported to the right cellular compartment and inserted into the axon as it grows, ensuring that growth cones respond properly and rapidly to complex extracellular stimuli encountered along the way (Goldberg, 2003).

Most building blocks needed for growth are synthetized in the cell body and subsequently transported into the growing axon. However, a large body of evidence suggests that long axons also rely on local axonal translation. Seemingly, local translation is tightly coupled to extracellular cues, enabling growth cones to respond to new signals with high adaptability and spatiotemporal control (reviewed in Jung and Holt, 2011, Deglincerti and Jaffrey, 2012). To integrate the environmental cues, growth cones are enriched in guidance receptors which recognize attractive or repellant molecules as well as cell-adhesion proteins that respond to the substrate. The side of the growth cone exposed to the external cue generally features a higher density of the appropriate receptors. The resulting

asymmetry leads to growth cone turning either toward (attraction) or away from the cue (repulsion), by generation of intracellular second messengers such as Ca^{2+} and cyclic nucleotides. In turn, the uneven distribution of second messengers within the growth cone results in changes of membrane trafficking, adhesion dynamics and most importantly in cytoskeletal reorganization to enable appropriate turning of the growth cone (reviewed in Tojima et al., 2011, Tojima, 2012, Vitriol and Zheng, 2012). Further evidence suggests that neurons do not extend axons constitutively, but that axon growth must be specifically signaled (Goldberg et al., 2002, Goldberg, 2003). Indeed, once the growth cone has reached its target region, axons generally arborize and contact appropriate postsynaptic partners. Consequently, the growth cone is transformed from a highly motile structure into a stable synaptic terminal. This developmental switch from a growing to a transmitting phase may represent one of the first steps in the loss of axon growth and regeneration ability (Enes et al., 2010, Tedeschi and He, 2010). Consequently, adult CNS neurons fail to convert to a rapidly regenerating mode and their axons stall at the lesion site after a traumatic injury. Paradoxically, neurons of the adult PNS are able to regenerate and often reestablish contact with their targets. Potential explanations for this differential regeneration potential of the CNS and PNS will be addressed in more detail in the following sections. Even though it is not clear to what extent axon regeneration in the adult nervous system may represent a recapitulation of neuritogenesis during development, the high similarity between these processes allows for the intriguing idea that basic developmental mechanisms could be reactivated in adult CNS neurons to facilitate regeneration (Snider et al., 2002, Harel and Strittmatter, 2006, Ylera and Bradke, 2007).

2.2 Spinal cord injury - the higher, the worse

The spinal cord is a long, cylindrical shaped bundle of nervous tissue surrounded and protected by a bony skeletal structure, the vertebral column. The primary function of the spinal cord is to ensure communication between the brain and other parts of the body. It conveys motor signals through descending pathways from the brain to peripheral muscles and organs, and relays sensory information through ascending nerve tracts from the periphery back to the brain. Finally, it

also contains neural circuits that can independently coordinate reflexes and central pattern generators. The spinal cord is organized into 31 segments, which can be grouped into four regions: the cervical, thoracic, lumbar and sacral spinal cord (**Figure 2.2**). Each segment of the spinal cord is associated with a pair of dorsal root ganglia located proximal to the spinal cord, which contain cell bodies of primary sensory neurons. Axons of these sensory neurons travel into the spinal cord via the dorsal roots. Ventral roots consist of axons from motor neurons, which convey information from the cell bodies within the CNS to the periphery. Dorsal and ventral roots adjoin and exit the intervertebral foramina as they become spinal nerves and connect to specific regions of the body. Consequently, the different segments have different areas of supply and function.

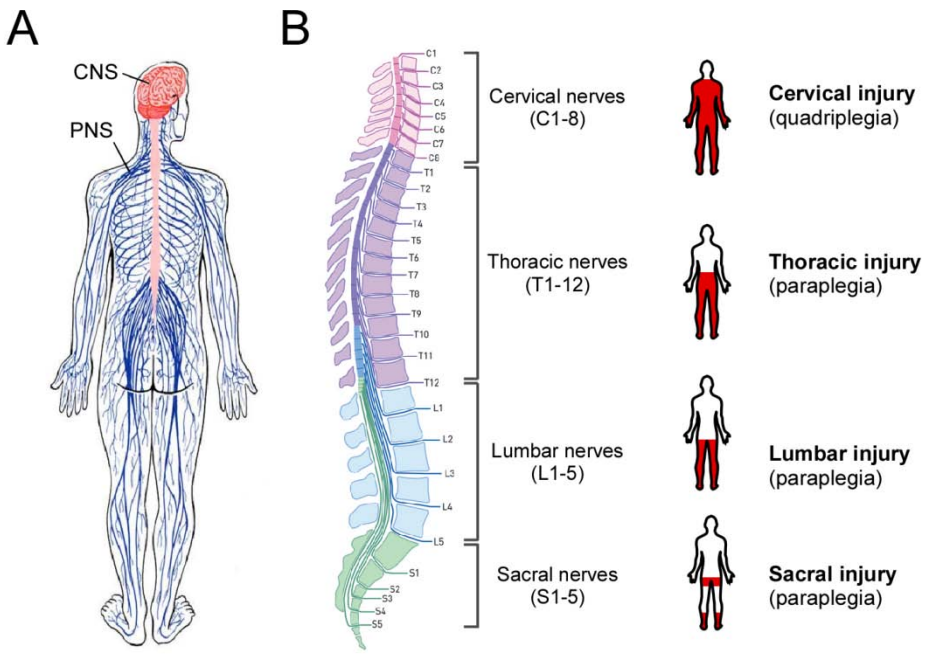

Figure 2.2. The nervous system and spinal cord injury. (A) The central nervous system (CNS) is composed of the brain and spinal cord. Its principal functions are to integrate sensory information, and to initiate and co-ordinate efferent responses. The peripheral nervous system (PNS) is composed of all the nervous tissue outside the CNS. Image adapted from studyblue.com/neurocytology. (B) The consequences of SCI depend on the severity of the injury and on the location along the spinal cord. Patients with cervical injuries may require a ventilator in order to breathe and all extremities are affected, leading to what is called quadriplegia. Patients with thoracic injuries can generally use their arms and hands but may have poor trunk control. In this case only the legs are paralyzed leading to what is called paraplegia. Patients with injuries at the lumbar level experience reduced control of their legs. The sacral nerves are responsible for bowel, bladder and sexual function as well as instructing the foot musculature. Images adapted from (Phillips et al., 1998) and www.wingsforlife.com.

Spinal cord injury (SCI) has devastating physical and psychological consequences and typically leads to irreversible loss of function. Communication between the brain and body parts below the level of injury is impaired. However, the type of disability occurring after SCI strongly depends on the severity and the level of the injury (**Figure 2.2**). In cases of complete SCI, all functions below the level of injury are lost, resulting in severe motor and sensory deficits, dysfunction of the autonomic system as well as neuropathic pain. Less well-known, but also detrimental to patients, SCI also affects bladder and bowel control, sexual performance and cardiovascular function.

Traumatic spinal cord injury represents a devastating but fortunately rare condition (10–83 cases per million people worldwide; Wyndaele and Wyndaele, 2006). Importantly, although SCI is a chronic condition, individuals suffering from incomplete lesions can attain a life expectancy that is close to normal. Hence, the number of individuals that are currently affected by SCI is much higher than the incidence rate would suggest (Chen et al., 2013), posing a significant economic burden to health care systems. Despite the urgent need to develop effective treatments for traumatic SCI, the knowledge of the cellular and molecular events underlying axonal damage and regeneration is limited. The search for novel therapeutic strategies to promote axon regeneration proves to be highly demanding and little progress has been made in the past decades. Since no treatment after spinal cord injury can thus far successfully propagate nerve regeneration to restore functionality in humans, therapeutic efforts mainly focus on preventing further damage and on sustaining intact functions. Indeed, the only clinically approved therapy to promote recovery of sensorimotor function in SCI patients so far is rehabilitative training (reviewed in Dietz and Fouad, 2014). But despite being efficient in preventing atrophy of denervated muscles and to some degree in promoting functional recovery in individuals with incomplete SCI, neurorehabilitation is rather focussed on ameliorating the patients´ symptoms without tackling the fundamental cause of the condition: the lack of functional axon regeneration. A list of clinical trials and therapies under research can be found in Thuret et al. (2006), Rossignol et al. (2007), Reier et al. (2012) or at www.clinicaltrials.gov.

2.3 Factors impeding regeneration after SCI

But why do axons of the PNS regenerate while central axons do not? To date, two main factors restricting CNS regeneration are known: the non-permissive extracellular environment and the reduced intrinsic growth potential of adult CNS axons. Within the first days after injury an impenetrable physical and molecular barrier is formed. First, the blood-brain-barrier (BBB) is disrupted, resulting in local hemorrhage and edema. Blood-borne immune cells like macrophages, as well as meningeal fibroblast and perivascular endothelial cells infiltrate the injured CNS parenchyma, where they mount a strong inflammatory wound healing response and gradually start to fill up the vacant space. Subsequently, glial cells contained in the CNS (including astrocytes, oligodendrocytes, oligodendrocyte precursor cells and microglia) are recruited to the lesion, where they are activated and proliferate (a process known as "reactive gliosis"), thereby forming a dense impenetrable network enclosing the lesion area (**Figure 2.3**).

The role of the glial scar is dichotomous. Despite being necessary for recovering CNS tissue homeostasis and thus preventing further damage, the glial scar constitutes a dense physical barrier to regenerating axons. It further contributes to the inhibition of regeneration by creating a molecular barrier (reviewed in Silver and Miller, 2004). Reactive astrocytes produce extracellular matrix (ECM) components and axon growth inhibitory molecules including chondroitin sulfate proteoglycans (CSPGs), as well as semaphorins and ephrins. In addition, debris of oligodendrocytes that usually make up the myelin sheath of axons up-regulate diverse secreted and transmembrane myelin associated inhibitors (MAIs; reviewed in Filbin, 2003), including neurite outgrowth inhibitor A (Nogo-A; Prinjha et al., 2000), oligodendrocyte myelin glycoprotein (OMgp; Habib et al., 1998), and myelin-associated glycoprotein (MAG; McKerracher et al., 1994). Importantly, seminal studies by Aguayo and colleagues showed that the use of peripheral nerve grafts in the spinal cord allows CNS axons to grow for considerable distances following injury (Richardson et al., 1980, David and Aguayo, 1981), suggesting that adult CNS neurons can activate a cell intrinsic program to support axonal regrowth if a permissive environment is created.

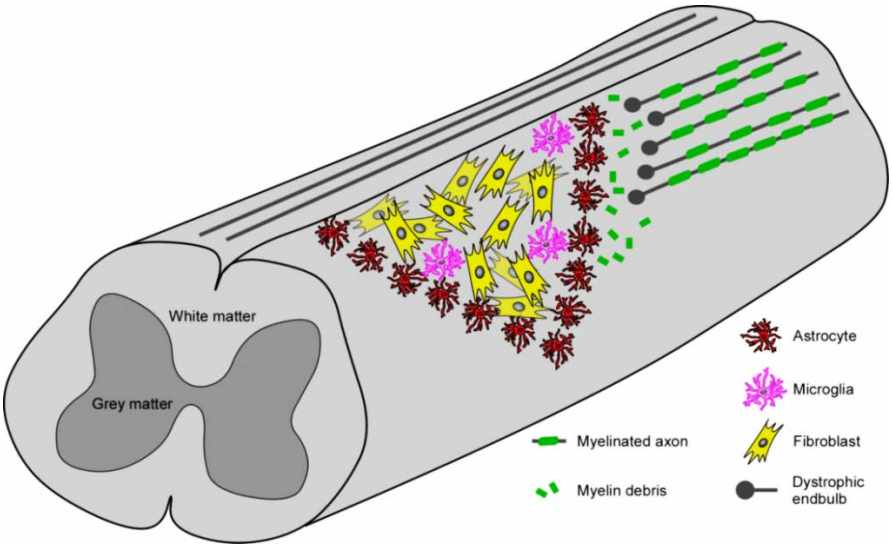

Figure 2.3. The scar – a dense physical and chemical barrier. Schematic illustration of the scar that forms upon traumatic injury to the spinal cord. The scar constitutes both a mechanical and a chemical barrier to regenerating axons. Upon lesion the axonal myelin sheath is damaged, resulting in the exposure of inhibitory molecules. Reactive astrocytes and microglia are recruited to the lesion periphery, secrete additional inhibitory molecules and form the glial scar. If the meninges are affected by the lesion as well, cells from the surrounding connective tissue, such as fibroblasts, infiltrate the lesion epicenter and form the fibrotic scar. Injured CNS axons cannot penetrate the scar and become dystrophic.

It is not surprising that a lot of effort has been invested into developing strategies making the hostile environment after SCI more permissible for regenerating axons by removing or counteracting inhibitory molecules (reviewed in Bradbury and McMahon, 2006, Lee and Zheng, 2012). Among the most famous examples are treatments with Nogo neutralizing antibodies (Bregman et al., 1995) and Nogo66 receptor agonists (GrandPre et al., 2002), as well as treatment with chondroitinase ABC (ChABC) which breaks down the inhibitory glycosaminoglycan (GAG) sugar chains of CSPGs (Bradbury et al., 2002). Several decades later however, increasing evidence suggests that both genetically and pharmacologically blocking the inhibitory environment only marginally improves axon regeneration *in vivo*.

Hence, a better understanding of alternative molecular mechanisms governing axon regeneration, like the intrinsic properties of axon growth, is fundamental (reviewed in Liu et al., 2011, Mar et al., 2014). In the transition phase from embryonic to adult, neurons undergo a profound loss in their intrinsic growth competence and increase their responsiveness to inhibitory cues to allow for proper synaptic development (Abe and Cavalli, 2008). In comparison to adult

neurons, embryonic neurons display a robust neurite outgrowth; they are more responsive to neurotrophic stimuli and react differently to myelin-associated inhibitors. Finally, the ability to activate growth genes and to form growth cones is greatly reduced in mature neurons of the adult CNS (reviewed in Sun and He, 2010, Yang and Yang, 2012). Intriguingly, injury to the adult PNS reactivates the intrinsic growth machinery and enables regeneration. In contrast, lesion to the CNS does not reactivate this growth program. Consequently, it would be innovative to find approaches to reactivate developmental processes in adult CNS neurons in order to make them grow like embryonic or peripheral neurons again. An ideal model system to study the intrinsic components underlying nerve regeneration, are dorsal root ganglia (DRG) neurons (Richardson and Issa, 1984). Because they constitute the focus of this study, they will be presented in detail in the following sections.

2.4 Dorsal root ganglia - a model to study spinal cord regeneration

DRG neurons are primary sensory neurons whose cell bodies lie in the dorsal root ganglia along the spinal cord. DRG neurons can be subdivided into groups according to the type of information that they convey: mechanosensation (touch and proprioception), thermoception (temperature) and nociception (pain). A unique feature of these pseudounipolar neurons is that they belong both to the central and to the peripheral nervous system. *In vivo* they typically feature two branches stemming from one unipolar axon. The peripheral branch conveys sensory information from peripheral targets, such as the skin and muscles, to the cell body, while the central branch projects into the dorsal column of the spinal cord and relays the sensory information to the brain (**Figure 2.4**).

However, these two branches of sensory axons differ with regard to their ability to regenerate after axotomy. Typically, the peripheral branch regenerates upon injury while the central branch does not (Ramon y Cajal, 1928, Schnell and Schwab, 1990, Xu et al., 1995). At first, this differential regenerative potential was attributed solely to the extrinsic environment, which is growth permissive in the PNS but inhibitory in the CNS (David and Aguayo, 1981). Intriguingly though, an increase in intrinsic growth potential prompted by a so called "conditioning" lesion can promote regeneration in the central branch as well. In brief, a primary

lesion to the peripheral branch of the DRG neuron prior to a secondary lesion to the central branch of the same neuron leads to enhanced axonal outgrowth of the central branch, if the primary lesion is conducted at the same time or prior to the secondary lesion (Figure 2.4; Richardson and Issa, 1984, Neumann and Woolf, 1999). Interestingly, a peripheral lesion performed after a central lesion (post-conditioning paradigm) does not improve axonal regeneration due to the assembly of a glial scar but still increases the intrinsic growth potential of DRG neurons (Ylera et al., 2009).

To date, the conditioning paradigm is still considered one of the most robust regeneration paradigms and is widely accepted as a suitable tool to study the intrinsic properties of axon regeneration. Of note, the growth promoting effects of a conditioning lesion can be nicely reproduced *in vitro,* thereby facilitating the study of the underlying molecular mechanisms. If a conditioning lesion is performed on the sciatic nerve (peripheral branch) 3-7 days prior to the dissection of the lumbar (L) 4 and 5 dorsal root ganglia, the conditioned neurons exhibit an enhanced axon outgrowth compared to naïve DRG neurons *in vitro* (**Figure 2.4, B**).

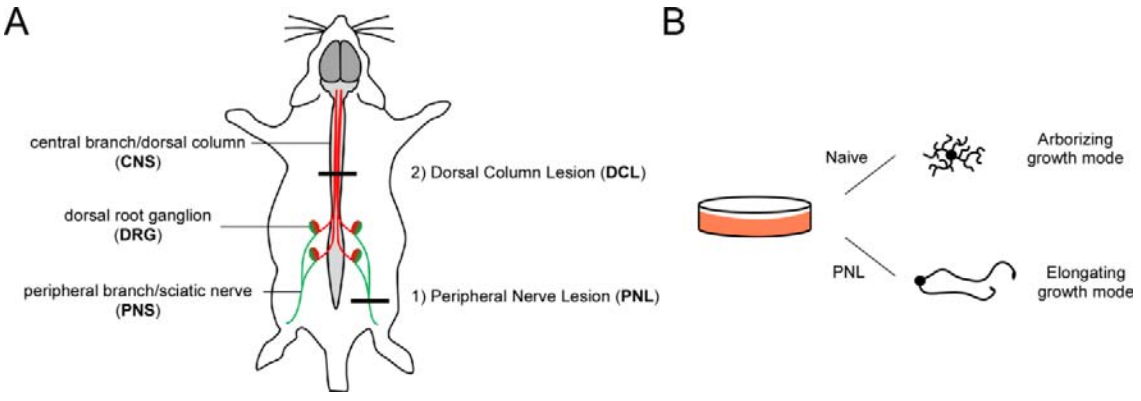

Figure 2.4. The conditioning paradigm. (A) Experimental setup: a unilateral axotomy of the peripheral DRG axons (sciatic nerve, green) is performed. One week after peripheral nerve lesion (PNL) the dorsal column (red) is lesioned (DCL). Alternatively, the dorsal root ganglia (green/red) of the lumbar segments 4 and 5 (L4/5) are dissected. (B) Ipsilateral (conditioned) and contralateral (naïve) L4/5 DRG neurons are dissected and cultured on permissive or inhibitory substrates. Conditioned neurons show an increase in intrinsic growth potential (enhanced axon length, lower branching frequency) compared to naïve DRG neurons.

The majority of naïve DRG neurons fail to extend neurites during the first day in culture, whereas conditioned cells extend processes within hours after plating (Smith and Skene, 1997). After approximately 16-18 hours *in vitro* naïve DRGs typically extend short and highly branched neurites, while conditioned neurons feature long and sparsely branched neurites. By the second day in culture, however, naïve DRG neurons also show a gradual transition from an arborizing to an elongating growth mode (Smith and Skene, 1997) attributed to the dissection process, which is comparable to a conditioning lesion.

2.5 Proposed signaling pathways involved in the conditioning effect

Although the conditioning lesion paradigm has been extensively investigated, the exact underlying cellular mechanisms remain poorly understood. It was proposed that the competence of DRG neurons for these distinct types of axon growth depends on different patterns of gene expression. While adult sensory neurons are constitutively competent to support arborizing axon growth, they are unable to initiate or sustain rapid, linear extension of axons, unless they undergo transcription-dependent changes in terms of gene expression and axonal transport (Smith and Skene, 1997). An interesting question is the nature of the injury signals resulting in the transcription-dependent transition by which DRG neurons enter into the growth-competent state after injury.

Mounting evidence suggests that injury signals may be either positive or negative. Indeed, seminal studies by Ambron and Walters (1996) suggested that temporally distinct but overlapping phases, during which signals enter the soma and prime the cell for the arrival of subsequent signals, may act complementarily or synergistically to each other upon a nerve lesion: (1) Arrival of injury-induced axonal potentials, that turn on early stage repair genes via the action of cAMP or calcium (2) discontinuation of extrinsic trophic support and repression from target-derived negative injury signals, and finally (3) retrograde transport of positive injury signals, such as proteins activated at the lesion site that are transported to the nucleus (reviewed in Abe and Cavalli, 2008, Liu et al., 2011, Mar et al., 2014). When these signals reach the cell body, they mediate the expression and activation of a number of transcription factors (TFs), that in turn regulate the

expression of regeneration associated genes (RAGs) involved in cell survival and neurite outgrowth (reviewed in Tedeschi, 2011).

Ever since the conditioning effect was first discovered, the list of signaling molecules whose expression and activity is modulated after peripheral lesion has become increasingly longer. Several TFs like c-Jun, cAMP response element-binding protein (CREB) and cAMP-dependent transcription factor 3 (ATF3; Tsujino et al., 2000, Raivich et al., 2004, Seijffers et al., 2007), signal transducer and activator of transcription 3 (STAT3; Qiu et al., 2005), mothers against decapentaplegic homolog 1 (Smad1; Zou et al., 2009), tumor protein 53 (p53; Di Giovanni et al., 2005, Di Giovanni et al., 2006) and several kruppel-like factor family members (KLF; Moore et al., 2009) have been identified. Among others, RAGs including arginase 1 (Arg1; Cai et al., 2002, Deng et al., 2009), neuropeptide Y (NPY; Xiao et al., 2002), vasointestinal peptide (VIP; Mohney et al., 1994), interleukin-6 (IL-6 ; Cao et al., 2006), growth-associated protein-43 (GAP-43; Skene, 1989, Bomze et al., 2001), cortical cytoskeleton associated protein-23 (CAP-23; Bomze et al., 2001), small proline-rich repeat protein 1A (SPRR1A; Bonilla et al., 2002) and galanin (Villar et al., 1989) are expressed to mount a robust regenerative response (reviewed in Richardson et al., 2009, Hoffman, 2010, Tedeschi, 2011, Mar et al., 2014, Ma and Willis, 2015). However, the precise contribution of each of the signaling molecules to the conditioning effect is still under debate and needs further elucidation. Some of the central pathways involved in mediating the conditioning response will be addressed in more detail in the following sections and are summarized in **Figure 2.5**.

2.5.1 Positive injury signals

One of the first injury signals is the influx of calcium into the axoplasm. Due to the inversion of the calcium/sodium flux, the axonal membrane is depolarized and antidromic waves of action potentials travel along the axon to the cell body. Interestingly, there is a direct correlation between the amplitude of these calcium waves and the success of regeneration as shown in *C. elegans* sensory neurons. In contrast, inhibition of voltage-gated calcium channels reduces the regenerative ability of axons (Ghosh-Roy et al., 2010). As a result of the calcium influx,

intracellular signaling pathways are activated that initiate resealing of the axonal membrane, local protein synthesis and assembly of a competent growth cone (reviewed in Bradke et al., 2012, Mar et al., 2014). Importantly, upon reaching the soma, the retrograde calcium wave leads to the activation of protein kinase C μ (PKCμ) and to the subsequent nuclear export of histone deacetylase 5 (HDAC5). Consequently, histone acetylation is enhanced and the pro-regenerative transcription program activated (Cho et al., 2013). Accordingly, treatment with the HDAC inhibitor valproic acid improved axonal growth of neurons *in vitro* and locomotion *in vivo* after SCI in rats (Lv et al., 2012).

A conditioning lesion is further correlated with a transient elevation of endogenous levels of the second messenger cAMP. The importance of cAMP signaling pathways in mediating the conditioning effect was elucidated by experiments showing that direct injection of a synthetic cAMP-analog (dibutyryl-cAMP) into DRGs *in vivo* prior to injury of the central branch, is sufficient to enhance SCI regeneration (Neumann et al., 2002, Qiu et al., 2002). In addition, the phosphodiesterase inhibitor Rolipram increased cAMP levels, leading to enhanced regeneration of serotonergic axons and functional recovery following SCI in rats (Nikulina et al., 2004). Interestingly, adult neurons have lower levels of cAMP than embryonic neurons and this decrease correlates with their inability to regenerate (Shewan et al., 2002). Moreover, lesion to the central branch of DRG neurons does not lead to a rise in intracellular cAMP. Nonetheless, the central role of cAMP remains controversial, as recent studies showed that the use of cAMP analogs only partially reproduce the conditioning effect *in vivo* (Blesch et al., 2012). Indeed, intracellular elevation of cAMP does not seem to directly increase the intrinsic growth ability of neurons, but rather supports axon regeneration by overcoming myelin-based inhibitors (reviewed in Hannila and Filbin, 2008). Finally, high cAMP levels are also not able to augment the slow component b (SCb) of axonal transport, which constitutes the rate-limiting step of axon growth (Han et al., 2004).

In response to injury, extracellular positive injury signals including neurotrophins (NT3, NGF) and cytokines (IL-6, LIF, CNTF), are expressed by peripheral nerves within the first few hours after a lesion (Ramer et al., 2000, Cafferty et al., 2001,

Cafferty et al., 2004). Neurotrophins bind and activate tyrosine receptor kinase (trk) receptors and lead to the phosphorylation and activation of extracellular-signal-regulated kinase (Erk). The resulting, transient inhibition of phosphodiesterase 4 (PDE4) activity triggers a rise in intracellular cAMP. Upon reaching a threshold level, cAMP activates protein kinase A (PKA), which phosphorylates and activates the transcription factor cAMP response element-binding protein (CREB). These events allow pre-axotomized neurons to overcome the growth inhibition associated with the binding of MAIs to a receptor complex consisting of Nogo-Receptor 1 or 2 (NgR1/NgR2), protein 75 neurotrophin receptor (p75(NTR)) or TROY, and leucine rich repeat and immunoglobin-like domain-containing protein 1 (LINGO-1). Finally, CREB activation leads to the transcription of RAGs like arginase 1, an enzyme which mediates the synthesis of polyamines (Cai et al., 2002). Polyamines are necessary for axon growth by interacting with cytoskeletal elements like tubulin. Accordingly, constitutively active CREB improves dorsal column regeneration *in vivo* (Gao et al., 2004), while expression of a dominant negative CREB results in less axon outgrowth *in vitro* and to a loss of the cAMP mediated repression from the growth inhibition mediated by MAIs (Redmond et al., 2002, Tedeschi, 2011).

Upon peripheral nerve injury, cytokines bind to receptor complexes containing the glycoprotein 130 (gp130) protein, thereby activating the Janus-kinase - signal transducer and activator of transcription (JAK-STAT) signaling pathway in a time-dependent manner. STAT3 is phosphorylated, activated and retrogradely transported to the nucleus in association with a dynein-importin complex (Hanz et al., 2003, Ylera and Bradke, 2007). This results in the accumulation of phospho-STAT3 in the nuclei of DRG neurons, where it induces transcription of growth promoting genes (Schwaiger et al., 2000, Qiu et al., 2005, Bareyre et al., 2011). Importantly, STAT3 activation only occurs upon peripheral and not central branch injuries, emphasizing its critical role in the pro-regenerative response (Schwaiger et al., 2000, Qiu et al., 2005). Accordingly, inhibition or specific deletion of STAT3 in DRG neurons resulted in an impairment of axon outgrowth *in vitro* and peripheral nerve regeneration, while overexpression of STAT3 promoted terminal and collateral sprouting upon dorsal column injury (Qiu et al., 2005, Bareyre et al., 2011). In addition, cytokines activate axoplasmic proteins containing nuclear

localization signals (NLS), which are then transported to the soma using fast axonal transport (0.4 m/day) via the β-importin-dynein motor complex (Levy and Darnell, 2002, Hanz et al., 2003, Liu et al., 2005). Interestingly, some genes that are expressed upon cytokine binding include some components of the injury signal itself, such as IL-6 and LIF, which may further amplify the injury signal via positive feedback.

2.5.2 Negative injury signals

In addition to enhanced positive injury signals, it was proposed that peripheral axotomy also leads to an increase in growth potential due to the interruption of constant retrograde transport of growth inhibitory factors from the growth cone to the soma. In fact, disruption of retrograde transport by application of the microtubule-depolymerizing agent colchicine was sufficient to initiate competence for elongating growth in naïve DRG neurons (Smith and Skene, 1997). This implies that the ability to sustain elongation is chronically suppressed in intact adult neurons by signals from peripheral growth cones. For successful synaptic development and circuit integration, target-derived signals must repress further axonal growth once a neuron has reached its appropriate target. However, regeneration can only occur if this inhibition is interrupted. Even though loss of negative cues appears to be another central mechanism in transducing the conditioning effect, surprisingly little is known about the underlying signalling mechanisms. A potential negative injury signal is the TGFβ/SMAD2/3 pathway. Upon peripheral nerve injury, SMAD2 levels are decreased, suggesting that SMAD2–dependent gene transcription may inhibit the intrinsic growth potential in naïve neurons and possibly that injury may lead to repression from this inhibition (reviewed in Abe and Cavalli, 2008). Similarly, expression of the transcription factor ATF-2 is rapidly decreased in neurons following injury (Martin-Villalba et al., 1998).

Another negative regulator of axonal growth is the dual phosphatase PTEN (phosphatase and tensin homolog), which was first identified as a tumor suppressor. Various intracellular signaling mechanisms involve the activation of receptor tyrosine kinase (RTK). Upon activation, phosphoinositide 3-kinase (PI3K) phosphorylates and converts the lipid second messenger phosphatidylinositol

(4,5) bisphosphate (PIP_2) into phosphatidylinositol (3,4,5) trisphosphate (PIP_3). PIP3, in turn, recruits and activates phosphatidylinositol-dependent kinase 1/2 (PDK1/2), resulting in the activation of protein kinase B (AKT; Song et al., 2005). In contrast, PTEN antagonizes PI3K and catalyzes the conversion from PIP3 to PIP2. Hence, inactivation of PTEN results in the accumulation of PIP3 and the activation of AKT. AKT controls a plethora of downstream molecules, including tuberous sclerosis complex 1 (TSC1/2). TSC1/2 in turn inhibits mammalian target of rapamycin (mTOR), which integrates various cellular signals, including nutrient availability to control protein translation, cell growth, and other processes (reviewed in He, 2010, Park et al., 2010). Importantly, mTOR activity is significantly down-regulated in injured CNS neurons, but not in PNS neurons (Park et al., 2008).

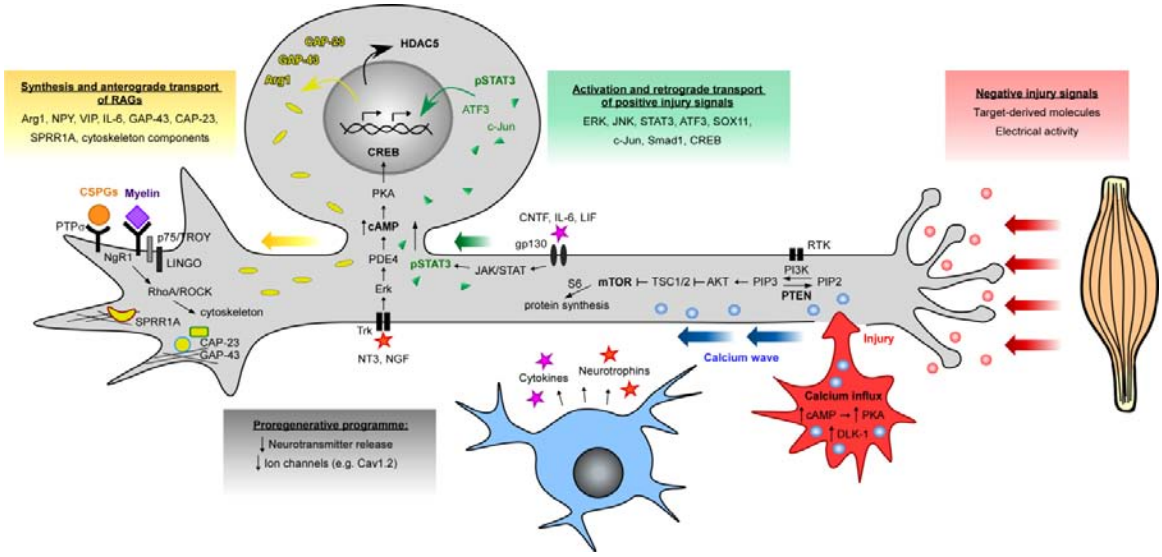

Figure 2.5. Signaling pathways involved in peripheral axon regeneration. A multitude of molecules have been implicated in mediating the conditioning effect. These include transcription factors, cytoskeletal proteins, molecular motors, cell-adhesion molecules and membrane receptors. Both positive and negative injury signals trigger the concerted activation and synthesis of these molecules upon peripheral injury. However the knowledge about the exact underlying mechanisms is still fragmentary. The initial calcium influx into the axoplasm leads to activation of intracellular signaling pathways that initiate resealing of the axonal membrane, local protein synthesis and assembly of a competent growth cone. To some extent, the growth response is also elicited by neurotrophins (NT3, NGF) and cytokines (IL-6, LIF, CNTF), which are overexpressed by Schwann cells in response to injury. In addition, disconnection from the target organs, and thus loss of electrical input, may constitute a possible early injury signal in peripheral neurons.

Accordingly, mTOR activity was suppressed and new protein synthesis was impaired upon optic nerve injury in wild-type adult retinal ganglion cells (RGCs). In contrast, RGC axons from PTEN knockout mice regenerated robustly (Park et al., 2008). Deletion of tuberous sclerosis complex 1 (TSC1), another negative regulator of the mTOR pathway, also allows axon regeneration. Hence, it is likely that a decrease in mTOR activity constitutes a major intrinsic obstacle for successful axon regeneration in CNS axons (reviewed in He, 2010).

Finally, electrical activity is another putative negative injury signal. Injury to peripheral axons leads to a large, sustained depolarization and antidromic propagation of action potentials from the lesion site to the soma (Mandolesi et al., 2004). Consequently, the axoplasm is invaded by a strong influx of calcium. Treatment with tetrodotoxin reduces the ability of peripheral axons to regenerate upon axotomy, suggesting that activation of voltage-gated sodium channels is necessary for the propagation of the calcium response and for successful regeneration (Mandolesi et al., 2004). However, the consequences of electrical activity remain controversial, possibly due to differences in stimulation paradigms (Abe and Cavalli, 2008, Tedeschi and He, 2010, Mar et al., 2014). Diverse studies showed that weak electrical stimulation improved regeneration of rat motor (Al-Majed et al., 2004) and sensory neurons (Udina et al., 2008), and increased intracellular cAMP to levels reminiscent of conditioned DRG neurons (Udina et al., 2008). In contrast, electrical stimulation of central axons did not promote regeneration, not even in the presence of a growth permissive environment (Harvey et al., 2005). Finally, strong electrical stimulation also significantly inhibited axon outgrowth in adult DRG neurons, and loss of electrical activity following PNS injury facilitated axonal regeneration in the PNS (Enes et al., 2010). In conclusion, electrical activity may constitute a pivotal early injury signal in peripheral neurons, but is probably insufficient to trigger regeneration of central neurons. Future investigations are needed to further explore the precise role of electrical activity in axonal regeneration.

Unfortunately none of the measures to counteract the inhibitory extracellular environment and to increase the intrinsic growth ability are able to fully reproduce the regenerative response induced by a conditioning lesion. This suggests that additional signaling mechanisms are required for successful

regeneration. To date, the most promising strategy to promote axon regeneration is to tackle CNS regeneration via a multifactorial approach, i.e. concurrently increasing the intrinsic growth potential of CNS neurons and decreasing the inhibitory effect of the lesion scar and CNS myelin. Interestingly, both extracellular and intracellular factors converge on a single common denominator: the growth cone cytoskeleton.

2.6 The growth cone cytoskeleton

The cytoskeleton is composed of three principle components: microtubules, intermediate filaments and actin filaments (also termed microfilaments). Analogous to the bony skeleton of the human body, the cytoskeleton´s principal function is to provide a structural framework to the cell. Contrary to the skeleton though, the cytoskeleton is capable of rapid assembly or disassembly in response to the cell´s requirements. It is centrally involved in almost all dynamic cellular events, including intracellular transport and signaling, cell division, migration and polarization. In the context of axonal regeneration, it is pivotal in controlling the growth cone machinery, regulating the migration and proliferation of scar-forming cells and constituting the fundamental down-stream target of inhibitory molecules.

2.6.1 Microtubules

Microtubules represent the largest component of the cytoskeleton and are hollow tubular polymers with an outer diameter of approximately 24 nanometers (**Figure 2.6**). They are most commonly composed of 13 protofilaments (Evans et al., 1985), which in turn, are formed by the polymerization of α-/β-tubulin heterodimers (Amos and Klug, 1974). Due to the specific head-to-tail association of these heterodimers, microtubules are polar structures with a fast-growing "plus-end", and a more stable slower-growing "minus-end" (Allen and Borisy, 1974). In axons of cultured mammalian neurons, microtubules are distributed with their plus-end towards the distal growth cone, while dendrites feature a mixed polarity (Baas et al., 1988, Baas, 1998).

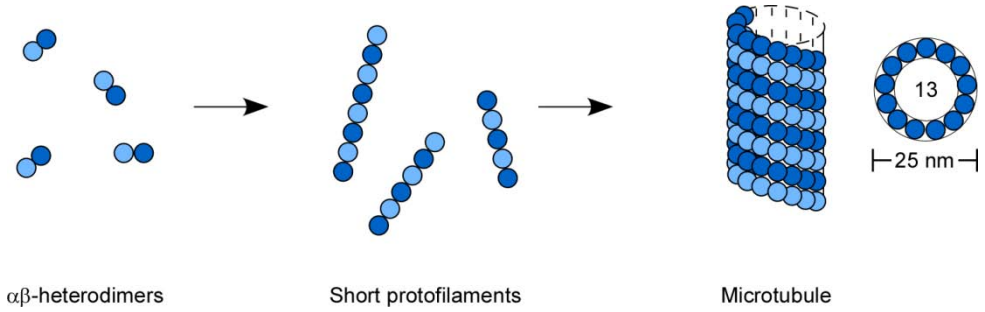

Figure 2.6. Microtubule polymerization. Microtubules are tubular polymers with a diameter of 24 nm, consisting of 13 shorter protofilaments (Evans et al., 1985), which in turn are composed of head-to-tail associated α/β-tubulin heterodimers (Amos and Klug, 1974). Scheme redrawn from Westermann and Weber (2003).

The polymerization of microtubules is driven by the propensity of tubulin-GTP dimers to bind to the plus-end of the microtubules. While the hydrolysis of GTP bound to α-tubulin is very slow, GTP is readily hydrolyzed to GDP after binding to ß-tubulin. Subsequently, GDP-tubulin is depolymerized and dissociated from the microtubule. Therefore, the tubulin polymers switch stochastically between phases of prolonged polymerization and rapid depolymerization, a phenomenon called "dynamic instability" (Mitchison and Kirschner, 1984). "Catastrophe" is the term describing the transition from growth to shrinkage, while "rescue" describes the transition from shrinkage to growth. Microtubule dynamics are regulated by two distinct sets of factors: microtubule-stabilizing and microtubule-destabilizing proteins (reviewed in Mandelkow and Mandelkow, 1995, Conde and Caceres, 2009). Microtubule-stabilizing factors may exert their function by either (1) preventing catastrophes, (2) by rescuing a depolymerizing microtubules or (3) by decelerating shrinkage. Examples include tau, diverse microtubule-associated proteins (MAPs) like MAP1b and MAP2, doublecortin (DCX), and several members of the plus end tracking protein family (+TIPs), including cytoplasmatic linker proteins (CLIPs), CLIP-associated proteins (CLASPs) and end-binding proteins (EB1 and EB3). +TIPs regulate microtubule growth and shrinkage by specifically binding to the plus-end of microtubules. In addition, +TIPs provide a link between microtubules and the actin cytoskeleton by binding to actin binding proteins (reviewed in Akhmanova and Steinmetz, 2008). By contrast, microtubule-destabilizing proteins act on microtubules, by (1) inducing catastrophes, (2) preventing rescues or by (3) accelerating shrinkage. Well-established examples include members of the kinesin-13 and kinesin-8 family, as well as Op18/stathmin.

In addition to microtubule stabilizing and destabilizing factors, the dynamics of microtubules are also regulated by post-translational tubulin modifications, including acetylation and deacetylation, tyrosination and detyrosination, generation of Δ2-tubulin, polyglutamylation, polyglycylation, palmitoylation and phosphorylation (reviewed in Janke and Kneussel, 2010).

Microtubules are fundamental for a variety of functions within the cell. They provide mechanical support to the cell, form the mitotic spindle which is necessary for cell division and control movement of cilia and flagella. They also serve as "highways" for molecular motors, such as kinesins and dyneins, which shuttle organelles and vesicles within the cytoplasm (reviewed in Goldstein and Yang, 2000, Drummond, 2011). In neurons, microtubules and their dynamic rearrangements are also vital for growth cone motility and steering, and subsequently for axon outgrowth (Forscher and Smith, 1988, Sabry et al., 1991, Dent and Gertler, 2003). In fact, local stabilization of microtubules by taxol is sufficient to steer the growth cone into the direction of taxol application, while nocodazole induced destabilization of microtubules, induces growth cones to turn away (Buck and Zheng, 2002). In addition, taxol treatment is sufficient to induce axon formation and thus to initiate polarization in hippocampal neurons *in vitro* (Witte et al., 2008). Moreover, microtubule stabilization increases the transport of vesicular cargoes, thus supplying the growth cone with the required materials for axonal growth such as membrane proteins and cytoskeletal elements (Zakharenko and Popov, 1998). Finally, microtubule stabilization is instrumental for growth cone formation after axonal injury. Upon injury, axons in the PNS usually form new growth cones and regenerate, while axons in the CNS form dystrophic end-bulbs (also called "retraction bulbs") that do not regenerate (reviewed in Bradke et al., 2012). Growth cone formation requires bundling and stabilization of microtubules in the distal part of the lesioned axon. In contrast, disorganized microtubules underlie the formation of retraction bulbs after injury and the subsequent failure of axonal regeneration *in vivo* (Erturk et al., 2007). Microtubule stabilization by low doses of taxol is sufficient to inhibit the formation of dystrophic end-bulbs, while destabilization by nocodazole or vincristine leads to the enhanced formation of these structures (Pan et al., 2003, Erturk et al., 2007). In summary, microtubule stabilization is central for the formation of a functional

growth cone and subsequently for axon outgrowth. Therefore, microtubules offer a well-suited target for potential multifactorial approaches to counteract intrinsic and extrinsic barriers in the CNS after trauma and to promote axon regeneration.

2.6.2 Intermediate filaments

As their name suggests, intermediate filaments have a mid-sized (relative to microtubule and actin filaments) average diameter of approximately 10 nanometers. Unlike microtubules and actin filaments, intermediate filaments are more heterogeneous and composed of a number of different protein subunits. The subunits organize into rod-shaped filaments which are non-polar and very stable. Due to the lack of dynamics, intermediate filaments are not centrally involved in cell motility. In fact, their main functions are primarily mechanical. They maintain the cell-shape and organize the internal structure of the cell, anchoring organelles and serving as structural components of the nuclear lamina. In addition, intermediate filaments have also been implicated in functions such as cell-to-cell communication, blood-brain-barrier (BBB) function and wound healing in the CNS (Liedtke et al., 1996). All eukaryotic cells contain intermediate filaments, but the composition of the various protein subunits is tissue-specific. Neurofilaments, for example, are found specifically in neurons (most abundantly in the axons), desmins in muscle cells, and keratins in epithelial cells. Other intermediate filaments like vimentins and lamins are distributed more widely, as detailed in Herrmann et al. (2007).

2.6.3 The actin cytoskeleton

Actin filaments (F-actin) are helical polymers about 7 nanometers in diameter that are composed of two strands formed from actin monomers (G-actin). There are three forms of G-actin subunits depending on the adenine nucleotide that is non-covalently associated with G-actin: ATP-actin, ADP-Pi-actin and ADP-actin (**Figure 2.7**). G-actin is composed of four subdomains and a deep ATP binding cleft between subdomain 2 and 4. The F-actin polymer is structurally polarized, since all subunits point towards the same end. The polymer end bound by an actin subunit that has its ATP binding cleft exposed is called the minus "(-)" or pointed end, while the opposite end (where the ATP-binding cleft is directed at an

adjacent monomer) is called the plus "(+)" or barbed end. The terms "pointed" and "barbed" end derive from their appearance under a transmission electron microscope after a preparation technique termed "decoration".

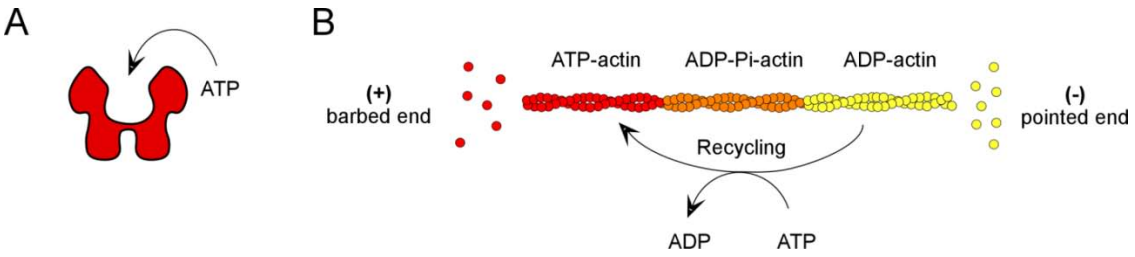

Figure 2.7: Actin filaments. Actin filaments are polymers composed of bi-helical strands of globular actin (G-actin) monomers. Polymerizing G-actin is non-covalently associated with ATP (red subunit), which undergoes two steps of hydrolysis, producing first ADP-Pi-actin (orange subunits) and then ADP-actin (yellow subunit). Consequently, ADP-actin dissociates from the pointed end and is again recycled to ATP-actin before the cycle restarts. At stead-state polymerization preferentially takes place at the "(+)" or "barbed" end, making it the rapidly-growing end. At steady-state depolymerization and severing occurs at the "(-)" or "pointed" end, and thus constitutes the slower growing end. Scheme adapted from (Dent and Gertler, 2003).

During polymerization, ATP-actin preferentially binds to the barbed end of the actin polymer. Bound ATP-actin then undergoes two phases of hydrolysis. First ATP-actin is hydrolyzed to ADP-Pi-actin and then to ADP actin, releasing Pi. Consequently, ADP-actin dissociates from the pointed end and is recycled to ATP-actin before the cycle starts again. As a consequence, the actin filament can be subdivided into three different areas depending on which adenine nucleotide is bound to it: ATP-actin is predominantly found at the barbed end, ADP-Pi-actin in the middle of the filament and ADP-actin close to the pointed end (**Figure 2.7**). Although ATP-actin and ADP-actin can dissociate from both the barbed (rapidly growing) and the pointed end (slower growing), dissociation of ADP-actin from the pointed end is favored (reviewed in Pak et al., 2008). This leads to polymerization at the barbed end and depolymerization from the pointed end, resulting in net growth of the filament at the barbed end (**Figure 2.7**).

It is interesting to note that actin monomers can spontaneously self-assemble into polarized, bi-helical filaments *in vitro*. With the aid of specific actin-binding proteins (ABPs, discussed in a later section) actin is then further organized into

higher order actin structures and networks that are required for growth cone motility (Pak et al., 2008). Three actin superstructures have been identified: (1) lamellipodia (also called veils) are flat regions containing a dense and branched meshwork of actin filaments, (2) filopodia (also called microspikes) are narrow, cylindrical bundles of actin filaments protruding several micrometers beyond the lamellipodial frontier, and (3) actin arcs are bundles of actin filaments running parallel to the growth cone leading edge. The growth cone can be divided into three distinct regions: the central (C) domain, the transition (T) zone, and the peripheral (P) domain (**Figure 2.8**).

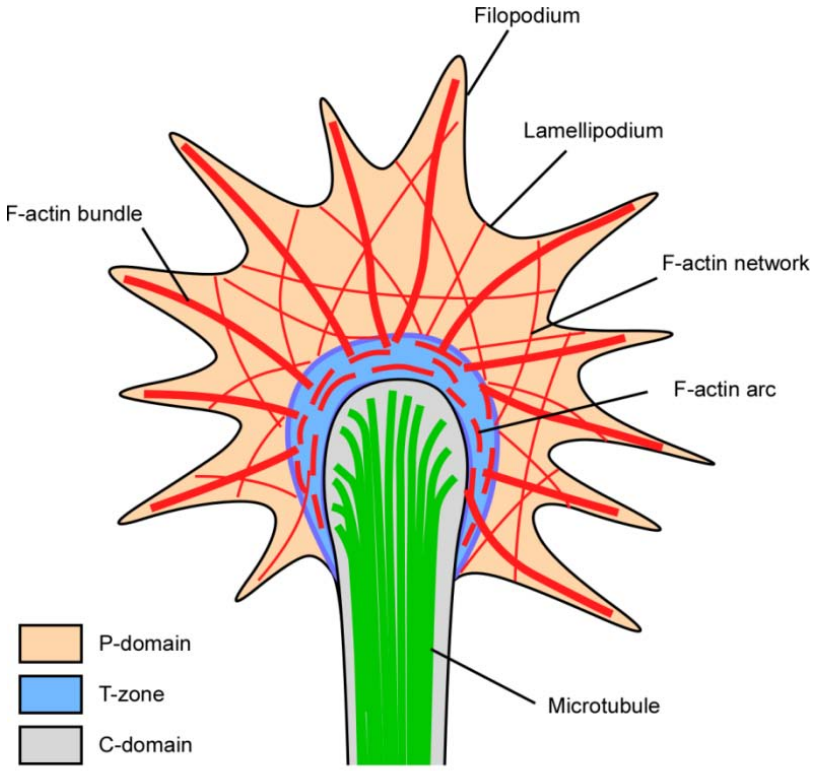

Figure 2.8: The axonal growth cone. The axonal growth cone can be subdivided into three distinct domains: the central (C) domain, the transition (T) zone and the peripheral (P) domain. Axonal microtubules invade the C domain of the axonal growth cone and occasionally protrude into the P domain, guided along filopodia. Filopodia are present in both the P and T domain, and are composed of dense bundles of actin filaments. Lamellipodia are primarily found within the P domain and are organized as a meshwork of actin filaments. Actin arcs are generated by myosin-II mediated contraction of F-actin filaments in the T domain and are oriented perpendicular to the growth axis.

The P domain is the thin, outermost region of the growth cone. It´s primary constituents are the actin-based lamellipodia and filopodia which are highly dynamic. Microtubules on the other hand only transiently enter the peripheral

region. In contrast, the C domain is located in the center of the growth cone in close proximity to the axonal shaft and is composed primarily of microtubules. It is thicker, and contains a multitude of organelles and vesicles. The T domain is the thin region between the C and P domains and is mainly characterized by the presence of F-actin arcs and myosin II.

F-actin filaments of both filopodia and lamellipodia are polarized and oriented with their barbed ends facing toward the distal membrane of the growth cone. As polymerization occurs at the barbed end, it causes actin filaments to extend and to push against the outer rim of the growth cone. At the same time, the membrane exerts force on the growing actin-filaments, and actin is severed and depolymerized at the pointed end, whereby the actin-filament moves away from the leading edge. This process is called "retrograde flow". In addition, myosin-II, a molecular motor that generates forces on F-actin, increases retrograde flow by contraction of F-actin filaments in the T domain, which results in the generation of actin arcs (**Figure 2.8**) (Schaefer et al., 2002). Actin arcs in turn, hinder microtubules from invading the P domain (Burnette et al., 2008, Lee and Suter, 2008, Schaefer et al., 2008, Lowery and Van Vactor, 2009). For axon outgrowth the growth cone undergoes repeated cycles of three specific stages termed protrusion, engorgement and consolidation (Goldberg and Burmeister, 1986, Lowery and Van Vactor, 2009) (**Figure 2.9**).

During protrusion, lamellipodia and filopodia explore the extracellular environment. Upon binding to attractive cues or adhesive substrates, receptors in the growth cone membrane activate intracellular signaling cascades that lead to the formation of a molecular "clutch" linking the substrate to the actin cytoskeleton. As a result, F-actin retrograde flow is temporarily decreased. At the same time, F-actin polymerization continues in front of the clutch site leading to the extension of lamellipodia and filopodia and subsequently to the forward expansion of the growth cone. As another consequence of the attenuation of retrograde flow, an actin free corridor is created between the adhesion site and the C domain, most likely because F-actin behind the clutch is severed and removed. During engorgement, actin arcs in the T-zone reorientate in the direction of growth and microtubules from the C domain invade the actin free

corridor. Concomitantly, vesicles, organelles and cytoskeleton modulating proteins are transported into the engorged area along the protruding microtubules. During consolidation, protruding microtubules are compressed by the myosin-II containing actin arcs at the growth cone neck to form a new segment of axon shaft. Finally, microtubules are bundled and stabilized by microtubule associated protein (MAPs) which are essential for the structural integrity of the axon (Conde and Caceres, 2009). Repetition of these three steps ultimately leads to axon outgrowth (reviewed in Lowery and Van Vactor, 2009, Stiess and Bradke, 2011).

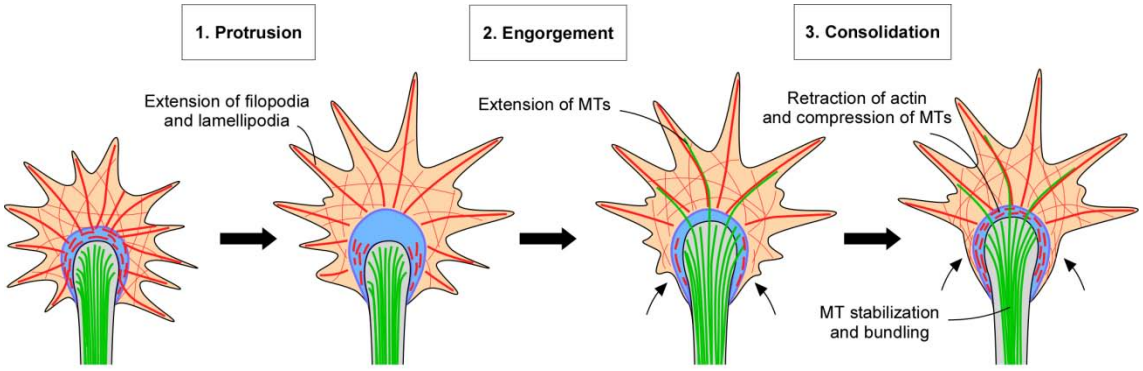

Figure 2.9: Phases of axon elongation. Axon elongation consists of three consecutive and repetitive steps. (1) Protrusion: adhesion of filopodia and lamellipodia to the substrate and subsequent polymerization of actin filaments result in growth cone extension. (2) Engorgement: dynamic microtubules engorge from the C domain into the former T zone, where actin filaments are disassembled and the remaining actin arcs reorientate along the axis of growth. Vesicles, organelles and cytoskeleton modulating protein are transported into the engorged area along microtubules. (3) Consolidation: microtubules are compressed by the action of myosin-II containing actin arcs in the newly localized C domain and are stabilized by MT-stabilizing proteins. The proximal part of the growth cone resumes a cylindrical shape and forms a new segment of the axonal shaft.

The interdependence of the actin and microtubule network was first demonstrated in studies where acute inhibition of actin assembly resulted in rapid microtubule advance into the peripheral domain of growth cones (Yamada et al., 1970, Forscher and Smith, 1988), and depolymerization of microtubules caused new growth cone like lamellipodial and filopodial protrusions along the usually quiescent axon shaft (Bray et al., 1978). These results gave rise to the idea of "steric-hindrance". The model postulates that microtubule extension and

consequently axon elongation is enhanced due to relief of physical restraints normally imposed on microtubules by peripheral actin networks. In fact, studies in sympathetic neurons demonstrated that the rate of growth cone advance may directly correlate with the size and dynamics of lamellipodia and filopodia (Argiro et al., 1984, 1985). In this context it is also interesting to note that sensory neurons can regenerate upon depletion of F-actin in the growth cones (Marsh and Letourneau, 1984, Letourneau et al., 1987, Jones et al., 2006). Similar results have been obtained in a variety of other neuronal systems. Most notably, localized actin network instability induced by cytochalasin D treatment caused axon formation in developing hippocampal neurons *in vitro* (Bradke and Dotti, 1999). Hence, regulation of actin assembly and dynamics is a prerequisite to modulate growth cone velocity and direction, and consequently axonal extension.

2.7 Regulation of actin dynamics by actin binding proteins

To enable the dynamic responses of the growth cone to a variety of intra- and extracellular cues, the precise control of actin nucleation, polymerization, depolymerization, bundling, and contraction is essential. Actin organization and dynamics are regulated by over 100 different actin-binding proteins (ABPs) that are grouped according to their function (**Figure 2.10**) (reviewed in Letourneau, 2009, Pollard and Cooper, 2009, Dent et al., 2011, Flynn, 2013).

"Actin sequestering proteins" like profilin, calbindin and thymosin-ß4 sequester or bind G-actin and thus restrict the availability of G-actin to minimize spontaneous actin nucleation and polymerization (Cassimeris et al., 1992, Sanders et al., 1992, Wills et al., 1999). However, profilin has also been found to catalyze the exchange of ADP-actin to ATP-actin, and thus to indirectly support actin polymerization by refreshing the G-actin pool (reviewed in Dent et al., 2011, Flynn, 2013).

Other ABPs, the so called "actin nucleators" stimulate the *de novo* actin filament assembly by facilitating the formation of an actin nucleus, the rate limiting step for actin-filament growth (Sept and McCammon, 2001). Four classes of actin nucleators have been identified, including the Arp 2/3 complex (Mullins et al., 1998), formin proteins (Pruyne et al., 2002), Spir proteins (Quinlan et al., 2005) and cofilin (Andrianantoandro and Pollard, 2006).

"Capping proteins" like CapZ bind the barbed end to terminate actin elongation or protect the filament end from polymerization-terminating capping proteins (Ishikawa and Kohama, 2007, Drees and Gertler, 2008). Other capping proteins like tropomodulin cap the pointed end to promote actin polymerization, while actin depolymerizing factor (ADF)/cofilin binds the pointed end to promote actin disassembly.

"Actin severing proteins" such as cofilin and gelsolin sever F-actin filaments into shorter protomers generating free actin filament ends that are accessible for further F-actin polymerization and depolymerization (reviewed in Ono, 2007).

Members of the family of "actin cross-linkers" bundle, cross-link and stabilize F-actin (Dent et al., 2011, Flynn, 2013). In general, smaller cross-linkers such as fascin, fimbrin and epsin organize F-actin into tight parallel bundles such as those found in filopodia (Sasaki et al., 1996, Cohan et al., 2001). By contrast, larger cross-linkers like filamin and α-actinin support gel-like, branched filament networks typical for lamellipodia (Lieleg et al., 2009). Tropomyosin, in turn, binds along actin filaments, thereby stabilizing them, and at the same time acts as a "gatekeeper" by regulating the access of other ABPs to the actin filament (Schevzov et al., 2012).

Diverse myosin motors, move cargo along actin filaments or move actin filaments themselves. Myosin V, for example, "walks" along actin filaments towards the barbed end and moves secretory vesicles and intracellular organelles (Pruyne et al., 2004, Fagarasanu and Rachubinski, 2007).

Finally, "actin tethering proteins" are responsible for anchoring F-actin to other cellular components such as the growth cone membrane (reviewed in (Letourneau, 2009, Dent et al., 2011). Spectrin mediates F-actin binding to the intracellular side of the plasma membrane and modulates the formation of the submembranous cortical spectrin network. Vinculin, talin and α-actinin link actin to integrin-mediated adhesion sites (Letourneau and Shattuck, 1989). And lastly, ERM (ezrin, radixin, moesin) proteins tether actin to diverse membrane proteins (Ramesh, 2004).

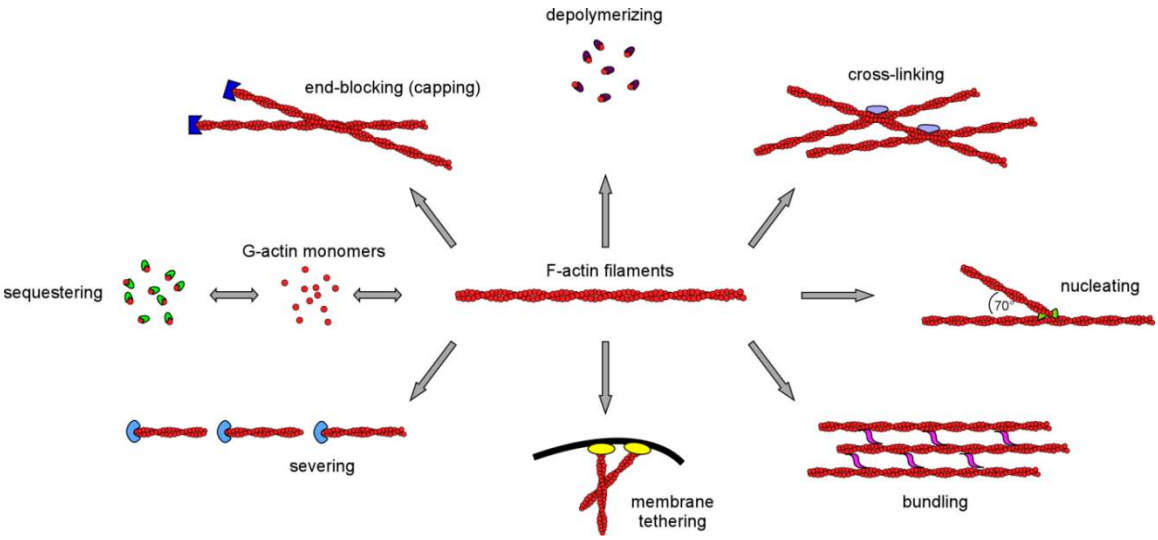

Figure 2.10. Actin binding proteins. Actin organization and dynamics are regulated by a plethora of diverse actin-binding proteins (ABPs) that are grouped according to their function. The major functions of ABPs include cross-linking, bundling, binding to the membrane, depolymerization, severing, sequestering, capping and nucleation of new actin filaments.

2.8 ADF/cofilin

As described earlier, actin-filament dynamics and reorganization play a pivotal role in motility, morphology, and directional movement of axonal growth cones. Growth cone motility is regulated by the assembly of actin filaments at the leading edge and disassembly at the T-zone (Lin and Forscher, 1995). This polarized growing and shrinking results in dynamic actin turnover and is fundamental for generation of protrusive forces in axons. A large body of evidence suggests that a single family of actin regulatory proteins - actin depolymerizing factor (ADF)/cofilin (AC) - is a critical regulator of this actin "treadmilling" and controls growth cone dynamics and neurite extension (**Figure 2.11**). (1) ADF and cofilin 1 are abundant in neuronal growth cones (Bamburg and Bray, 1987, Jensen, 1993, Garvalov et al., 2007). (2) *Xenopus* ADF/cofilin increased the length of neurite outgrowth when expressed in rat cortical neurons or chick spinal cord neurons (Meberg and Bamburg, 2000). (3) AC proteins and their upstream regulators positively regulate growth cone dynamics and the rate of neurite extension in dissociated embryonic chick DRG neurons (Endo et al., 2003). (4) More recently, our group showed that AC also regulates neuritogenesis during development by driving actin turnover and organization in embryonic

hippocampal and cortical neurons (Flynn et al., 2012). Given their pivotal role in development, I asked if AC proteins are also critical regulators of axon regeneration and involved in the conditioning response?

AC proteins are small (~19 kDa) actin-binding proteins and essential regulators of actin dynamics in all eukaryotes (Bernstein and Bamburg, 2010). AC proteins bind preferentially to ''aged'' ADP-actin filaments, thereby altering their conformation (McGough et al., 1997), and thus increasing fragmentation at the boundaries between cofilin-decorated and bare filaments (Andrianantoandro and Pollard, 2006, Pavlov et al., 2007, Suarez et al., 2011, Elam et al., 2013). AC proteins enhance actin dynamics in at least three ways (**Figure 2.11**): by depolymerization (accelerating monomer loss at the pointed end), by severing F-actin filaments into shorter protomers (generating free actin filament ends that are accessible for F-actin polymerization and depolymerization), and by directly or indirectly facilitating actin filament growth at the barbed end (Hawkins et al., 1993, Hayden et al., 1993, Carlier et al., 1997, Andrianantoandro and Pollard, 2006, Michelot et al., 2007, Bernstein and Bamburg, 2010).

There are three tissue specific AC family members in mammals: the muscle specific cofilin 2 (also termed m-cofilin) and the two nonmuscle specific isoforms cofilin 1 (n-cofilin) and ADF (destrin). During development, cofilin 1 is the predominant isoform and remains expressed ubiquitously in most adult tissues. Postnatally, ADF is upregulated and most abundantly expressed in epithelial and endothelial tissues, albeit generally at lower concentrations than cofilin 1. During late embryogenesis, and after birth, it is known that cofilin 2 replaces cofilin 1 in striated, skeletal and cardiac muscle (Ono et al., 1994, Vartiainen et al., 2002, Gurniak et al., 2005, Nakashima et al., 2005, Bellenchi et al., 2007, Gurniak et al., 2014). Other studies have shown that unlike cofilin 1 and ADF, cofilin 2 is expressed very late in development and most abundantly in postnatal muscle and brain tissue (Vartiainen et al., 2002, Gurniak et al., 2014, Kremneva et al., 2014).

Despite sharing certain expression patterns, the specific biochemical and functional properties distinguishing muscle from nonmuscle isoforms are largely unknown. The exact biochemical and functional properties of all three isoforms are unclear, with cofilin 2 being the least understood member of the AC family. Although AC proteins share certain functions (Hotulainen et al., 2005), ADF

depolymerizes actin filaments more efficiently than cofilin 1, whereas cofilin 1 severs filaments better than ADF (Bernstein and Bamburg, 2010). Cofilin 2 has a weaker actin filament depolymerization activity and displays a much higher affinity for ATP-actin monomers than ADF and cofilin 1 (Vartiainen et al., 2002). But it was shown recently, that in contrast to other isoforms, cofilin 2 can also bind and disassemble ADP-Pi F-actin filaments (Kremneva et al., 2014).

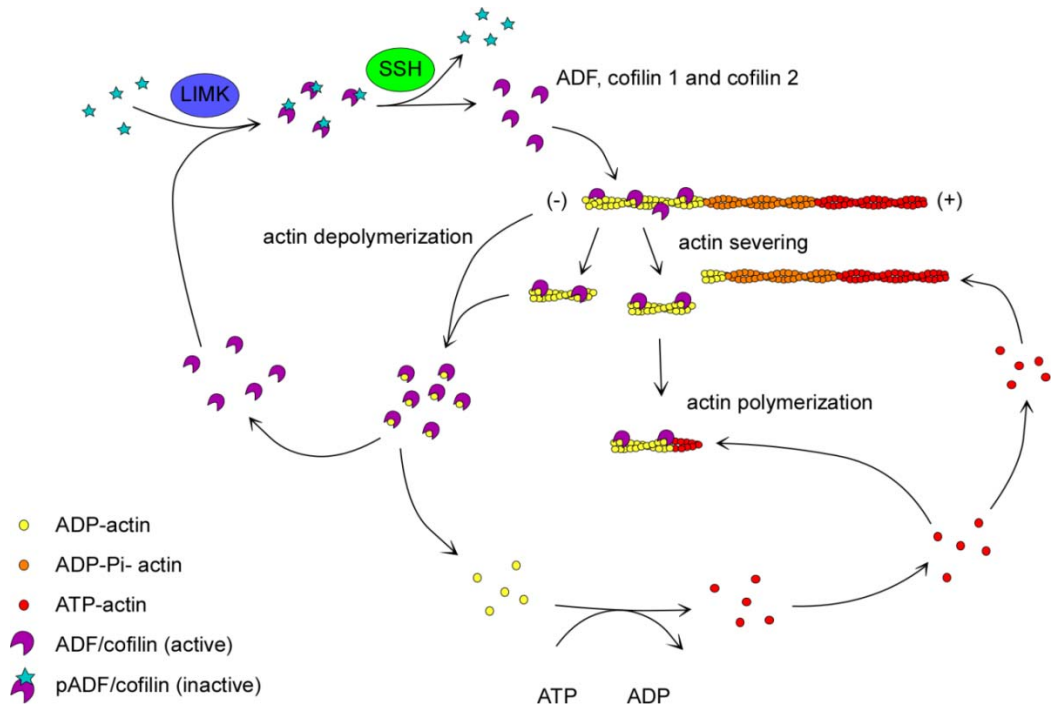

Figure 2.11. Regulation of actin dynamics by ADF/cofilin. ADF/cofilin preferentially binds to the ADP-actin rich region of the F-actin filament, thereby altering its twist. This conformational change in turn leads to enhanced fragmentation (severing and/or depolymerization) at the boundaries between cofilin-decorated and bare regions on the actin filament. Subsequently, short actin protomers are accessible for further F-actin polymerization and depolymerization, while dissociated ADP-actin monomers are recycled to ATP-actin and reenter the pool of G-actin monomers that are available for polymerization. ADF/cofilin activity is reversibly regulated by phosphorylation (LIMK) and dephosphorylation (SSH) at serine 3.

Diverse mechanisms regulate the activity of AC proteins, including phosphorylation and dephosphorylation (collectively termed phosphoregulation), binding to phosphatidyl inositol phosphates (PIP_2), by synergistic or competitive interactions with other ABPs and scaffolding proteins, as well as by pH (reviewed

in Van Troys et al., 2008). However to date, most research has focused on the reversible regulation of AC via phosphorylation (**Figure 2.11**). LIM kinases (LIMK, in which LIM is an acronym of the three gene products Lin-11, Isl-1, and Mec-3) (Arber et al., 1998, Scott and Olson, 2007) and the related testicular (TES) kinases (Toshima et al., 2001b, Toshima et al., 2001c) phosphorylate and thus inactivate AC proteins, while phosphatases such as slingshot homolog (SSH) (Niwa et al., 2002) and chronophin (CIN) (Gohla et al., 2005, Wiggan et al., 2005) reactivate AC proteins through dephosphorylation. LIM kinases in turn are also regulated through phosphorylation by the Rho GTPase effectors Rho kinase (ROCK) and p21-activated kinase (PAK) (Edwards et al., 1999, Ohashi et al., 2000) whereas the TES kinases are downstream of integrin signals that require Rho but not ROCK or PAK (Toshima et al., 2001a).

2.9 Objectives of this study

In conclusion, adult CNS neurons lose the ability to regenerate after development. This is due to an inhibitory extracellular environment and to a reduced intrinsic growth competence. Interestingly, both extracellular and intracellular factors converge on a single common denominator: the growth cone cytoskeleton. In particular, the actin and microtubule network is especially important for the dynamics and outgrowth of axons. Hence, in order to find new approaches to promote regeneration in the adult nervous system, a better understanding of the cellular and molecular mechanisms that govern the axonal growth ability is indispensable. However, to date, not much is known about the intracellular basis of the conditioning paradigm – a model for successful regeneration - at the level of the cytoskeleton.

In my PhD project, I hypothesized that the strikingly different growth modes of naïve and conditioned primary sensory neurons is reflected in changes at the level of the cytoskeleton. Accordingly, I addressed three main questions. (1) Which changes of the actin and microtubule network are correlated to the increase in axonal outgrowth after conditioning? (2) What is the physiological relevance of changes happening at the level of the cytoskeleton for enhanced axonal

outgrowth after conditioning? (3) Which are the potential signalling pathways and molecular players involved in mediating the conditioning effect after peripheral axotomy?

To test my hypothesis, I performed live-cell imaging of naïve and conditioned DRG neurons and observed that increased growth cone and actin dynamics are correlated with and necessary for the rapid axon outgrowth following a conditioning lesion. Subsequently, I focused my investigation on the actin regulatory protein family of actin depolymerizing factor(ADF)/cofilin (AC), as it was shown to regulate actin dynamics and neurite outgrowth in other neuronal cell types (Endo et al., 2003, Flynn et al., 2012). To investigate the role of AC proteins in the conditioning response, I asked whether genetic depletion or overexpression of AC proteins interferes or promotes axon growth, respectively. My data show that AC proteins are necessary for axon growth both *in vitro* and *in vivo*. Furthermore, I show that AC proteins are sufficient to promote axon outgrowth *in vitro*. Future studies will be needed to clarify whether AC proteins also hold promise for enhancing axon regeneration *in vivo*. I conclude that AC protein mediated actin turnover facilitates axon growth and is necessary for regeneration by recapitulating processes that occur during neurite initiation in development.

3 RESULTS

3.1 Rapid axonal growth after PNL correlates with an increase in growth cone dynamics

A primary lesion to the peripheral branch of dorsal root ganglion (DRG) neurons followed by a second lesion to the central branch of the same neurons results in a robust growth response of the central branch *in vivo* (Richardson and Issa, 1984, Smith and Skene, 1997, Neumann and Woolf, 1999). This growth phenomenon is also reflected in cell culture, and hence nicely suited as tool to investigate the intrinsic mechanisms underlying the conditioning effect. To obtain a first idea about potential differences between naïve and conditioned DRG neurons, I started out by characterizing the conditioning growth response in cell culture. To this end I conditioned DRG neurons by performing a peripheral nerve lesion (PNL), i.e. I ligated and transected the left sciatic nerve of adult rats. Seven days later, I dissected the conditioned lumbar (L) 4 and 5 DRGs as well as their contralateral naïve counterparts, dissociated and plated them on the permissive substrate laminin.

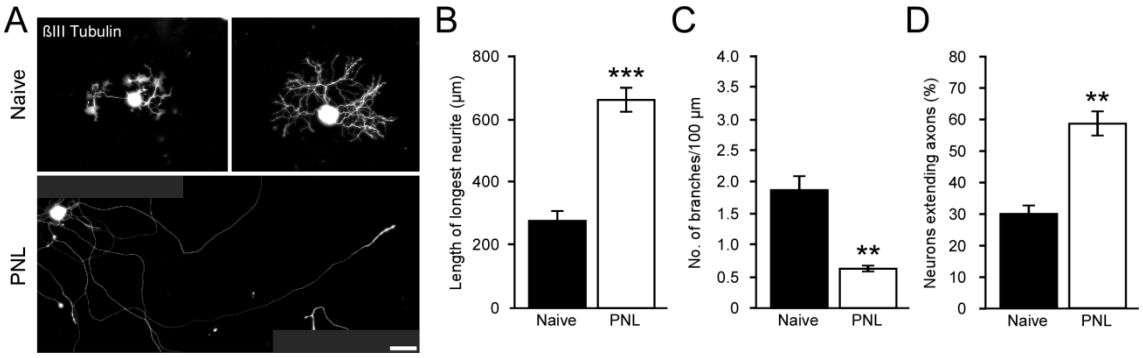

Figure 3.1. Conditioned DRG neurons extend longer axons and branch less frequently. After 16-18 hours in culture, naïve and conditioned neurons were fixed with 4% paraformaldehyde and immunostained with antibodies against ßIII-tubulin (Tuj1). Images were aquired using fluorescence microscopy. The length of the longest neurite per neuron (B), the number of branches per 100 µm (C) and the percentage of neurons extending axons (D) was quantified (*** $p < 0.001$, ** $p < 0.01$ by t-test; $n > 90$ neurons from three independent experiments, mean ± SEM; scale bar 50 µm).

Approximately 16-18 hours after plating, neurons were fixed using 4% paraformaldehyde and immunostained for the neuron specific ßIII-tubulin (Tuj1). Naïve neurons typically displayed short neurites often terminating in large,

complex growth cones (**Figure 3.1, A**). In comparison, conditioned DRG neurons extended long axons that branched rarely and often fasciculated with one another (**Figure 3.1, A**). On average, naïve DRG neurons extended 277 µm ± 30 µm long axons. In contrast, neurites of conditioned neurons grew 666 µm ± 69 µm in length, an increase of almost 3-fold ($p < 0.001$; **Figure 3.1, B**). The number of branches along the axon decreased from 1.9 ± 0.2 in naïve to 0.6 ± 0.1 in conditioned DRGs ($p < 0.01$; **Figure 3.1, C**). The percentage of neurons extending axons doubled from 29.9 % ± 2.5 % to 58.5 % ± 3.8 % upon PNL ($p < 0.01$; **Figure 3.1, D**). In summary, the observed differences in the growth response were similar to those first described by Smith and Skene (1997). Thus, I could reproduce the conditioning effect successfully *in vitro* and use it as a mean to study possible intracellular mechanisms underlying the increase in growth potential after PNL.

As described above, conditioned DRG neurons grow longer axons than naïve controls if grown for the same period of time. This implies that the two groups should show clear differences in their growth behavior. As the growth cone contains the necessary machinery to drive axon growth (reviewed in Coles and Bradke, 2015), I next sought to analyze the growth cone dynamics of conditioned DRG neurons and to compare them to naïve controls using video live-microscopy. To this end, I prepared naïve and conditioned DRG cultures and allowed them to grow for 15-16 hours. Subsequently, cells displaying typical features of naïve (short and highly branched axons) and conditioned (long and sparsely branched axons) DRG neurons were selected and their growth cones observed for 1 hour using the live cell imaging setup described in the methods section.

General observations revealed that axons of naïve neurons branched frequently and that growth cones were morphologically more complex than in conditioned neurons. These features of naïve DRG neurons were associated with a slower, albeit continuous growth and the concomitant extension and retraction of short filopodia (**Figure 3.2, A-C**). In contrast, conditioned DRGs showed a typical step-like growth curve with alternating phases of growth arrest and rapid growth spurts. While periods of no growth correlated with the formation of typical torpedo-shaped, tapered growth cones, rapid growth was associated with the frequent ejection of long and thin filopodia-like structures from these bulbous endings (**Figure 3.2, A-C**). Conditioned DRG neurons grew more than three times

faster than naïve DRG neurons (0.30 ± 0.06 µm/min for naïve vs. 0.90 ± 0.12 µm/min for PNL; $p < 0.001$), and reached maximum speeds of up to 1-2 µm/min (**Figure 3.2, D and E**). In addition, long filopodia-like structures exceeding 5 µm in length were extended more frequently and the average and maximum length of these actin-based structures was 2 to 3-fold higher in conditioned DRGs, respectively (**Figure 3.2, F and G** and **Figure 3.3, A**).

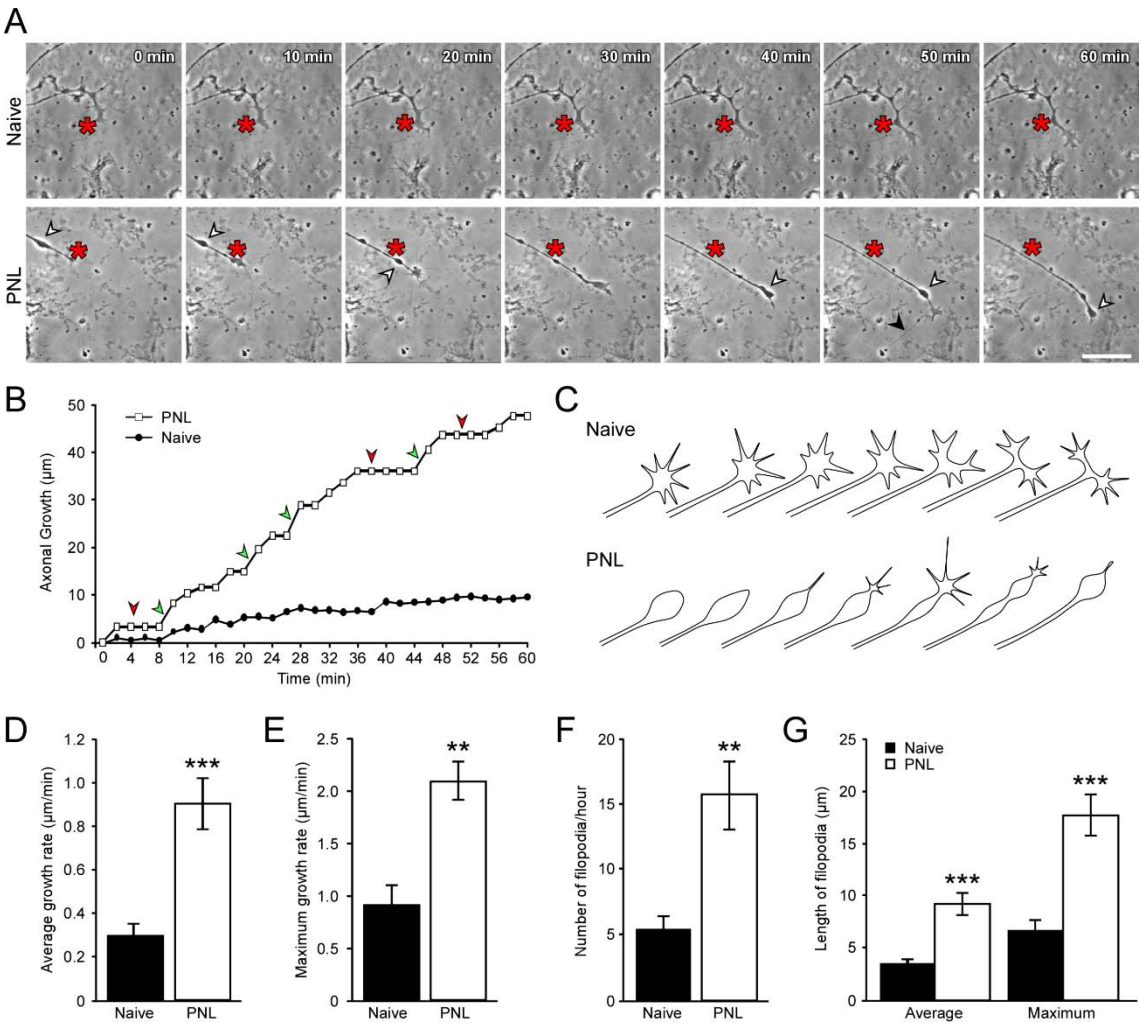

Figure 3.2. Growth cones of conditioned DRG neurons elongate faster. (A) Naïve and conditioned DRG neurons were cultured for 15-16 hours prior to live cell imaging. Phase images were recorded every minute for 1 hour. Conditioned DRG neurons typically feature bulbous growth cones (white arrowhead) and extend very long and thin filopodia-like structures (black arrowhead). Red asterisks represent stable landmarks across time-points (B) Time-course of the growth pattern of two individual cells. Conditioned DRG neurons feature a typical step-like growth curve with alternating phases of rapid growth (green arrowhead) and phases of growth arrest (red arrowhead). (C) Model of the average growth pattern. (D+E) Average and maximum growth rates are increased by more than 3-fold and 2-fold upon PNL, respectively. (F+G) The number and length of thin and long filopodia is augmented after PNL (*** $p < 0.001$; ** $p < 0.01$ by t-test, $n > 15$ neurons from three independent experiments, mean ± SEM, scalebar 20 µm).

3.2 PNL leads to rearrangements of the actin cytoskeleton

I hypothesized that the observed differences in growth behavior between naïve and conditioned primary sensory neurons must be reflected in changes at the level of the cytoskeleton. Subsequently, I assessed whether the actin and microtubule network is altered in DRG neurons upon PNL. For this purpose, naïve and conditioned DRG neurons were cultured for 16-18 hours and then fixed. Neurons were then treated with phalloidin conjugated to rhodamine to visualize actin. Phalloidin is a toxin derived from the death cap (*Amanita phalloides)* and binds specifically at the interface between F-actin subunits, locking adjacent subunits together. Thus, fluorescently labelled phalloidin can be used to visualize actin specifically. Subsequently, the morphologies of growth cones of naïve and conditioned DRG neurons were compared. Conditioned growth cones predominantly had a simple tapered shape. Characteristically, they featured a bulbous microtubule-based enlargement of the axon proximal to the axon tip. Often, thin and long (> 5 µm in length) actin-based structures protruded from these bulbous endings. In contrast, naïve growth cones were more complex and fan-like (25.4% ± 2.3% simple growth cones for naïve vs. 71.6% ± 1.2% for PNL; $p < 0.001$; **Figure 3.3, A and B**). In summary, I showed that rapid axonal growth after PNL is correlated with changes in growth cone morphology and actin structure.

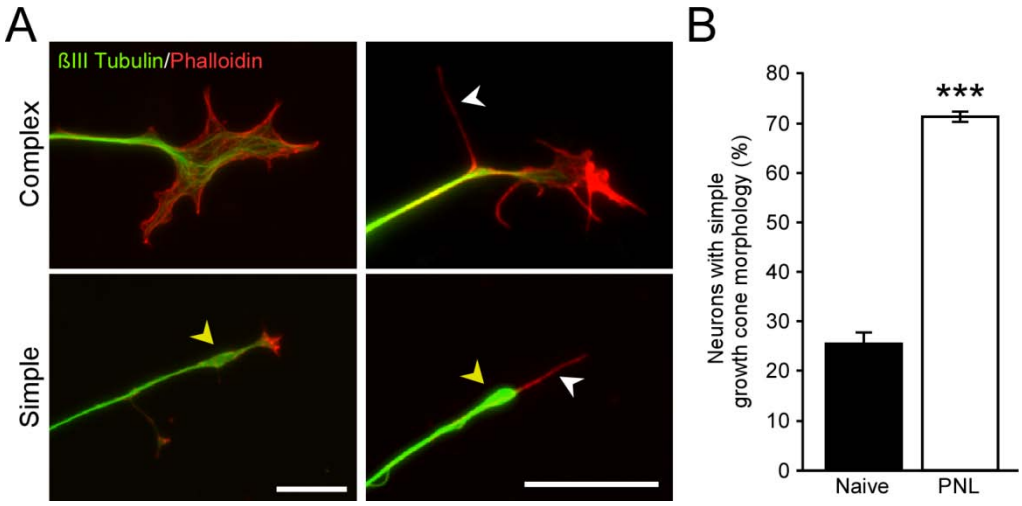

Figure 3.3. Growth cones of conditioned DRG neurons are morphologically less complex. (A) Naïve and conditioned DRG neurons were cultured for 16-18 hours prior to fixation and staining for F-Actin (phalloidin) and ßIII-tubulin (Tuj1). Axonal growth cones of conditioned DRG neurons predominantly have a simple, bulbous morphology (yellow arrowhead), frequently extending long and thin actin based filopodia-like structures (white arrowhead). (B) Quantification of the percentage of neurons with simple growth cone morphology PNL (*** $p < 0.001$ by t-test, $n > 90$ neurons from three independent experiments, mean ± SEM, scalebars 10 µm).

3.3 Actin depolymerization via cytochalasin D increases axon outgrowth

Whether simple growth cones are necessary for rapid axon outgrowth is not fully clear. In general, rapidly growing growth cones have the tendency to be small, while slow moving or paused growth cones are very large (Dent et al., 2003). Moreover, chicken sensory neurons can regenerate in the absence of F-actin in the growth cones (Marsh and Letourneau, 1984, Letourneau et al., 1987, Jones et al., 2006) and localized actin network instability induced by cytochalasin D treatment supports axon elongation in hippocampal neurons (Bradke and Dotti, 1999). My findings suggested that a reduced morphological growth cone and actin complexity is associated with rapid elongation typical for conditioned DRG neurons and that peripheral axotomy may enhance axon growth through destabilization of the peripheral actin network. Hence, I postulated that pharmacologically induced reduction of the actin cytoskeleton in naïve DRG neurons may lead to enhanced axonal growth.

To test my hypothesis, I cultured naïve DRG neurons under standard conditions. 2-4 hours after plating (once cells had settled and attached firmly to the substrate), I applied 3 nM of the actin depolymerizing drug cytochalasin D to the culture. Cytochalasins are well-known fungal metabolites that inhibit actin polymerization by capping the barbed end of actin filaments. In addition, they may also have other disruptive effects on actin filament networks (Flanagan and Lin, 1980, Goddette and Frieden, 1986, Cooper, 1987, Forscher and Smith, 1988). After 16-18 hours in culture, I fixed the DRG neurons and stained them for ßIII-tubulin (Tuj1). Subsequently, the axonal length and axonal branching frequency were quantified (**Figure 3.4, A-C**). As postulated, the average length of the axons increased from 274 µm ± 13 µm to 357 µm ± 20 µm ($p < 0.05$) upon cytochalasin D treatment. The branching frequency was not affected by the treatment. Even though moderate destabilization of actin via cytochalasin D was able to increase axonal outgrowth, the effect only partially mimicked the conditioning response. Nevertheless, I confirmed the assumption that rearrangement of the actin cytoskeleton enhances axon outgrowth and may therefore contribute to mediating the conditioning effect.

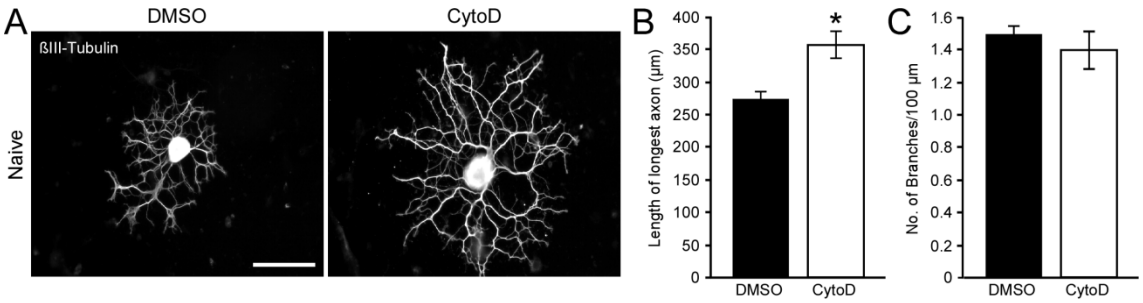

Figure 3.4. Actin depolymerization via cytochalasin D increases axon length. (A) Naïve DRG neurons were treated with DMSO (0.2%) or Cyto D (3 nM) 2-4 hours after plating and cultured for 16-18 hours prior to fixation and staining for ßIII-tubulin (Tuj1). Cyto D treated axons are longer than DMSO treated controls, while branching frequency is not affected. (B) Quantification of the axonal length and (C) number of axonal branches per 100 µm (* $p < 0.05$ by t-test, $n > 120$ neurons from 4-5 independent experiments, mean ± SEM, scalebar 200 µm).

3.4 Microtubules are more stable upon PNL

Increasing evidence suggests that not the actin cytoskeleton alone, but also microtubule dynamics play a considerable role in growth cone propagation and path finding. The interdependence between the actin and microtubule cytoskeleton was first observed in studies where acute inhibition of actin assembly resulted in rapid microtubule advance into the peripheral domain of growth cones (Forscher and Smith, 1988). Moreover, it was shown that the stabilization of microtubules alone can lead to axon formation and elongation (Witte et al., 2008). With these results in mind, it appeared plausible that the diverging growth behavior of naïve and conditioned neurons might also be attributed to differences in microtubule stability. The stability of microtubules is reflected by post-translational modifications of the tubulin subunits. Newly formed, dynamic microtubules are mainly composed of subunits containing tyrosinated α-tubulin. In more stable and persistent microtubules, on the other hand, α-tubulin gradually becomes detyrosinated and acetylated (Gomis-Ruth et al., 2008, Janke and Bulinski, 2011). Therefore, I compared the ratio of acetylated (stable) to tyrosinated (dynamic) microtubules in naïve and conditioned DRG neurons. DRG neurons were dissociated and cultured for 16-18 hours under standard conditions. While acetylated α–tubulin is restricted to microtubules, unpolymerized tyrosinated α–tubulin is also found in the cytoplasm. Hence, cells were extracted during fixation to remove unpolymerized tubulin subunits. Thereafter, neurons were stained for the two posttranslational modifications of α–tubulin and their distribution evaluated (**Figure 3.5, A-C**). Expectedly,

acetylation levels did not differ in the distal axon shaft and the axon tip between naïve and conditioned neurons, reflecting their dynamic state required for steering and elongation (Tanaka et al., 1995). However, the ratio between acetylated and tyrosinated α–tubulin was enhanced at the axon base (0.92 ± 0.09 in naïve vs. 1.66 ± 0.18 in conditioned DRGs; $p < 0.05$) and in the proximal axon shaft (0.70 ± 0.09 in naïve vs. 1.77 ± 0.12 in conditioned DRGs; $p < 0.01$) (**Figure 3.5, C**). In summary, I showed that peripheral nerve lesion leads to enhanced stability of microtubules in the proximal portion of DRG axons.

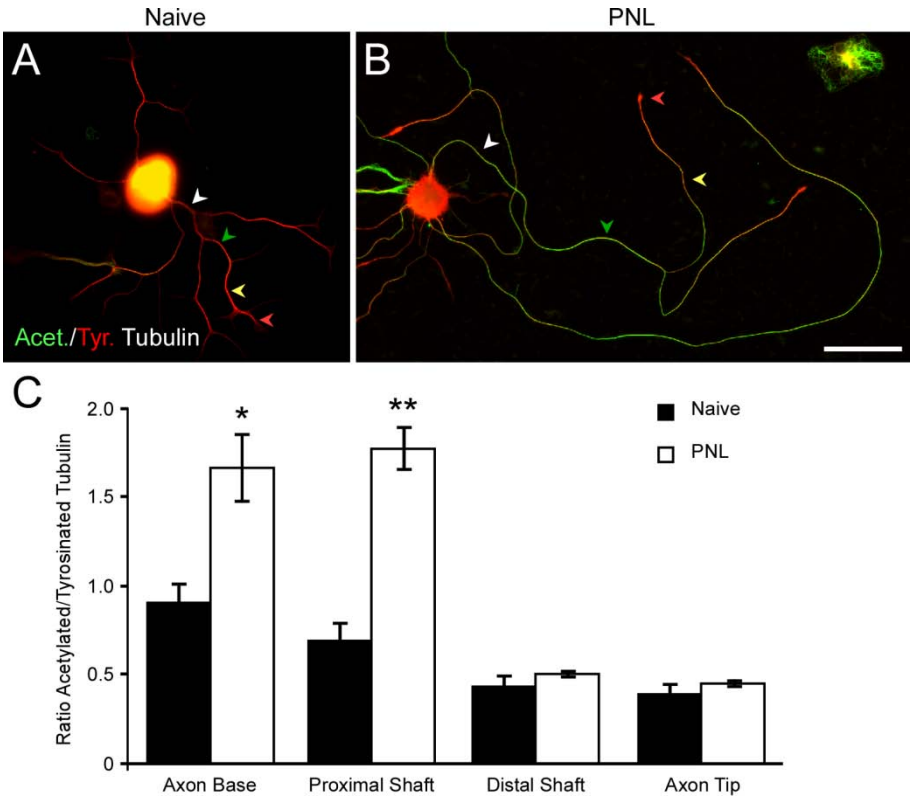

Figure 3.5. Differential distribution of acetylated and tyrosinated microtubules in naïve and conditioned DRG neurons. (A) Naïve and (B) conditioned DRG neurons stained for acetylated (green) and tyrosinated (red) α–tubulin. Neurons were permeabilized during fixation to remove unpolymerized tubulin subunits, therefore only α-tubulin incorporated in microtubules was assessed. In the axon base (white arrowhead) and the proximal axon shaft (green arrowhead), a high ratio of acetylated to tyrosinated α-tubulin was found in microtubules of conditioned DRG neurons in comparison to microtubules of naïve DRG neurons. (C) Ratio quantification of fluorescence intensities of acetylated and tyrosinated α-tubulin in microtubules of naïve and conditioned DRG neurons (** $p < 0.01$; * $p < 0.05$ by t-test, $n > 90$ neurons from three independent experiments, mean ± SEM, scalebar 50 µm).

3.5 Stabilization of microtubules leads to reduction in branching

Accordingly, I postulated that moderate stabilization of the microtubule cytoskeleton in naïve DRG neurons may be sufficient to enhance axonal growth. To test my hypothesis, I cultured naïve DRG neurons under standard conditions. After 2-4 hours in culture (once cells had settled and attached firmly to the substrate) I added 1 nM taxol to the culture. Taxol, originally identified as anti-cancer drug, is known to bind to free and polymerized β-tubulin subunits (Bollag et al., 1995, Giannakakou et al., 2000). Upon binding to free tubulin, taxol enables polymer assembly without the need for GTP (Diaz and Andreu, 1993). Taxol binding to polymerized tubulin, on the other hand, leads to the stabilization of lateral contacts between the individual subunits (Wade, 2009). Thereby, taxol shifts the dynamic equilibrium towards microtubule growth and protects the polymer against depolymerization. 14-16 hours after taxol treatment, I fixed naïve DRG neurons with 4% paraformaldehyde and stained them for ßIII-tubulin (**Figure 3.6, A-C**). As hypothesized, the length of the axons increased from 340 µm ± 5 µm to 411 µm ± 20 µm ($p < 0.05$) upon taxol treatment, an increase of 21%. However, the effect was smaller than anticipated. More remarkably, the number of branches along the axon decreased to almost half from 1.52 ± 0.06 to 0.91 ± 0.04 ($p < 0.001$). Hence, moderate microtubule stabilization via taxol was able to decrease axonal branching and thus to mimic one of two key aspects of the elongating growth typical for conditioned DRG neurons.

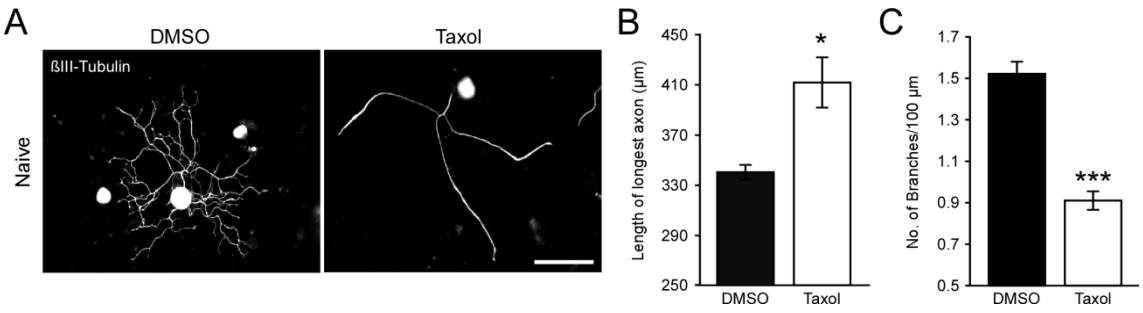

Figure 3.6. Microtubule stabilization via taxol increases axon length and decreases axon branching. (A) Naïve DRG neurons were treated with DMSO (0.2%) or taxol (1 nM) 2-4 hours after plating and cultured for 16-18 hours prior to fixation and staining for ßIII-tubulin (Tuj1). Taxol treated axons were only moderately longer than DMSO treated controls, but displayed considerably less branches. (B) Quantification of the axonal length and (C) number of axonal branches per 100 µm (*** $p < 0.001$; * $p < 0.05$ by t-test, $n > 90$ neurons from three independent experiments, mean ± SEM, scalebar 200 µm).

3.6 The fine structure of naïve and conditioned DRG growth cones

To supplement the immunocytochemical characterization of naïve and conditioned DRG neurons, I compared the fine structure of their growth cones using electron microscopy (EM). This approach allows the analysis of intracellular structures with an improved resolution and detail. To this end, naïve and conditioned DRG neurons were cultured for 16-18 hours prior to fixation with medium containing 2% glutaraldehyde. Cells were then processed for electron microscopy as described in the materials and methods section. The neuronal identity of the analyzed cells was confirmed by immunofluorescence and by their morphology. After acquisition of the electron micrographs, microtubules were pseudo-colored to facilitate quantification and the angle of deviation of the microtubules measured in relation to the direction of axonal growth. I chose to analyze three specific regions within the individual growth cones: the distal tip of the growth cone, the growth cone center and the axonal shaft (**Figure 3.7, A and 3.8, A**).

In both naïve and conditioned DRG neurons, microtubules were highly organized in the axonal shaft, as well as in the distal growth cone tip. In fact, microtubules were arranged in parallel arrays and did not deviate significantly from the direction of growth (**Figures 3.7, B and 3.8, B**). In contrast, microtubules in the growth cone center were disoriented as seen by the deviation angle which was significantly higher than in the axon shaft and growth cone tip. In general, naïve and conditioned DRG growth cones displayed similar features and did not differ significantly (**Figure 3.9**).

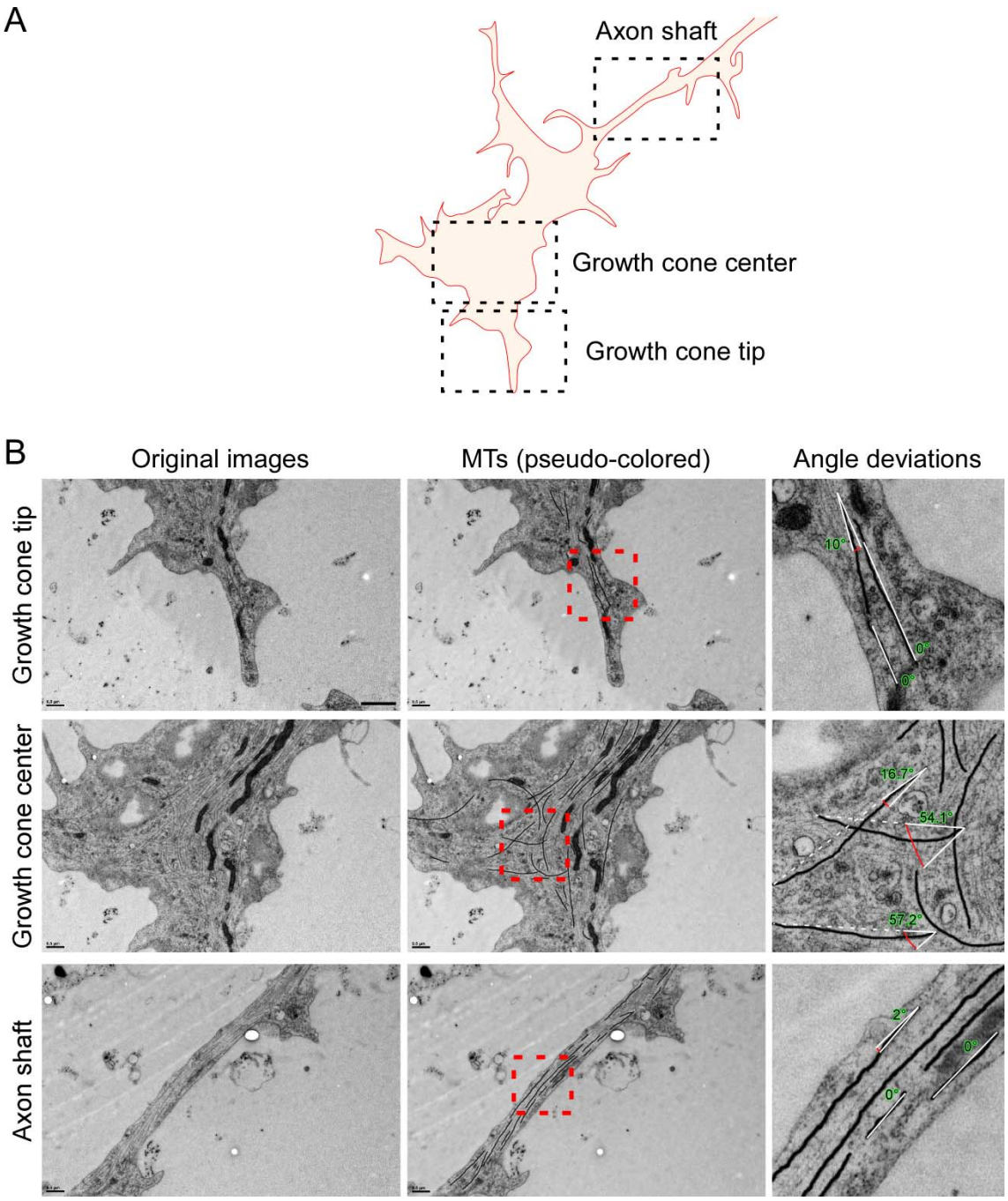

Figure 3.7. Ultrastructure of a naïve DRG growth cone. (A) Schematic drawing of the naïve DRG neuron depicted in (B). Three regions were analyzed: the distal growth cone tip, the growth cone center and the axon shaft. (B) Electron micrographs of the respective regions of a naïve DRG neuron. Cells were cultured for 16-18 hours, fixed with 2% glutaraldehyde and processed for electron microscopy. After acquisition of electron micrographs (left panel), the microtubules were pseudo-colored (middle panel) and the microtubule angles of deviation measured in respect to the direction of growth (right panel). Microtubules are oriented along the axis of growth in the distal axon tip and the axon shaft. The growth cone center contains disorganized microtubules; scalebar 1 µm.

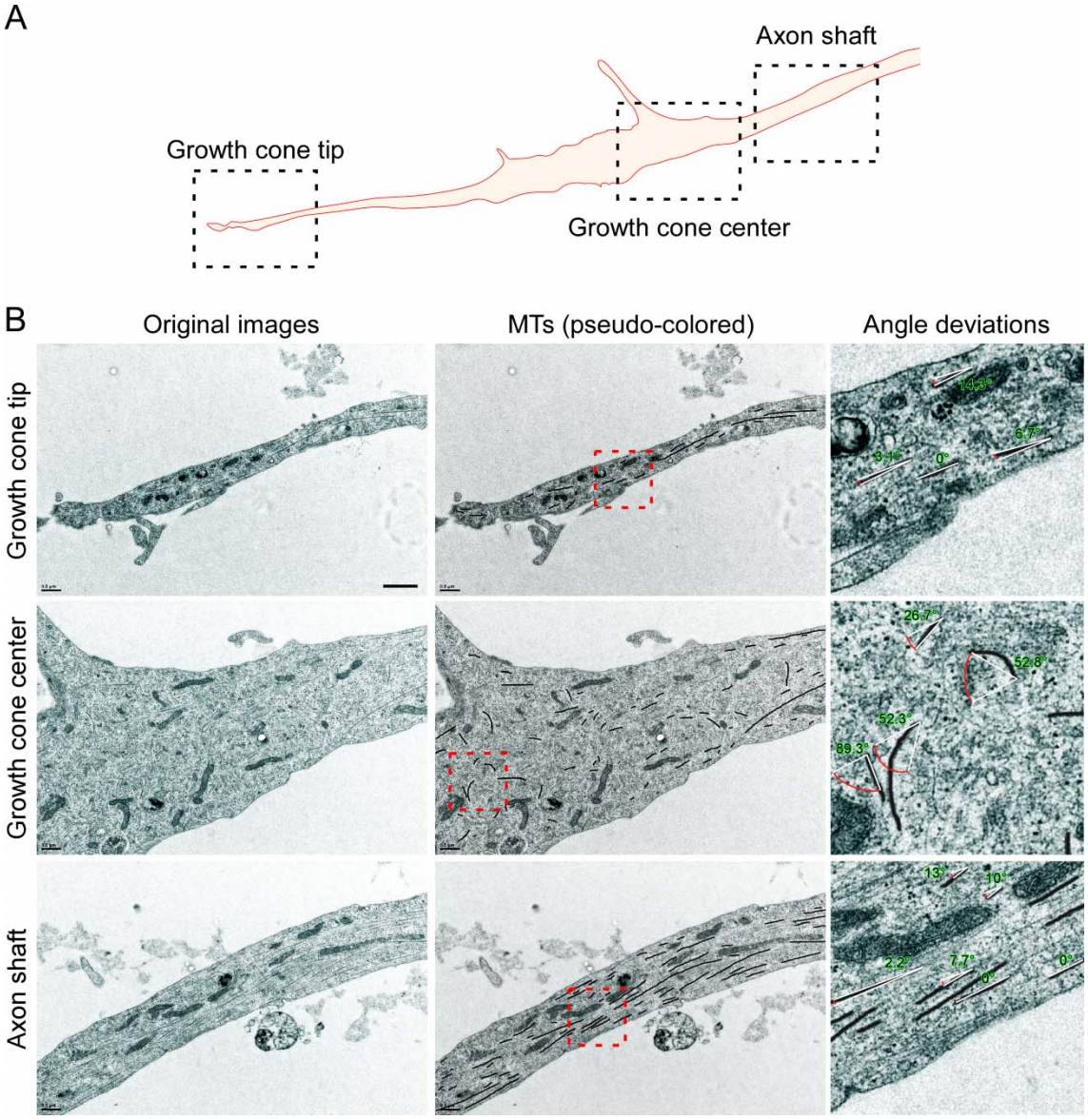

Figure 3.8. Ultrastructure of a conditioned DRG growth cone (A) Schematic drawing of the conditioned DRG neuron depicted in (B). Three regions were analyzed: the distal growth cone tip, the bulbous growth cone center and the axon shaft. (B) Electron micrographs of the respective regions of a conditioned DRG neuron. Cells were cultured for 16-18 hours, fixed with 2% glutaraldehyde and processed for electron microscopy. After acquisition of electron micrographs (left panel), the microtubules were pseudo-colored (middle panel) and the microtubule angles of deviation measured in respect to the direction of growth (right panel). Microtubules are oriented along the axis of growth in the distal axon tip and the axon shaft. The growth cone center contains disorganized microtubules; scalebar: 1 µm.

In fact, both groups showed similar angles of deviation within the axon shaft and growth cone tip (axon shaft: 5.03° ± 0.88° in naïve vs. 7.56° ± 0.69° in conditioned DRG neurons; growth cone tips: 12.98° ± 1.97° in naïve vs. 9.31° ± 1.14° in conditioned DRG neurons, $p > 0.05$). Solely the angles of deviation in the growth cone center were higher in neurons that had previously undergone a conditioning lesion (20.49° ± 2.04° in naïve vs. 25.75° ± 1.04° in conditioned DRG neurons, $p <$

0.05), suggesting that microtubules are highly disorganized in the bulbous endings typical for conditioned DRG neurons. Seeing that the overall structure of microtubules is not significantly modified upon PNL, in future, it will be interesting to test whether the dynamic behavior of microtubules might differ between naïve and conditioned DRG neurons.

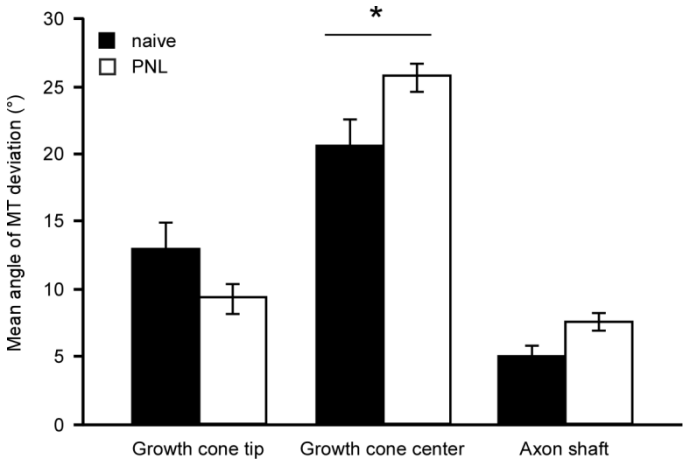

Figure 3.9. Microtubules are disoriented in the growth cone center of naïve and conditioned DRG neurons. Quantification of the mean angle of deviation of microtubules in respect to the direction of growth. Microtubules in the growth cone tip and in the axon shaft are highly ordered, while microtubules in the growth cone center are disoriented (* $p < 0.05$ by t-test, n = 129 microtubules counted from 4 cells (naïve) and 608 microtubules counted from 9 cells (conditioned); three independent experiments, mean ± SEM).

3.7 PNL leads to accumulation of mitochondria in bulbous growth cones

Neurons are dependent on high levels of energy, which is provided by cell organelles called mitochondria. Some axons have to span extremely long distance between the cell soma in the brain and their targets in the spinal cord or periphery of the body. In consequence, appropriate energy levels - often far from the neuronal cell bodies - need to be ensured and the precise regulation of mitochondrial transport and distribution of mitochondria along the axon is indispensable to maintain neuronal physiology. However, the knowledge about the precise role of mitochondria in spinal cord injury and regeneration is limited. To test whether naïve and conditioned DRG neurons show differences in their mitochondrial distribution, I prepared cultures of DRG neurons and stained the neurons with rhodamine 123. Rhodamine 123 is a cationic fluorescent dye that is mainly used to label respiring mitochondria (Chazotte, 2011). Comparison of naïve

and conditioned DRGs revealed that conditioned DRG growth cones are enriched in rhodamine 123, especially in the axonal bulbous endings (**Figure 3.10, A and B**). However, rhodamine 123 is not suited for quantitative analyses regarding mitochondrial content. Subsequently, I examined the electron micrographs that I prepared to measure the microtubule angles and counted the number of mitochondria in growth cones of naïve and conditioned DRG neurons in several consecutive sections. Analysis of the mitochondrial density showed that conditioned DRG neurons contain more than double the amount of mitochondria than naïve control neurons (**Figure 3.10, C-E**; 0.32 ± 0.08 in naïve vs. 0.69 ± 0.14 in conditioned DRG growth cones; $p < 0.05$). This is consistent with the idea that mitochondria are enriched in regions of high energy turnover and rapid growth (Morris and Hollenbeck, 1993).

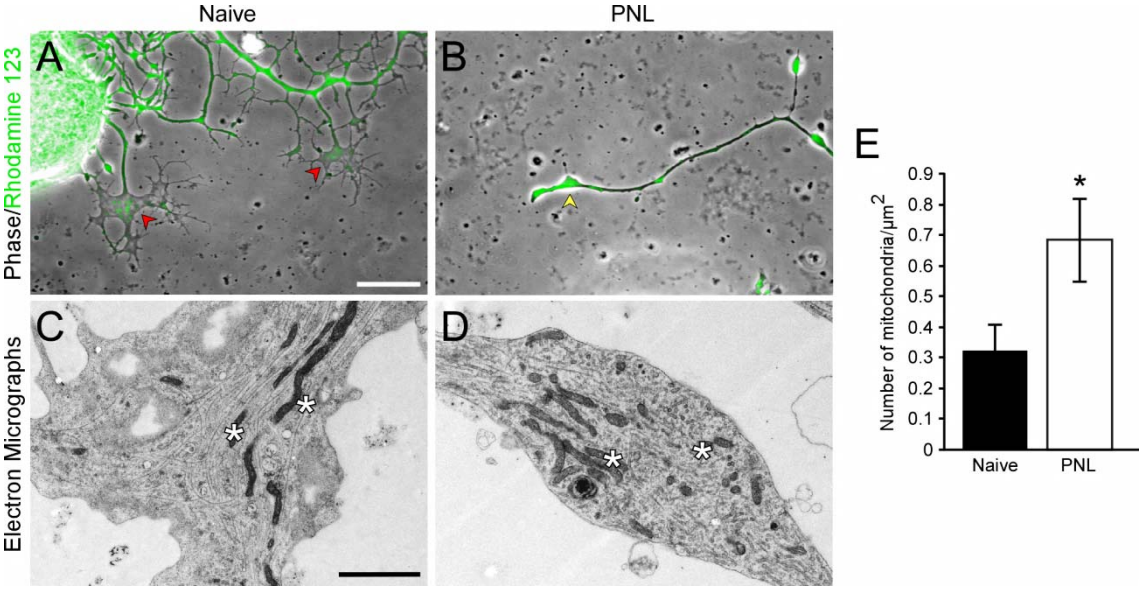

Figure 3.10. A conditioning lesion results in accumulation of mitochondria in the growth cones of DRG neurons. Naïve and conditioned DRG neurons were cultured for 16-18 hours, (A+B) stained with the mitochondrial marker rhodamine 123 and images acquired using our live imaging setup, or (C+D) prepared for electron microscopy as described in the materials and methods section. Growth cones of naïve DRG neurons contain sparse mitochondria (red arrowhead), while the bulbous axonal endings of conditioned DRGs are packed with mitochondria (yellow arrowhead). Asterisks depict mitochondria in the electron micrographs. (E) Quantification of the number of mitochondria per µm² (* $p < 0.05$ by t-test, n = 3 (naïve) and 9 (conditioned) neurons from three independent experiments, mean ± SEM, scalebars: 20 µm (A+B) and 2 µm (C+D)).

3.8 Growth cone and actin dynamics are enhanced following PNL

Seeing that there were few apparent differences in the microtubule composition and structure of naïve and conditioned DRG growth cones, I decided to focus on the actin cytoskeleton. Previous results had shown that the growth cone and actin is restructured following a peripheral nerve lesion. To pinpoint potential differences I first performed short-interval time lapse microscopy. I captured phase images of naïve and conditioned DRG growth cones every 2 seconds over a period of 2 minutes. Subsequently, the relative changes in growth cone area were measured frame per frame. The analysis of the data revealed that conditioned growth cones, in contrast to naïve controls, rapidly changed their morphology and extended long actin based filopodia (**Figure 3.11, A and B**). In fact, relative changes in growth cone area increased by more than double upon peripheral nerve lesion (0.60 ± 0.05 in naïve DRGs vs. 1.38 ± 0.08 upon PNL; $p < 0.001$), clearly showing that conditioned DRG neurons are more dynamic (**Figure 3.11, B**). This is in line with the finding that growth cones that oscillate strongly and rapidly, tend to make forward progress faster (Goodhill et al., 2015).

To analyze the underlying actin dynamics, I electroporated naïve and conditioned DRG neurons with plasmid DNA expressing Lifeact fused to green fluorescent protein (GFP), a versatile marker to image actin dynamics with minimal photobleaching and phototoxicity (Riedl et al., 2008) and performed fluorescent time lapse microscopy 15-16 hours after plating the neurons. Fluorescence images were acquired every 2 seconds for 5 minutes using a specialized live-cell imaging set-up described in the materials and methods section. Linescans around the perimeter of growth cones of naïve and conditioned neurons were used to measure different aspects of actin dynamics: retrograde flow, protrusion frequency and protrusion distance. Kymograph analyses revealed that retrograde flow was augmented from 3.03 ± 0.19 µm/min in naïve to 4.41 ± 0.15 µm/min in conditioned growth cones (**Figure 3.11, C-E**). In addition, actin-based protrusions doubled in frequency (0.41 ± 0.03 #/min for naïve vs. 0.78 ± 0.04 #/min for PNL; $p < 0.001$; **Figure 3.11, F**) and extended a greater distance (1.51 ± 0.14 µm for naïve vs. 2.56 ± 0.15 µm for PNL; $p < 0.001$; **Figure 3.11, G**) after peripheral nerve lesion.

In summary, my results show that rapid axonal growth following a conditioning lesion is correlated with an increase in growth cone and actin dynamics.

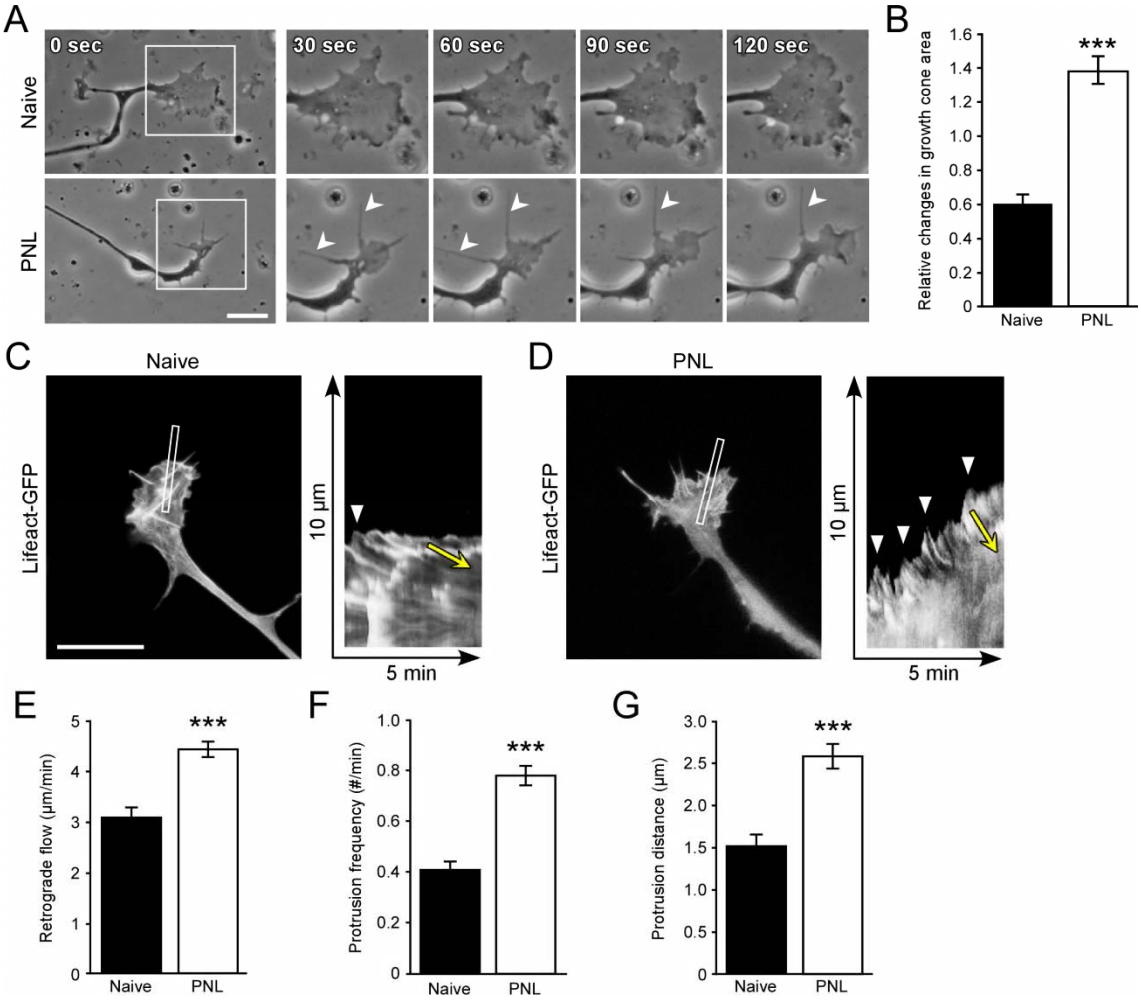

Figure 3.11. Growth cone and actin dynamics are enhanced following peripheral nerve lesion. (A) Naïve and conditioned DRG neurons were cultured for 15-16 hours prior to live-cell imaging. Appropriate cells were chosen and phase images recorded every 2 seconds for a period of 2 minutes. Growth cones of naïve DRG neurons are static and do not change their morphology as frequently as conditioned DRG neurons, which often extend long filopodia (white arrowheads). (B) Quantification of the relative changes in growth cone area. Conditioned DRG growth cones are more dynamic and change their morphology more frequently than naïve control neurons. Single frames from live-cell imaging series of a naïve (C) and a conditioned DRG neuron (D) expressing Lifeact-GFP. Frames were captured every 2 seconds for a period of 5 minutes. The lines indicate sites where line scans were taken. The kymographs show actin retrograde flow from the indicated line scans. Yellow arrows indicate actin translocation. White arrowheads indicate sites of actin protrusions. Quantification of actin retrograde flow (E), protrusion frequency (F) and protrusion distance (G) in naïve and conditioned DRG neurons. (*** $p < 0.001$ by t-test, $n > 30$ neurons from three independent experiments, mean ± SEM, scalebars 10 µm).

3.9 High actin turnover is essential for rapid axonal growth

In a next step I wanted to determine whether high actin turnover is necessary for rapid axonal extension. Therefore, I treated naïve and conditioned adult rat DRG neurons with the F-actin stabilizing drug jasplakinolide 2-4 hours after plating and fixed them after 16-18 hours in culture. Subsequently, I performed morphometric analyses of axon length and branching frequency. Jasplakinolide, originally isolated from marine sponges, is an actin filament polymerizing and stabilizing drug (Holzinger, 2009). I postulated that jasplakinolide mediated actin stabilization should inhibit the conditioning growth response, if actin dynamics are indeed a prerequisite for the robust axon outgrowth after PNL.

In fact, nanomolar doses of jasplakinolide were sufficient to suppress axon extension and increase branching frequency in conditioned DRG neurons, an effect which was concentration dependent (**Figure 3.12, A-C)**. Axonal length was decreased from 891 µm ± 48 µm (DMSO) to 839 µm ± 72 µm (1nM Jasp), 620 µm ± 15 µm (5 nM Jasp), 404 µm ± 14 µm (10 nM Jasp) and finally to 105 µm ± 9 µm (20 nM Jasp). At 10 nM, conditioned DRG neurons assembled morphologies reminiscent of naïve neurons. The branching frequency was inversely correlated to the axon length (**Figure 3.12, A-C**). In contrast, naïve neurons were not affected significantly from the treatment with jasplakinolide (**Figure 3.12, A-C**). 5 nM and 10 nM jasplakinolide had neither an effect on average axon length (891 µm ± 48 µm [DMSO]; 620 µm ± 15 µm [5 nM Jasp]; 404 µm ± 14 µm [10 nM Jasp]) nor axon branching frequency (1.25 ± 0.18 [DMSO]; 1.35 ± 0.26 [5 nM Jasp]; 1.29 ± 0.18 [10 nM Jasp]). The average axonal length only dropped to 183 µm ± 23 µm at the highest concentration of 20 nM jasplakinolide. The branching frequency, however, was still unaffected (0.34 ± 0.11). Jasplakinolide treatment further resulted in a less mobile actin network of conditioned DRG neurons (**Figure 3.12, D-G**) as assessed by live-cell imaging. Actin retrograde flow dropped to an average rate of 2.33 ± 0.42 µm/min ($p < 0.01$ compared to PNL + DMSO; (**Figure 3.12, E**) and there was a comparable reduction in both protrusion frequency (**Figure 3.12, F**) and protrusion distance (**Figure 3.12, G**) in jasplakinolide treated conditioned DRG neurons. Thus, I provide strong evidence for the hypothesis that high actin turnover is necessary for rapid axonal growth following PNL.

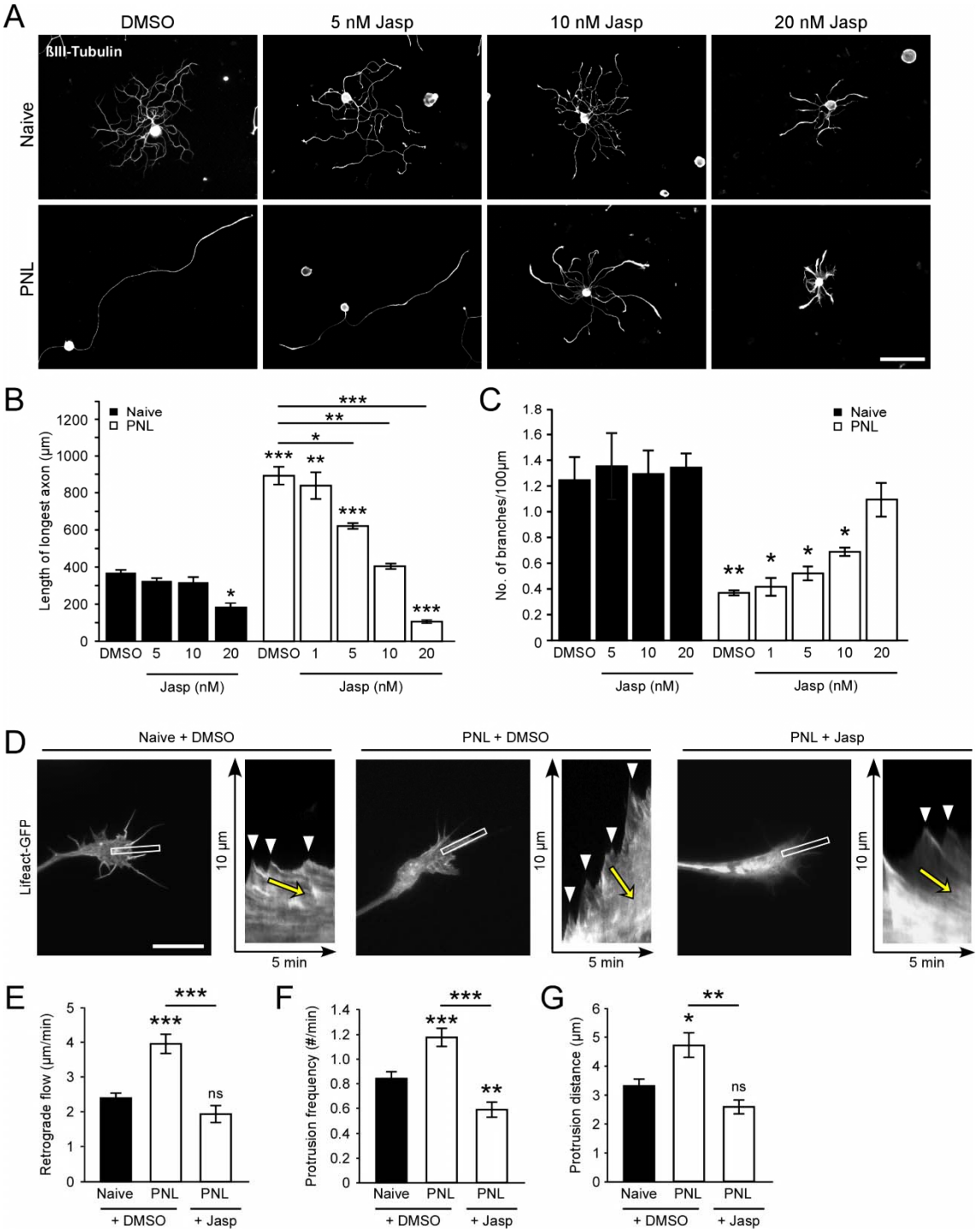

Figure 3.12. Actin dynamics are essential for rapid axonal growth. (A) Naïve and conditioned DRG neurons were treated with the actin-polymerizing drug jasplakinolide (Jasp) and cultured for 15-16 hours prior to fixation and staining for ßIII-tubulin. (B) Quantification of the length of the longest axon and (C) the branching frequency. (D) Single frames from live-cell imaging series of a naïve and a conditioned DRG neuron expressing Lifeact-GFP and treated with 0.2% DMSO or 5 nM jasplakinolide. Frames were captured every 2 seconds for a period of 5 minutes. The lines indicate sites where line scans were taken. The kymographs show actin retrograde flow from the indicated line scans. Yellow arrows indicate actin translocation. White arrowheads indicate sites of actin protrusions. Quantification of actin retrograde flow (E), protrusion frequency (F) and protrusion distance (G) in DMSO and jasplakinolide treated naïve and conditioned DRG neurons. (* $p < 0.05$; ** $p < 0.01$; *** $p < 0.001$ by t-test, $n > 90$ (A and B) and $n > 30$ (C-G) neurons from three independent experiments, mean ± SEM, scalebars: (A) 200 µm (D) 10 µm).

3.10 Cofilin activity is enhanced upon PNL

As AC proteins are critical regulators of axon growth, we asked whether the activity of cofilin and its upstream regulators is modulated after a conditioning lesion (**Figure 3.13, A**). To this end we dissected L4 and L5 DRGs from adult rats that had undergone a sham or PNL lesion 7 days previously. Subsequently, DRGs were processed for western blotting. Analysis of the biochemical extracts revealed that protein levels of neither total ADF, nor cofilin 1 or cofilin 2 were altered between PNL and naïve conditions (**Figure 3.13, B**). However, protein levels of phosphorylated (inactive) cofilin - were decreased by more than 5-fold in PNL samples compared to naïve controls (**Figure 3.13, B**). Thus, the overall activity of cofilin was increased, as measured by the ratio of phosphorylated to total cofilin levels (**Figure 3.13, D**). Consistently, the levels of the phosphorylated form of the cofilin phosphatase slingshot homolog (SSH) 1 were also decreased. Hence, the ratio of phosphorylated to total SSH1 levels was also decreased in the PNL condition, suggesting that SSH1 is more active after PNL (**Figure 3.13, C and E**).

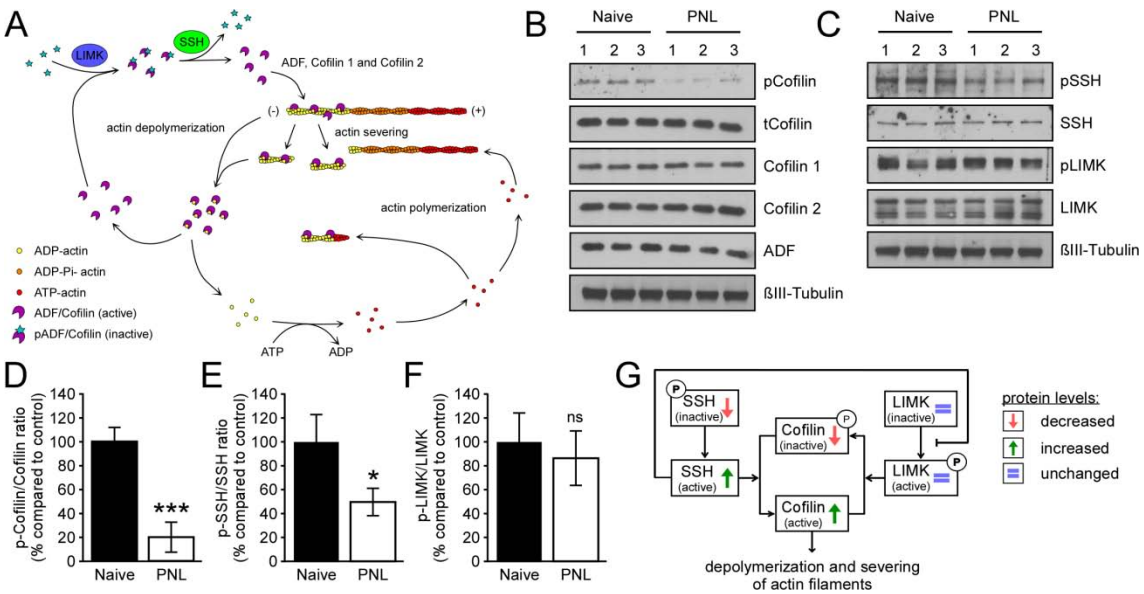

Figure 3.13. Cofilin and SSH1 activity is increased following PNL. (A) Schematic representation of the signaling pathway involving ADF/cofilin (AC) and its upstream regulators slingshot homolog (SSH) 1 and LIM kinase (LIMK) 1. AC is dephosphorylated (activated) by dephosphorylated (active) SSH1. AC then binds to ADP-actin, resulting in disassembly of the actin filament via depolymerization and severing. Subsequently, AC is dissociated from the ADP-actin subunits and deactivated by LIMK1 through phosphorylation. ADP-actin is recycled to ATP-actin and available for further polymerization. (B+C) Western blot of naïve and conditioned DRG extracts. (D-F) Quantification of the ratio of phosphorylated to total protein levels for cofilin, SSH1 and LIMK1, respectively. (G) Diagram illustrating the reversible regulation of cofilin via phosphorylation through SSH1 and LIMK1 ($p < 0.001$ by t-test, mean ± SEM; n >3 for each condition).

In contrast, the activity of LIM kinase (LIMK) 1 - a second major upstream regulator of cofilin - was unchanged (**Figure 3.13, C and F**). Thus, I provide first evidence that AC proteins and their upstream regulator SSH1 are activated upon peripheral nerve lesion (**Figure 3.13, G**). These findings gave rise to the idea that AC proteins might also be required for the regenerative growth upon conditioning.

3.11 Knockout of ADF and cofilin 1 leads to reduction in actin turnover, axon length and regeneration

To assess the physiological role of AC proteins for the conditioning response, I wanted to test whether double knockout of ADF and cofilin 1 (from now on referred to as "AC1 KO") would have a detrimental effect on axon outgrowth following PNL. To this end, I made use of the ADF$^{-/-}$Cofilin1$^{flox/flox}$ mouse line with genomic ablation of ADF and expressing floxed cofilin 1 alleles (Bellenchi et al., 2007, Flynn et al., 2012). However, crossing these mice with the established brain-specific Nestin-Cre driver line to obtain the AC1 double knockout was not feasible since these AC1 KO mice die postnatally. Hence, I chose to use an adeno-associated-viral (AAV) vector based approach. I aimed to obtain a targeted, conditional ablation of AC proteins in adult DRG neurons by injecting ADF$^{-/-}$ Cofilin1$^{flox/flox}$ mice with AAV-Cre or AAV-CreGFP into the sciatic nerve or directly into the L4/5 DRG. To date, inducible knockout approaches using Cre recombinase and acute virus-based gene delivery have been successfully used to modulate gene expression in specific neuronal subsets (Rothermel et al., 2013). However, I first had to test the efficacy of our viral vectors in specifically infecting adult L4/5 DRG neurons. To this end, I injected an AAV expressing enhanced GFP (AAV-eGFP) into the sciatic nerves of wild-type C57BL/6J animals. 2 weeks post-injection I perfused the animals and dissected the L4/5 DRGs, the sciatic nerves and the spinal cords. Quantification of the eGFP expressing neurons and axons in the dorsal column and sciatic nerve showed that the transduction rate was as high as 70-80% in all tissues analyzed, confirming that the viral approach chosen was appropriate for our purpose (**Figure 3.14, A and B**). Upon direct injection of AAV-eGFP into the L4/L5 DRGs, transduction efficiency could even be maximized, reaching levels up to 90% eGFP expressing DRG neurons.

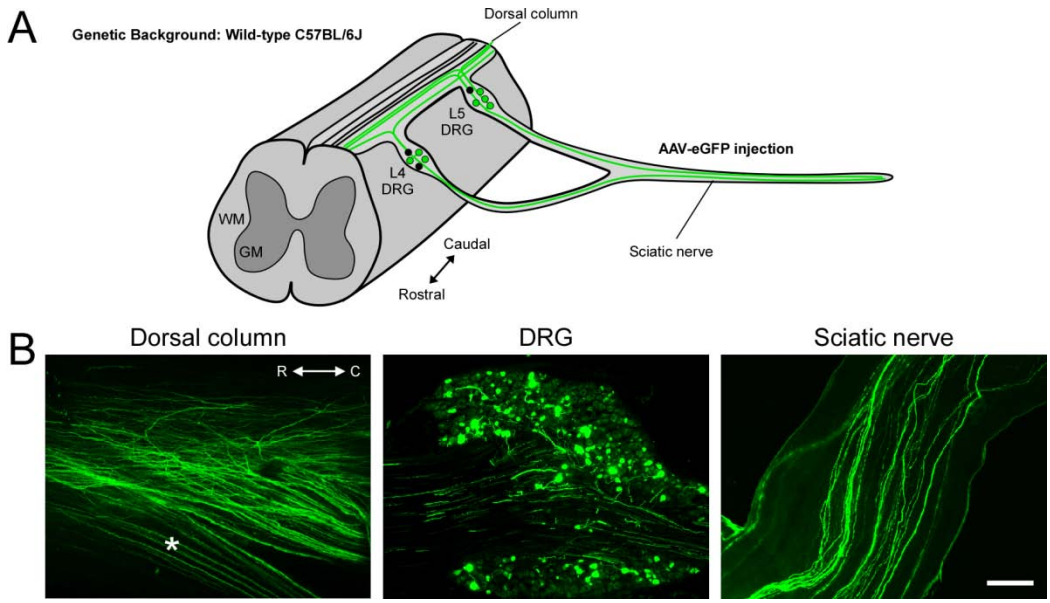

Figure 3.14. Tracing of dorsal column and sciatic nerve axons using an adeno-associated-viral (AAV) approach. (A) Schematic illustration of the experimental setup. (B) Representative fluorescent images of dorsal column, DRG and sciatic nerve sections from wild-type mice that were transduced by injecting AAV-eGFP into the sciatic nerve (R: rostral; C: caudal, GM: grey matter, WM: white matter; white asterisk depicts dorsal root entry zone (DREZ); scalebar 200µm)

In a second pilot experiment, I injected AAVs expressing enhanced GFP (AAV-eGFP) and Cre recombinase (AAV-Cre) mixed 1:1 into the sciatic nerves of adult Gt(ROSA)26Sor$^{tm9(CAG\text{-}tdTomato)Hze}$/J mice, a Cre reporter line expressing the fluorescent protein tdTomato upon Cre recombination (**Figure 3.15, A**). 2 weeks post-injection, animals were transcardially perfused, the DRGs dissected, cut and mounted onto slides. Quantitative analysis revealed that the transduction rate was remarkable, with approximately 46% of all transduced neurons being eGFP-positive and 54% being tdTomato-positive (**Figure 3.15, B and C**). Conveniently, 68% of all eGFP-positive neurons were also tdTomato-positive; thus inferring that almost 70% of all eGFP positive axons will also be AC1 KO neurons in our system.

Finally, adult ADF$^{-/-}$Cofilin1$^{flox/flox}$ mice were injected with an AAV-eGFP or AAV-CreGFP into the sciatic nerve. Two weeks after AAV injection, the animals were subjected to PNL. One week later, conditioned L4/5 DRGs were dissected, dissociated and plated. Immunocytochemistry and biochemical extracts showed a substantial reduction in total cofilin levels upon Cre mediated recombination, suggesting that our knockout approach is effective. However, much to our surprise, there were still some residual levels of cofilin left in the AC1 knockout neurons (**Figure 3.15, D-F**).

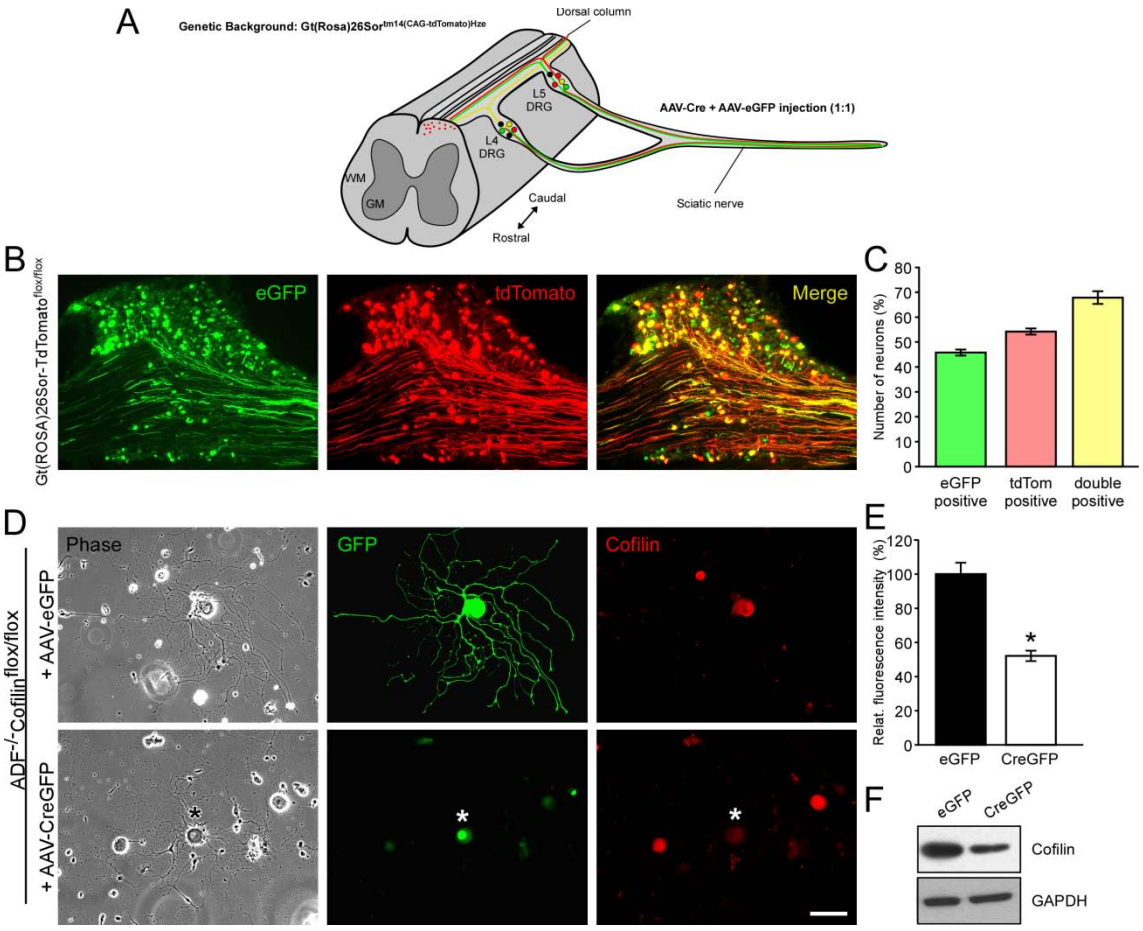

Figure 3.15. Targeted and conditional ablation of AC proteins in adult DRG neurons using an adeno-associated-virus (AAV) based approach. (A) Schematic illustration of the experimental setup. (B) Representative fluorescent images of DRG sections from Gt(ROSA)26Sor$^{tm9(CAG-tdTomato)Hze}$/J mice that were transduced by injecting a mixture of AAV-eGFP and AAV-Cre (1:1) into the sciatic nerve. (C) Quantification of the percentage of transduced neurons. (D) Phase and fluorescent images of AAV-eGFP and AAV-CreGFP transduced ADF$^{-/-}$Cofilin1$^{flox/flox}$ DRG neurons 16-18 hours after plating. Neurons were stained using an antibody specific for total cofilin. Asterisk depicts CreGFP-positive neuron with lower levels of cofilin (AC1 KO). (E) Quantification of the relative fluorescence intensities of cofilin in dissociated ADF$^{-/-}$Cofilin1$^{flox/flox}$ DRG neurons injected with either AAV-eGFP or AAV-CreGFP. (F) Western blot of ADF$^{-/-}$Cofilin1$^{flox/flox}$ DRGs injected with either AAV-eGFP or AAV-CreGFP ($p < 0.05$ by t-test, $n = 4$ (A+B) and $n > 35$ (C+D); mean ± SEM; scalebar 200µm).

Accordingly, actin dynamics were only moderately decreased in adult conditioned AC1 KO DRG neurons (**Figure 3.16, A - D**). Kymograph analyses showed that the average retrograde flow rate was reduced from 2.81 ± 0.04 µm/min in conditioned wild-type (WT) DRG neurons to 2.08 ± 0.10 µm/min in conditioned AC1 KO DRGs ($p < 0.01$; **Figure 3.16, B**). Similarly, protrusion frequency and protrusion distance were only mildly reduced (**Figure 3.16, C and D**). Effects of the AC1 KO on axon growth were also less profound than expected (**Figure 3.16, E-H**). While axons of conditioned control DRG neurons grew 707 µm ± 11 µm, conditioned AC1 KO

neurons on average still grew 445 µm ± 8 µm ($p < 0.001$; **Figure 3.16, E and F**). The branching frequency on the other hand was almost doubled and increased from 0.62 ± 0.05 in WT to 1.01 ± 0.06 in AC1 KO DRG neurons ($p < 0.001$; **Figure 3.16, G**) The percentage of neurons extending axons was unaltered after AC1 ablation (58.5 % ± 3.9 % for WT+ PNL vs. 61.6 % ± 1.6 % AC1 KO + PNL; **Figure 3.16, H**).

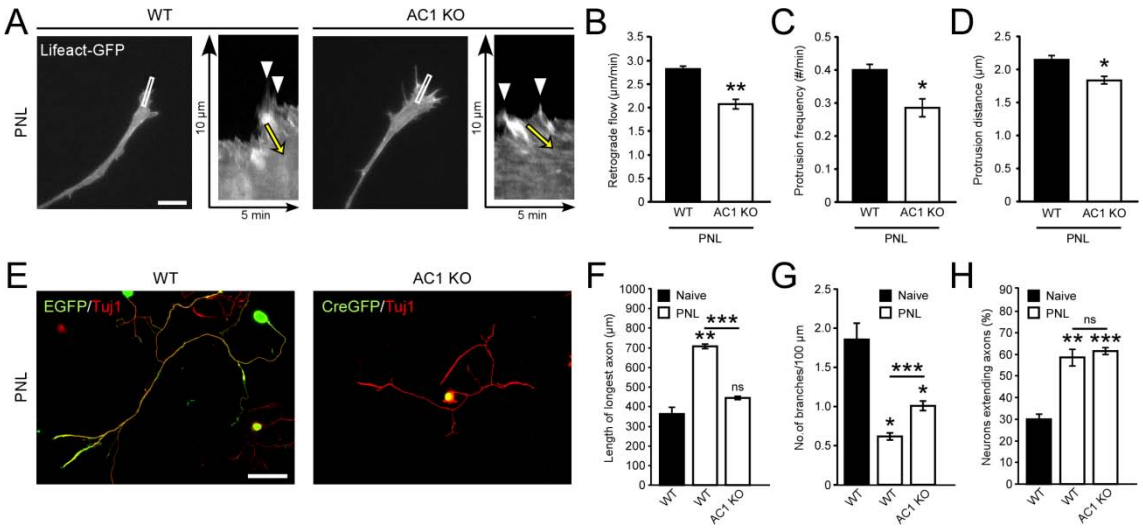

Figure 3.16. Actin dynamics and axon length are moderately decreased in conditioned AC1 KO DRG neurons. (A) Single frames from live-cell imaging series of conditioned DRG neurons from wild-type (WT) or ADF/cofilin1 double knockout (AC1 KO) DRG neurons expressing Lifeact-GFP. Frames were captured every 2 seconds for a period of 5 minutes. The lines indicate sites where line scans were taken. The kymographs show actin retrograde flow from the indicated line scans. Yellow arrows indicate actin translocation. White arrowheads indicate sites of actin protrusions. Quantification of actin retrograde flow (B), protrusion frequency (C) and protrusion distance (D). (E) Representative fluorescence images of conditioned adult dissociated DRG neurons from WT and AC1 KO mice transduced with AAV-eGFP or AAV-CreGFP and stained for ßIII-tubulin (Tuj1). (F) Quantification of the length of the longest axon, (G) the branching frequency and (H) the percentage of neurons extending axons (* $p < 0.05$; ** $p < 0.01$; *** $p < 0.001$ by t-test, $n > 30$ (A-D) and $n > 90$ (E-H) neurons from three independent experiments, mean ± SEM, scalebars: (A) 10 µm (E) 200 µm).

The just described moderate effect of the AC1 KO in cell culture was also reflected *in vivo* as conditioned AC1 knockout neurons regenerated their axons similarly well to the conditioned wild-type controls (**Figure 3.17, A-C**). To visualize double knockout axons in the spinal cord, ADF$^{-/-}$Cofilin1$^{flox/flox}$ animals were crossed with the Gt(ROSA)26Sor$^{tm9(CAG-tdTomato)Hze}$/J Cre reporter strain. Adult ADF$^{-/-}$ Cofilin1$^{flox/flox}$tdTomato$^{flox/flox}$ mice were injected with AAV-Cre into the sciatic nerve unilaterally (**Figure 3.17, A**). 2 weeks after AAV injection, the animals were subjected to a sham or conditioning lesion of the same sciatic nerve followed by

an ipsilateral spinal cord injury (SCI) of the central DRG axons, also known as dorsal column (DC), at thoracic level (T) 12 one week later. In wild-type (WT) and AC1 KO mice AAV-transduction efficiency was comparable (**Figure 3.17, C**). Cofilin levels were significantly decreased in the tdTomato positive AC1 KO neurons (**Figure 3.17, C**), suggesting that the knockout approach is effective.

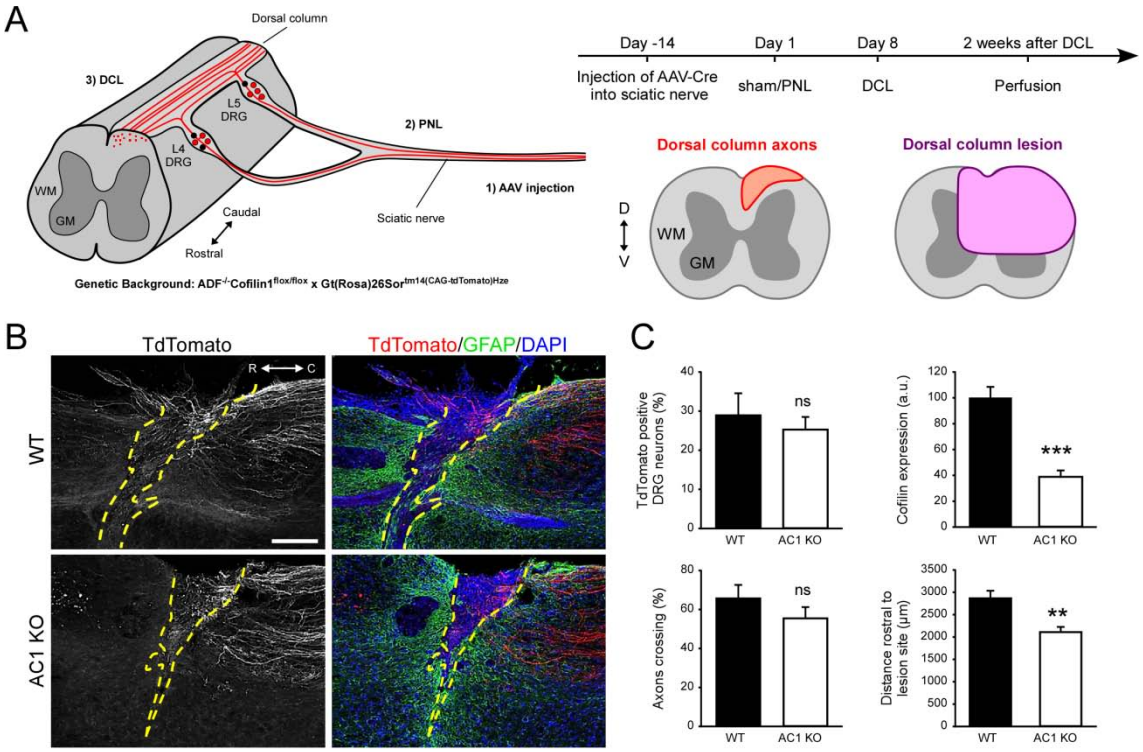

Figure 3.17. Axon regeneration in AC1 KO mice. (A) Left panel: Schematic representation of the experimental procedure. WT (ADF^{WT}Cofilin1^{WT}tdTomato$^{flox/flox}$) and AC1 KO (ADF$^{-/-}$Cofilin1$^{flox/flox}$ tdTomato$^{flox/flox}$) mice were injected with AAV-Cre into the sciatic nerve. Then, a peripheral nerve lesion (PNL) followed by a dorsal column lesion (DCL) was performed. Upon Cre-mediated recombination, neurons expressed tdTomato. Right panel: Timeline and schematic drawing of longitudinal ascending dorsal column axons and the spinal cord injury model used to completely transect them (D: dorsal, V: ventral, WM: white matter, GM: grey matter). (B) Sagittal sections of the injured spinal cord expressing tdTomato and stained for GFAP. DAPI stained nuclei. The yellow dashed line indicates the lesion border. (C) Quantification of AAV transduction efficiency, cofilin expression levels and axon regeneration across the lesion site in WT and AC1 KO mice (*** $p < 0.001$, ** $p < 0.01$ by t-test; mean ± SEM; scalebar 200 µm, n = 5). (D) Western blot showing ADF, cofilin 1 and cofilin 2 expression levels in L4/5 DRGs of WT and AC1 KO mice. GAPDH is shown as loading control (n=3 independent replicates per condition).

Nonetheless, both conditioned WT control and AC1 KO DRG axons grew into and beyond the lesion site upon dorsal column lesion (DCL) (**Figure 3.17, B and C**). Merely the distance that axons grew rostral to the lesion site was moderately reduced in AC1 KO animals (2857.1 µm ± 178.1 µm in WT + PNL vs. 2101.8 µm ± 123.8 µm in AC1 KO + PNL; $p < 0.01$). Collectively, both the *in vitro* and the *in vivo* loss of function data suggest that, besides ADF and cofilin 1, other molecular players seem to be involved in regulating actin dynamics, axon growth and regeneration upon conditioning.

3.12 Loss of ADF and cofilin 1 is compensated by cofilin 2 expression

We wondered whether cofilin 2, the third member of the AC protein family, might compensate for the loss of ADF and cofilin 1 in AC1 KO neurons. This possibility could theoretically account for the residual cofilin levels found after AC1 ablation (**Figure 3.15, C-E**) and explain why the effect of the double knockout is not as severe as expected. To test this hypothesis, we injected AAV-eGFP or AAV-CreGFP directly into the L4/5 dorsal root ganglia of WT and ADF$^{-/-}$Cofilin1$^{flox/flox}$ mice, respectively. Two weeks post-injection L4/5 DRGs were dissected and processed for western blotting. Protein levels of ADF, cofilin 1 and cofilin 2 were compared by using custom-made antibodies specific for each protein (**Figure 3.18, A**). As anticipated, protein levels of ADF could not be detected, and cofilin 1 was substantially reduced in the AC1 KO DRGs. Indeed, cofilin 2 levels were elevated considerably. This result fostered the idea that the three AC family members can functionally compensate for each other. To provide further evidence for this hypothesis, we tested the effect of each possible single and double knockout on axon growth and morphology (**Figure 3.18, B-D**). The following mouse lines were used for the experiment: ADF$^{-/-}$ (ADF KO), Cofilin1$^{flox/flox}$ (C1 KO), ADF$^{-/-}$ Cofilin1$^{flox/flox}$ (AC1 KO), ADF$^{-/-}$ Cofilin2$^{flox/flox}$ (AC2 KO) and Cofilin1$^{flox/flox}$Cofilin2$^{flox/flox}$ (C1C2 KO) (Cofilin2$^{flox/flox}$ (C2 KO) were not yet available at the time of my thesis submission). The appropriate adult mice were injected with AAV-CreGFP into the sciatic nerve. 2 weeks post-injection, a peripheral nerve lesion was performed, followed by dissection of the DRGs 1 week after PNL. 15-16 hours after plating, the neurons were fixed and stained for ßIII-tubulin.

Subsequently, axon length, branching frequency and percentage of neurons extending axons were quantified. The single knockouts for ADF and cofilin 1 had no adverse effect on axon growth of conditioned DRG neurons (**Figure 3.18, C and D**). However, simultaneous depletion of any combination of two AC proteins - ADF and cofilin 1 (AC1 KO), ADF and cofilin 2 (AC2 KO) or cofilin 1 and cofilin 2 (C1C2 KO) - all had a similar effect.

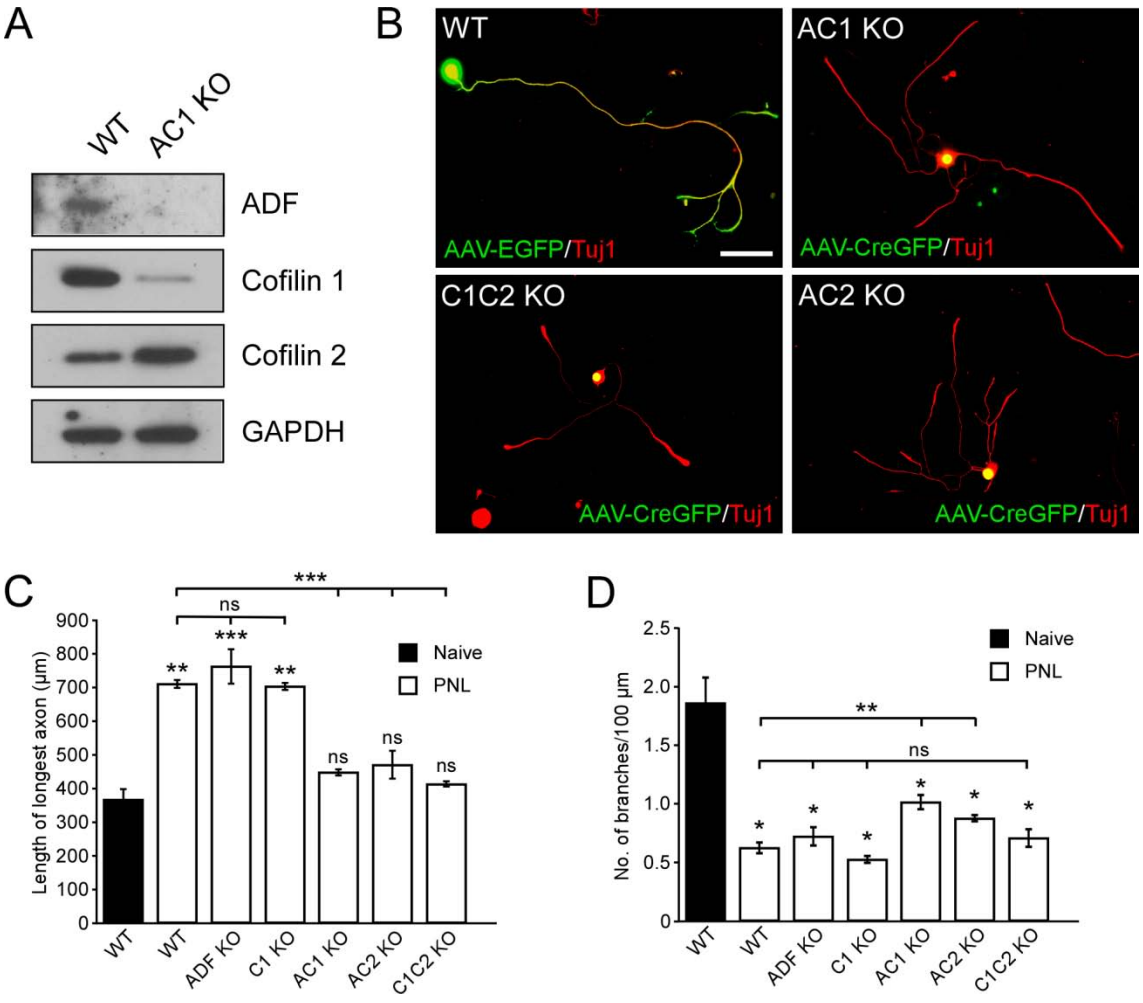

Figure 3.18. Genetic ablation of ADF and cofilin 1 leads to upregulation of cofilin 2 and functional compensation. (A) Western blot showing ADF, cofilin 1 and cofilin 2 expression levels in L4/5 DRGs of wild-type (WT) and AC1 KO mice that were previously injected with AAV-eGFP or AAV-CreGFP, respectively. GAPDH is shown as loading control (n=3 independent replicates per condition). (B) Representative fluorescence images of conditioned adult dissociated DRG neurons transduced with AAV-eGFP or AAV-CreGFP and stained for ßIII-tubulin (Tuj1). The following mouse lines were used: WT ($ADF^{WT}Cofilin1^{WT}Cofilin2^{WT}$), AC1 KO ($ADF^{-/-}Cofilin1^{fl/fl}$), AC2 KO ($ADF^{-/-}Cofilin2^{fl/fl}$) and C1C2 KO ($Cofilin1^{fl/fl}Cofilin2^{fl/fl}$). Neurons were fixed 15-16 hours after plating. (C) Quantification of the average length of the longest axon and (D) branching frequency (* $p < 0.05$; ** $p < 0.01$; *** $p < 0.001$ by t-test, $n > 90$ individual cells from three independent experiments, mean ± SEM, scalebar 200 µm)

All three combinations resulted in a reduction of axon length by approximately 50% and an increase in branching by more than 3-fold to levels reminiscent of naïve DRG neurons (**Figure 3.18, B-D**). However, none of the three double knockouts had an effect on the percentage of neurons extending axons. These findings proved that, in contrast to embryonic neurons, AC protein family members can compensate for each other to some extent in adult DRG neurons.

3.13 Knockout of ADF, cofilin 1 and cofilin 2 results in a complete loss of the conditioning effect

Remarkably, the effect of none of the three double knockouts was remotely comparable to the severe effect of the AC1 double KO observed during development in hippocampal and cortical neurons (Flynn et al., 2012). In each case, this was presumably due to the compensation by the third non-ablated family member. Hence, to ablate all ADF/cofilin activity in adult DRG neurons I tested the effects on the conditioning response upon depletion of all three AC family members: ADF, cofilin 1 and cofilin 2 (from now on referred to as "AC1C2 KO"). Wild-type control and triple transgenic ADF$^{-/-}$Cofilin1$^{flox/flox}$Cofilin2$^{flox/flox}$ (Bellenchi et al., 2007, Gurniak et al., 2014) mice were injected with AAV-eGFP or AAV-CreGFP into the sciatic nerve, respectively. 2 weeks later, animals were subjected to PNL and L4/5 DRGs were dissected, dissociated and electroporated with Lifeact-GFP one week following PNL. 15-16 hours after plating, fluorescence live-cell imaging was performed and different aspects of actin dynamics were measured as described in previous sections.

As opposed to conditioned wild-type controls, growth cones of AC1C2 triple knockout neurons had an immobile actin network (**Figure 3.19, A and B**). Kymograph analyses showed that control neurons had an average retrograde flow rate of 2.97 ± 0.13 µm/min, while AC1C2 KO neurons only had an average rate of 0.88 ± 0.16 µm/min, a more than 3-fold reduction ($p < 0.001$, **Figure 3.19, A, B and D**). A similar reduction in protrusion frequency was observed in AC1C2 KO compared to conditioned wild-type neurons (**Figure 3.19, E and F**), dropping from 0.81 ± 0.06 protrusions/min in WT controls to 0.19 ± 0.06 protrusions/min in AC1C2 KO DRG neurons ($p < 0.001$). However, protrusion distance was not altered

significantly upon depletion of AC proteins ($p > 0.05$). To test whether reintroduction of cofilin could restore actin dynamics in AC1C2 KO neurons, I injected ADF$^{-/-}$Cofilin1$^{flox/flox}$Cofilin2$^{flox/flox}$ animals with a mixture of AAV-CreGFP and AAV-CofWT-RFP, an AAV vector expressing human wild-type cofilin 1 conjugated to red fluorescent protein (RFP). In fact, reintroduction of wild-type cofilin 1 was able to rescue all aspects of actin dynamics to wild-type control levels (**Figure 3.19, C-F**).

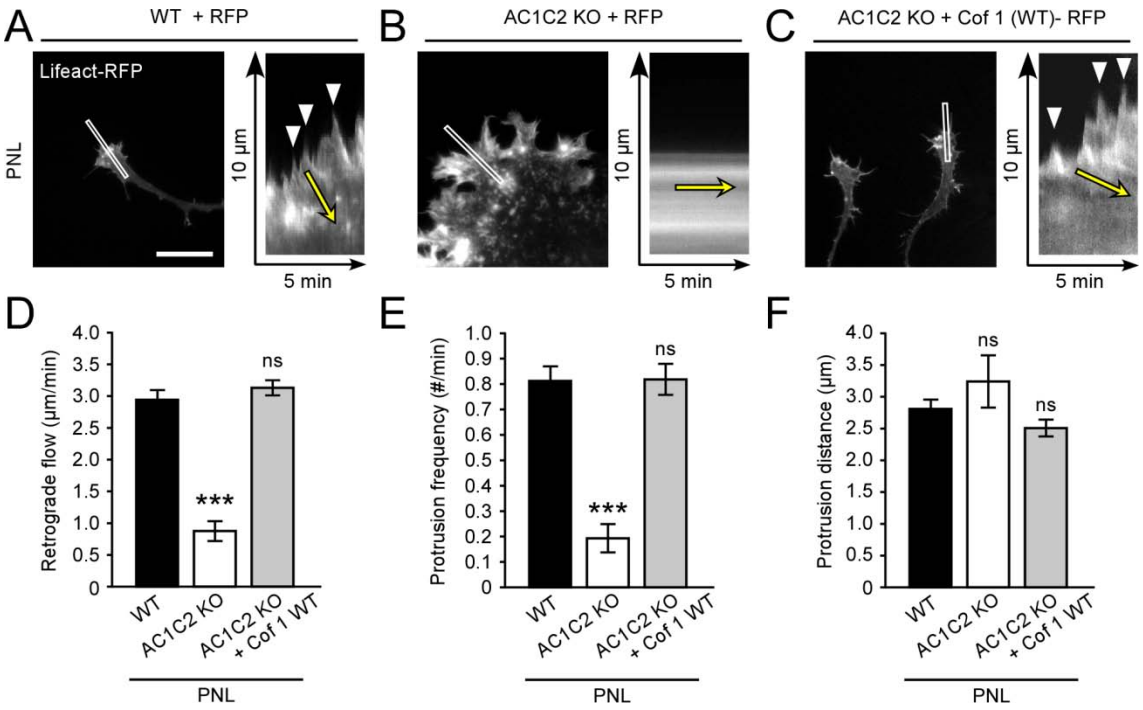

Figure 3.19. The actin network is immobile in conditioned AC1C2 KO DRG neurons. (A) Single frames from live-cell imaging series of conditioned DRG neurons from wild-type (WT) or AC1C2 triple knockout DRG neurons expressing Lifeact-GFP, CreGFP and RFP or CofWT-RFP, respectively. Frames were captured every 2 seconds for a period of 5 minutes. The lines indicate sites where line scans were taken. The kymographs show actin retrograde flow from the indicated line scans. Yellow arrows indicate actin translocation. White arrowheads indicate sites of actin protrusions. Quantification of (B) actin retrograde flow, (C) protrusion frequency and (D) protrusion distance (* $p < 0.05$; ** $p < 0.01$; *** $p < 0.001$ by t-test, $n > 30$ neurons from three independent experiments, mean ± SEM, scalebar 10 µm).

Concomitantly, far less conditioned AC1C2 KO neurons extended axons (58.5% ± 3.8% in wild-type control vs. 15.6% ± 2.1% in AC1C2 KO; $p < 0.01$; **Figure 3.20, A - D**), which additionally were short and highly branched as opposed to typical WT conditioned axons. Wild-type conditioned DRGs extended axons of 707 ± 11 µm length, whereas axons of AC1C2 KO neurons were only 145 ± 22 µm long ($p <$

0.001; **Figure 3.20, A and B**). Conversely, the branching frequency was increased from 0.62 ± 0.05 in WT controls to 3.0 ± 0.4 branchpoints/100 µm in AC1C2 KO neurons ($p < 0.01$; **Figure 3.20, C**). The effects on axon growth in AC1C2 KO neurons were fully rescued by reintroduction of wild-type cofilin 1 (**Figure 3.20, A - D**). Together, these data provide unambiguous evidence that AC proteins are necessary for actin turnover and axon growth after conditioning.

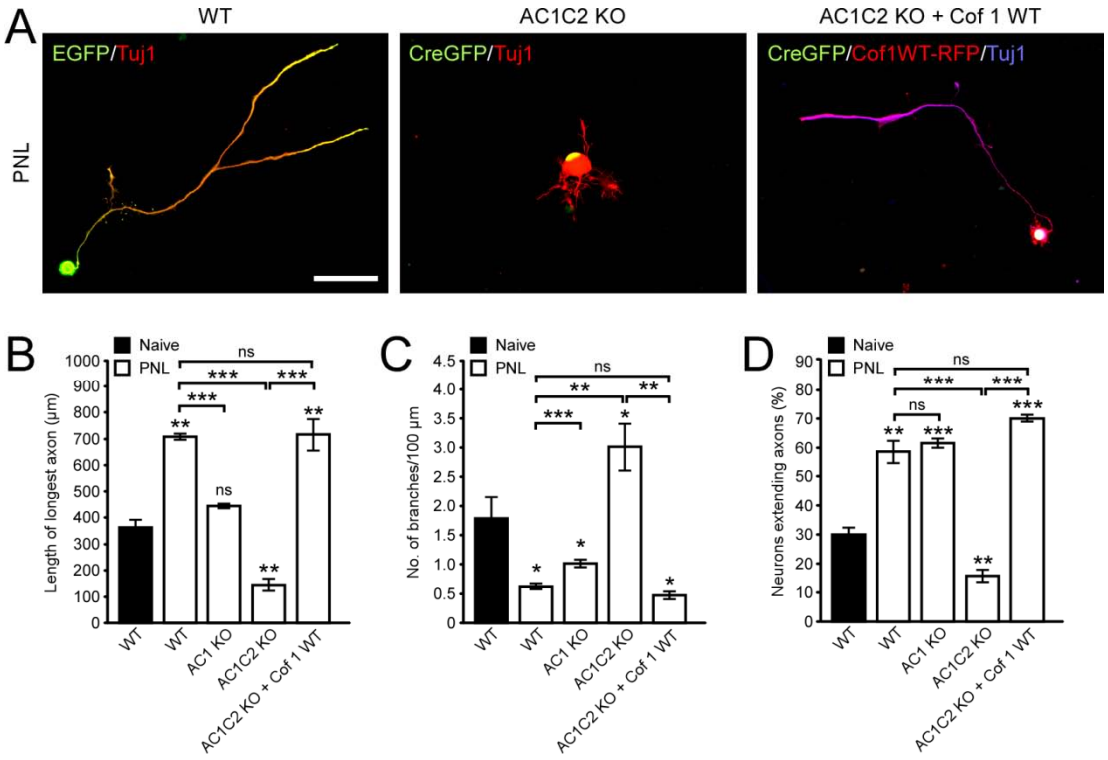

Figure 3.20. The conditioning effect is lost in AC1C2 KO DRG neurons in vitro. (A) Representative fluorescence images of conditioned adult dissociated DRG neurons from wild-type (WT) and AC1C2 KO mice transduced with AAV-eGFP or AAV-CreGFP and AAV-CofWT-RFP, and stained for ßIII-tubulin (Tuj1). (B) Quantification of the length of the longest axon, (C) the branching frequency and (D) the percentage of neurons extending axons (* $p < 0.05$; ** $p < 0.01$; *** $p < 0.001$; ns: not significant by t-test, $n > 90$ neurons from three independent experiments, mean ± SEM, scalebar 200 µm).

3.14 ADF/cofilin proteins are necessary for axon regeneration *in vivo*

To determine whether AC proteins are also vital for the growth response following a conditioning lesion *in vivo*, I tested two different regeneration paradigms. First, I wanted to test whether AC proteins play a role in peripheral nerve regeneration (**Figure 3.21, A**). Therefore, L5 DRGs of adult WT control and AC1C2 animals were injected with AAV-Cre. In addition, I injected AAV-eGFP into the same DRG to visualize the axons in the sciatic nerve. One week later, the sciatic nerves were crushed ipsilaterally. Three days after crush-injury, the animals were perfused and the sciatic nerves dissected.

As previously described (Shin et al., 2012), control axons robustly regenerated three days after injury. In contrast, peripheral AC1C2 KO axons failed to regenerate over long distances (**Figure 3.21, B and C**; 4.29 mm ± 0.16 mm for WT vs. 0.84 mm ± 0.16 mm for AC1C2 KO).

Secondly, I tested whether axon regeneration is also impaired in the central nervous system of AC1C2 KO animals (**Figure 3.21, D-F**). To this end, I injected AAV-Cre into the sciatic nerves of WT control and AC1C2 animals unilaterally. To visualize dorsal column (DC) axons in the spinal cord, we co-injected AAV-eGFP into the sciatic nerve to transduce L4-6 DRGs. 2 weeks after injection a sham or peripheral nerve lesion was performed, followed by a complete unilateral transection of the dorsal column at thoracic level (T) 12 one week later. Using two-photon imaging of the unsectioned adult spinal cord, we observed that regeneration of DC axons across the lesion is strongly impaired in AC1C2 KO animals compared to WT controls 4 weeks after spinal cord injury ($p < 0.01$; **Figure 3.21, E and F**). On average, axons of conditioned WT mice regenerated 2-3 folds more into and rostral to the lesion site in comparison to axons of conditioned AC1C2 animals. In fact, the level of AC1C2 axon regeneration was reminiscent to sham lesioned WT controls ($p > 0.05$). Collectively, these data support the hypothesis that AC proteins are strictly necessary for axon regeneration both in the peripheral as well as in the central nervous system following a conditioning lesion.

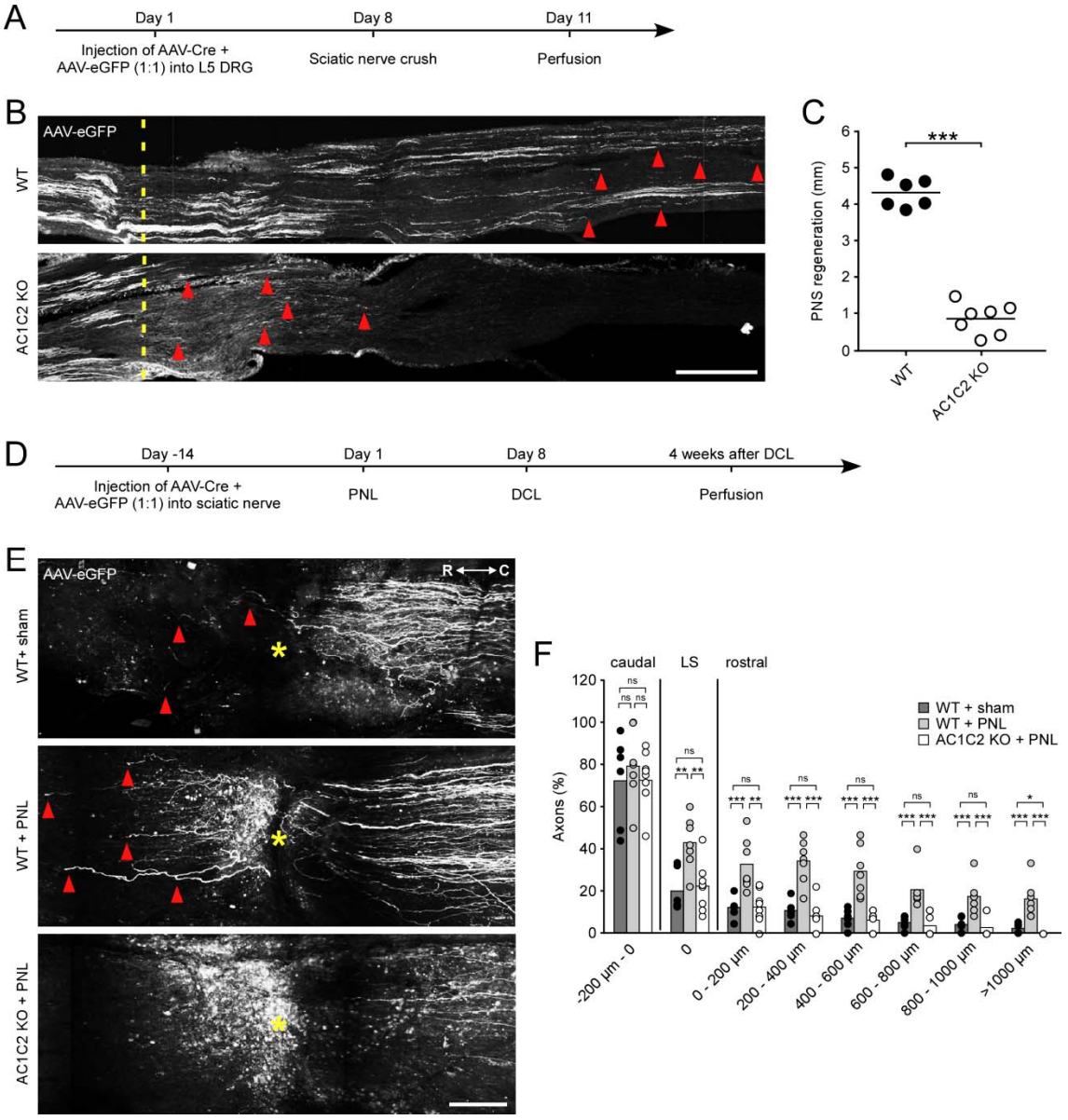

Figure 3.21. Peripheral nerve and spinal cord regeneration are impaired in AC1C2 KO mice. (A) Timeline of the experiment to assess peripheral nerve regeneration. (B) Longitudinal sections of sciatic nerves 3 days after crush injury. Seven days before injury, L5 DRGs were injected with AAV-GFP and AAV-Cre (1:1). Red arrowheads indicate regenerating axons. Yellow dashed lines indicate the injury site. (C) Quantification of (B). (***p < 0.001; scatter plot with mean; WT n=6 and AC1C2 KO n=7 animals; 12-28 axons/animal; scalebar 1 mm). (D) Timeline of the experiment to assess spinal cord regeneration. (E) Multiphoton scan of the unsectioned adult spinal cord 4 weeks after SCI. DC axons were labeled by injecting AAV-eGFP into the left sciatic nerve. Red arrowheads indicate regenerating axons. Yellow asterisks indicate the lesion site (LS). (R: rostral, C: caudal). (F) Quantification of regenerating axons (*p < 0.05, ** p < 0.01 and ***p < 0.001 using permutation test; scatter plot with mean; WT + sham n=6, WT + PNL n= 7 and AC1C2 + PNL n=9 animals; scalebar 200 µm).

3.15 The severing activity of AC proteins regulates actin turnover and axon extension

It is known that AC proteins enhance actin dynamics in two major ways: by depolymerization, i.e. disassembly of G-actin monomers at the pointed end, and by severing F-actin filaments into shorter protomers, thus generating free actin filament ends that are accessible for F-actin polymerization and depolymerization (Hawkins et al., 1993, Hayden et al., 1993, Carlier et al., 1997, Du and Frieden, 1998, Andrianantoandro and Pollard, 2006, Michelot et al., 2007, Bernstein and Bamburg, 2010). It was shown that when Tyr82 is mutated to Phe (Y82F), cofilin loses its depolymerizing activity. Conversely, when Ser94 is mutated to Asp (S94D), cofilin loses its severing activity but retains its depolymerizing activity (**Figure 3.22**) (Moriyama and Yahara, 1999, 2002). To address the question which of these two activities is pivotal for increasing actin turnover and thus axon growth after a peripheral nerve lesion, we tested the efficiency of these two activity mutants of cofilin in rescuing the profound AC1C2 triple knockout phenotype. To this end, we injected a mixture of AAV-CreGFP and either AAV-RFP, AAV-CofS94D-RFP or AAV-CofY82F-RFP into the sciatic nerves of AC1C2 animals. Approximately 10-14 days later, animals were subjected to a peripheral nerve lesion. DRGs were dissected, dissociated and electroporated with a plasmid encoding Lifeact-GFP.

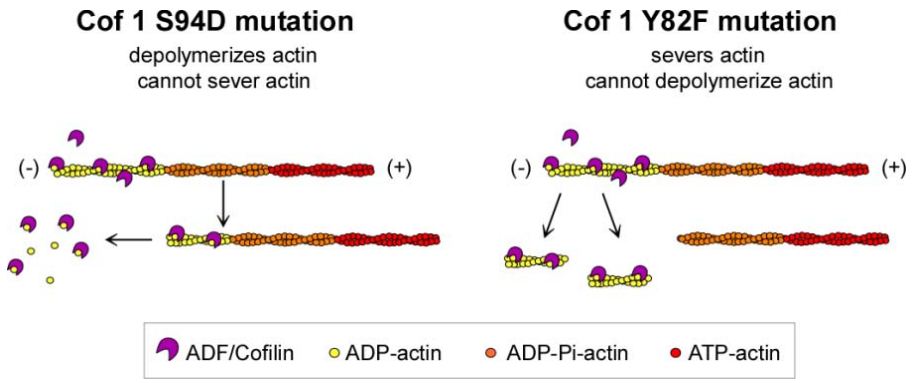

Figure 3.22. S94D and Y82F, two activity mutants of cofilin. Cofilin with a tyrosine-82 to phenylalanine (Y82F) mutation retains the ability to sever F-actin filaments but depolymerizes filaments into G-actin monomers only to a small degree (Moriyama and Yahara, 1999). Cofilin with a serine-94 to aspartate (S94D) mutation retains the ability to depolymerize filaments into G-actin monomers but severs only weakly (Moriyama and Yahara, 2002).

15-16 hours after plating, fluorescent live-cell imaging was performed and actin dynamics were analyzed as previously described. Expression of the CofS94D mutant, which can depolymerize but cannot sever actin filaments, showed only little restoration of actin dynamics in conditioned AC1C2 KO neurons (**Figure 3.23, A-D**). By contrast, the expression of the CofY82F mutant, which can only sever but cannot depolymerize actin filaments, fully restored actin retrograde flow to levels reminiscent of conditioned wild-type neurons (**Figure 3.23, A and B**) and partially rescued protrusion dynamics (**Figure 3.23, C and D**). Retrograde flow was not changed between AC1C2 KO controls (0.71 ± 0.21 µm/min) and CofS94D-expressing AC1C2 KO neurons (1.04 ± 0.10 µm/min; $p > 0.05$), but considerably increased in CofY82F-expressing AC1C2 KO neurons (2.84 ± 0.17 µm/min), a 4-fold increase ($p < 0.001$; **Figure 3.23, A and B**).

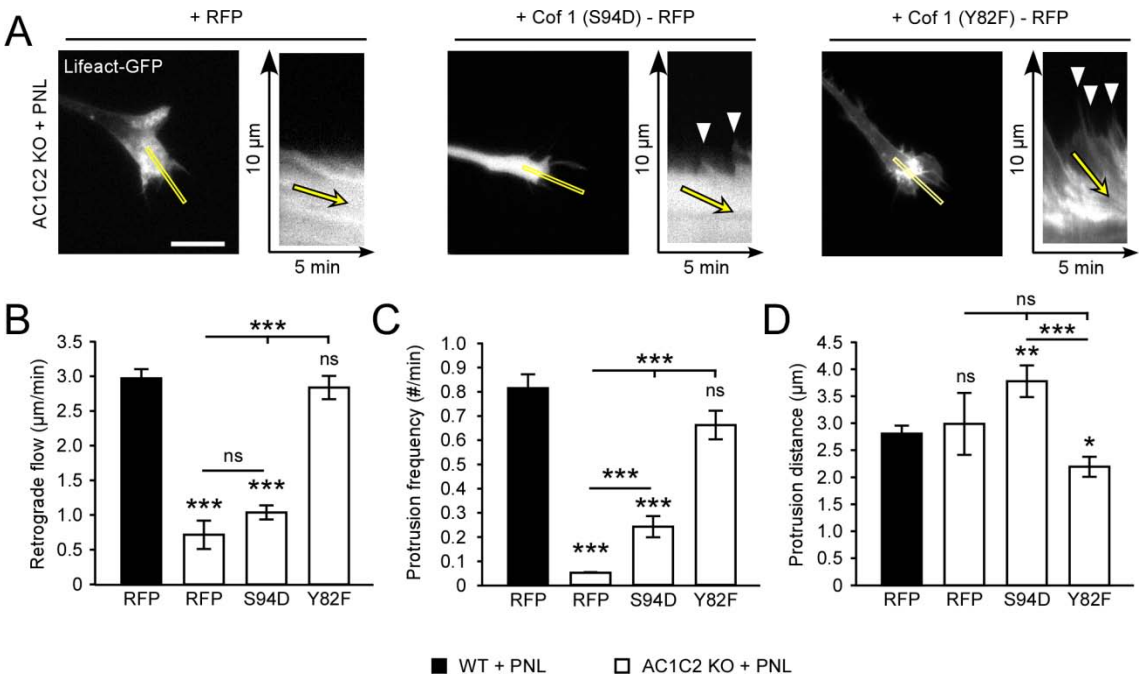

Figure 3.23. The CofY82F mutant rescues actin dynamics in conditioned AC1C2 KO DRG neurons. (A) Single frames from live-cell imaging series of conditioned DRG neurons from AC1C2 triple knockout DRG neurons expressing Lifeact-GFP, CreGFP and RFP, CofS94D-RFP or CofY82F-RFP, respectively. Frames were captured every 2 seconds for a period of 5 minutes. The lines indicate sites where line scans were taken. The kymographs show actin retrograde flow from the indicated line scans. Yellow arrows indicate actin translocation. White arrowheads indicate sites of actin protrusions. (B) Quantification of actin retrograde flow, (C) protrusion frequency and (D) protrusion distance (* $p < 0.05$; ** $p < 0.01$; *** $p < 0.001$; ns: not significant by t-test, $n > 3$-37 neurons from two independent experiments, mean ± SEM, scalebar 10 µm).

In addition, CofY82F expression led to a rescue of the protrusion frequency back to wild-type levels, and CofS94D expression also partially rescued the AC1C2 KO phenotype (0.05 ± 0.01 #/min in AC1C2 KO + RFP vs. 0.24 ± 0.04 #/min in AC1C2 KO + CofS94D vs. 0.66 ± 0.06 #/min in AC1C2 KO + CofY82F; $p < 0.001$; **Figure 3.23, C**). Surprisingly though, protrusion distance was decreased by CofY82F expression and increased by CofS94D expression (**Figure 3.23, D**).

Consistently, analysis of axon growth and branching frequency showed that the severing Y82F mutant is capable of fully rescuing the AC1C2 KO phenotype. While the S94D mutant only moderately increased axon length in AC1C2 KO neurons from 113 µm ± 17 µm to 141 µm ± 12 µm ($p < 0.05$) , the Y82F mutant increased axon length by nearly 3-fold to 347 µm ± 28 ($p < 0.01$; **Figure 3.24, A and B**).

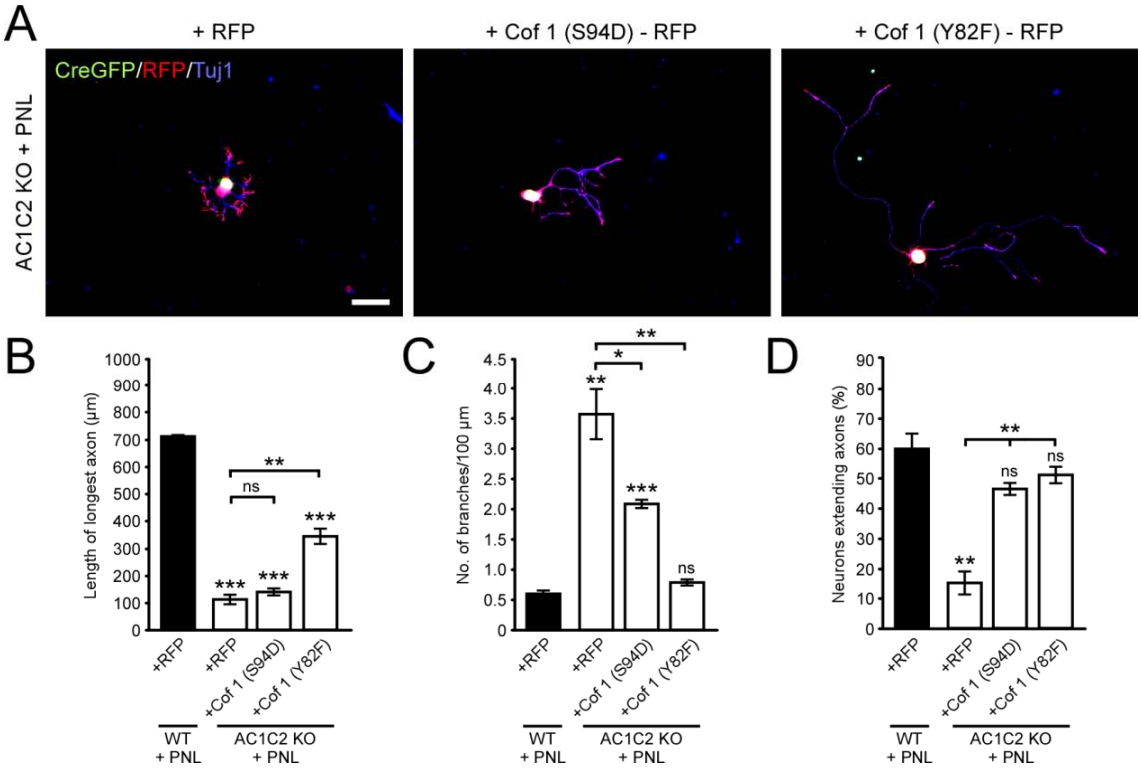

Figure 3.24. The Y82F mutant rescues axon growth in conditioned AC1C2 KO DRG neurons. (A) Representative fluorescence images of conditioned adult dissociated DRG neurons from AC1C2 KO mice transduced with AAV-CreGFP and AAV-RFP, AAV-CofS94D-RFP or AAV-Y82F (1:1) and stained for ßIII-tubulin (Tuj1). (B) Quantification of the length of the longest axon, (C) the branching frequency and (D) the percentage of neurons extending axons (* $p < 0.05$; ** $p < 0.01$; *** $p < 0.001$; ns: not significant by t-test, $n > 90$ neurons from three independent experiments, mean ± SEM, scalebar 100 µm).

The branching frequency in AC1C2 knockout DRG neurons decreased from 3.55 ± 0.41 branchpoints per 100 µm in RFP controls to 2.07 ± 0.07 in CofS94D-RFP expressing neurons and even further to 0.78 ± 0.05 in CofY82F expressing neurons, almost reaching levels of conditioned WT neurons (**Figure 3.24, C**). Both mutants were equally adept at restoring the percentage of neurons extending axons (**Figure 3.24, D**). Taken together, these data provide conclusive evidence that the severing activity of AC proteins drives actin retrograde flow and protrusion dynamics and is necessary for rapid axon growth in regenerating adult DRG neurons.

3.16 Overexpression of cofilin is sufficient to enhance axon growth in vitro

In the previous sections I provided clear evidence that AC proteins are centrally involved in the transduction of the conditioning effect. In fact, they seem to be strictly necessary for actin turnover and growth cone dynamics associated with rapid axon outgrowth after a peripheral nerve lesion. But are AC proteins also sufficient to drive regenerative growth in naïve DRG neurons?

First, I tested whether enhancing actin turnover by overexpressing AC proteins would be sufficient to increase axon growth *in vitro*. To this end, I electroporated naïve dissociated adult rat DRG neurons with plasmid DNAs expressing either (1) red fluorescent protein (RFP) alone, (2) human wildtype cofilin 1 (CofWT) conjugated to RFP, or (3) the unphosphorylatable, constitutively active form of cofilin 1 (CofS3A), which bears a serine-3 to alanine (S3A) mutation, and plated them on the growth-permissive substrate laminin (**Figure 3.25**).

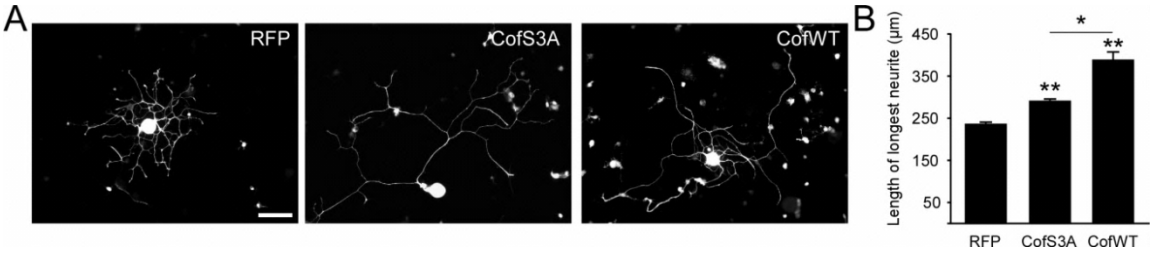

Figure 3.25. Cofilin drives axon growth in naïve DRG neurons plated on laminin. (A) Representative fluorescence images of adult naïve dissociated rat DRG neurons electroporated with plasmids encoding red fluorescent protein (RFP), constitutively active cofilin 1 (CofS3A-RFP) or wild-type cofilin 1 (CofWT-RFP). (B) Quantification of the length of the longest axon (* $p < 0.05$; ** $p < 0.01$ by t-test, $n > 90$ neurons from at least three independent experiments, mean ± SEM, scalebar 100 µm).

16-18 hours after plating, DRG neurons were fixed and axon length was quantified. On average, RFP-expressing control neurons extended axons of 234 µm ± 4 µm. Expression of CofS3A enhanced axon length by approximately 28% to 288 µm ± 7 µm ($p < 0.01$) and expression of wild-type cofilin, enhanced axon length to 386 µm ± 20 ($p < 0.01$), an increase of 33% (**Figure 3.25, A and B**). Despite not being a very large increase in axon outgrowth, the effect was highly consistent and reproducible. Moreover, the effect was comparable to the treatment of naïve DRG neurons with the actin depolymerizing drug cytochalasin D. Remarkably, 20-22 hours after plating, CofS3A-RFP and CofWT-RFP expressing neurons also grew considerably better than RFP control neurons on the two non-permissive substrates Nogo-A and CSPGs (**Figure 3.26)**.

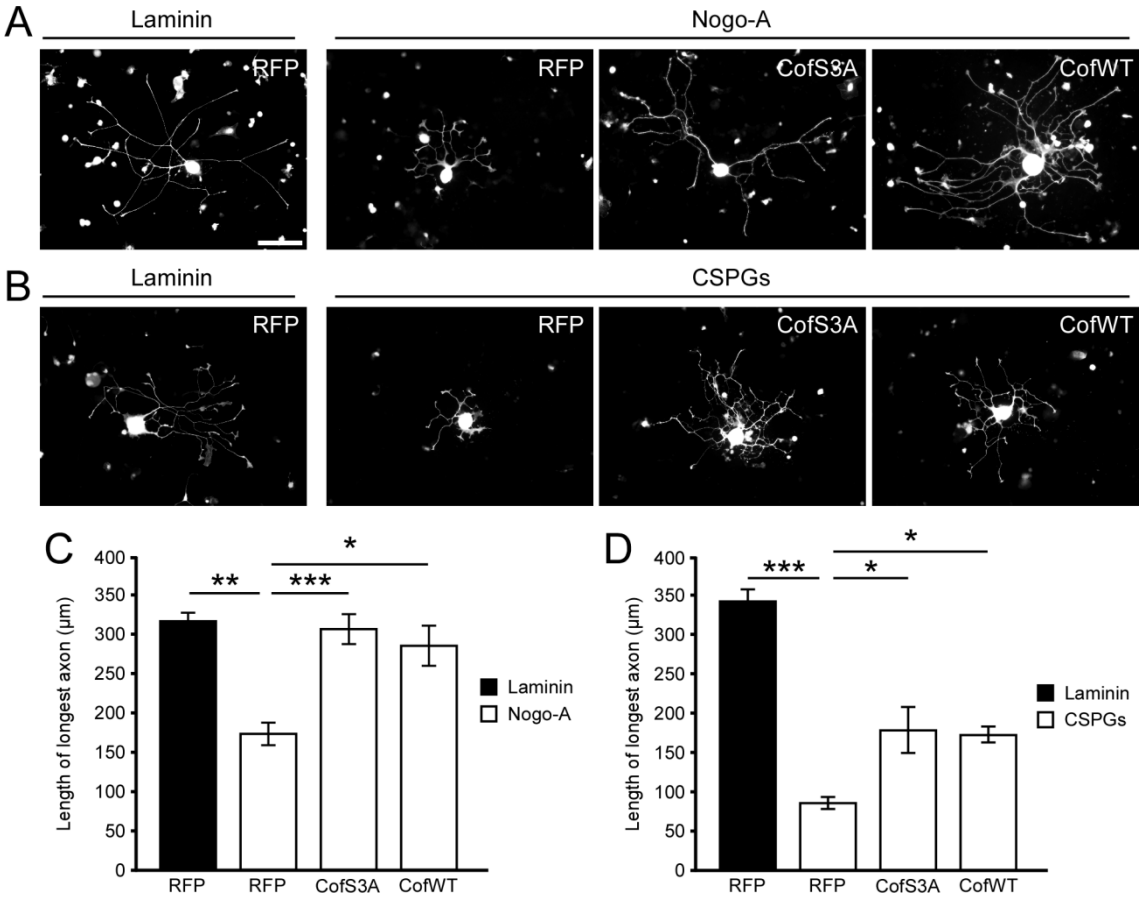

Figure 3.26. Cofilin drives axon growth in naïve DRG neurons plated on inhibitory substrates. (A+B) Representative fluorescence images of adult naïve dissociated rat DRG neurons electroporated with plasmids encoding red fluorescent protein (RFP), constitutively active cofilin 1 (CofS3A-RFP) or wild-type cofilin 1 (CofWT-RFP) plated on two different inhibitory substrates: (A) Nogo-A and (B) CSPGs. (C) Quantification of (A). (D) Quantification of (B) (* $p < 0.05$; ** $p < 0.01$; *** $p < 0.001$ by t-test, $n > 90$ neurons from at least three independent experiments, mean ± SEM, scalebar 100 µm).

In fact, on Nogo-A axon length increased from 172 µm ± 14 µm (RFP) to 305 µm ± 16 µm (CofS3A-RFP; $p < 0.001$) and to 284 µm ± 25 µm (CofWT-RFP; $p < 0.01$), thus fully restoring the axon outgrowth to levels on the permissive substrate laminin (315 µm ± 15 µm; **Figure 3.26, A and C**). The same trend was observed in DRG cultures supplemented with growth inhibitory CSPGs. Axon length increased from 86 µm ± 7 µm (RFP) to 178 µm ± 29 µm (CofS3A-RFP; $p < 0.05$) and to 172 µm ± 10 µm (CofWT-RFP; $p < 0.01$), thus restoring axon outgrowth to approximately 50% of control levels on laminin (345 µm ± 13 µm; **Figure 3.26, B and D**). These results suggest that cofilin overexpression is sufficient to enable adult primary sensory neurons to grow neurites in an otherwise growth-restraining environment. My results so far showed that elevation of the availability of intracellular cofilin (by overexpression) is correlated with an increase of axon growth in naïve DRG neurons.

Next, I wanted to find out whether cofilin is involved in enhancing axon growth via the same pathways as the conditioning effect. To test this hypothesis, I overexpressed wild-type cofilin 1 in conditioned DRG neurons. I expected that there should not be a further increase in axon length of conditioned DRG neurons upon cofilin overexpression, if cofilin should be involved in the same pathway. In fact, axon length of conditioned DRG neurons was not significantly affected by further increasing cofilin levels in conditioned DRG neurons (593 µm ± 42 µm [RFP] vs. 615 µm ± 8 µm [CofWT-RFP]; $p > 0.05$). These data insinuate that peripheral axotomy itself potentially leads to a full activation of the cofilin pathway. This activity then cannot be further augmented by introducing even more cofilin.

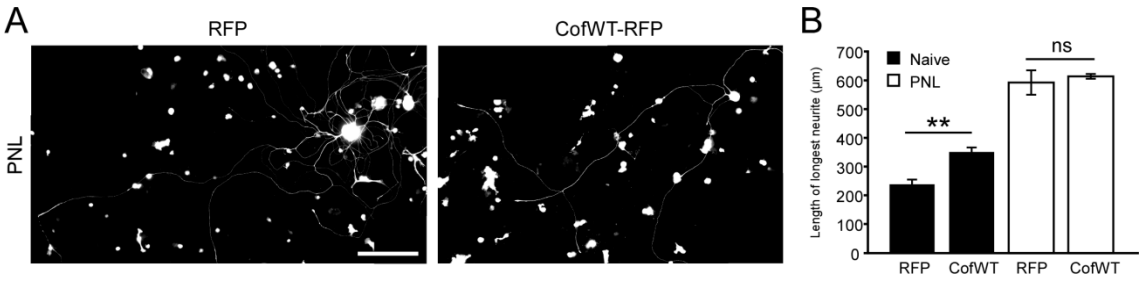

Figure 3.27. Cofilin overexpression and the conditioning response are not additive. (A) Representative fluorescence images of adult conditioned dissociated rat DRG neurons electroporated with plasmids encoding red fluorescent protein (RFP) or wild-type cofilin 1 (CofWT-RFP). (B) Quantification of the length of the longest axon (** $p < 0.01$ by t-test, $n > 90$ neurons from at least three independent experiments, mean ± SEM, scalebar 200 µm).

3.17 The severing activity of cofilin drives axon growth in vitro

So far, I provided conclusive evidence that cofilin 1 is involved in transducing the conditioning effect. Although ADF and cofilin are sharing certain functions (Hotulainen et al., 2005), ADF depolymerizes actin filaments better than cofilin 1, and cofilin 1 severs filaments better than ADF (Bamburg and Bernstein, 2010). Cofilin 2 in turn has a weaker actin filament depolymerization activity and displays a much higher affinity for ATP-actin monomers than ADF and cofilin 1 (Vartiainen et al., 2002). But it was also shown, recently, that in contrast to other isoforms, cofilin 2 can bind and disassemble ADP-Pi F-actin filaments (Kremneva et al., 2014). Hence, I wanted to test whether other members of the AC family of actin regulatory proteins are also able to increase the growth response in naïve DRG neurons and if so, by which mechanisms they exert their function. To this end, I electroporated naïve dissociated adult rat DRG neurons with plasmid DNAs expressing wild-type cofilin 1, cofilin 2 or ADF fused to either red or green fluorescent protein. As seen previously (**Figure 3.25**), overexpression of wild-type cofilin 1 increased axon growth from 278 µm ± 12 µm in RFP expressing control neurons to 386 µm ± 20 µm ($p < 0.01$; **Figure 3.28, A and D**). Interestingly though, overexpression of neither ADF nor cofilin 2 increased axon length significantly in naïve DRG neurons plated on laminin (270 µm ± 16 µm in cofilin 2 expressing neurons vs. 315 µm ± 15 µm in ADF expressing neurons). Analogous to the loss of function experiments in the triple AC1C2 KO animals, I next tested which function of cofilin 1 is essential for mediating this increase in axon growth. To this end I electroporated adult dissociated, naïve DRG neurons with plasmid DNAs encoding either the severing (Y82F) or depolymerizing (S94D) mutant of cofilin and plated them on permissive (laminin) or inhibitory (CSPGs) substrates. After 16-18 hours in culture, overexpression of the depolymerizing mutant CofS94D-RFP did not yield an increase in axon growth on either of the substrates (**Figure 3.28, B-F)**. By contrast, overexpression of the severing mutant CofY82F-RFP resulted in increased axon extension on both laminin (**Figure 3.28, B and E)** and CSPGs (**Figure 3.28, C and F**). These findings argue in favor of the hypothesis that the severing activity of cofilin 1 is essential for the augmented actin turnover necessary for rapid axonal growth.

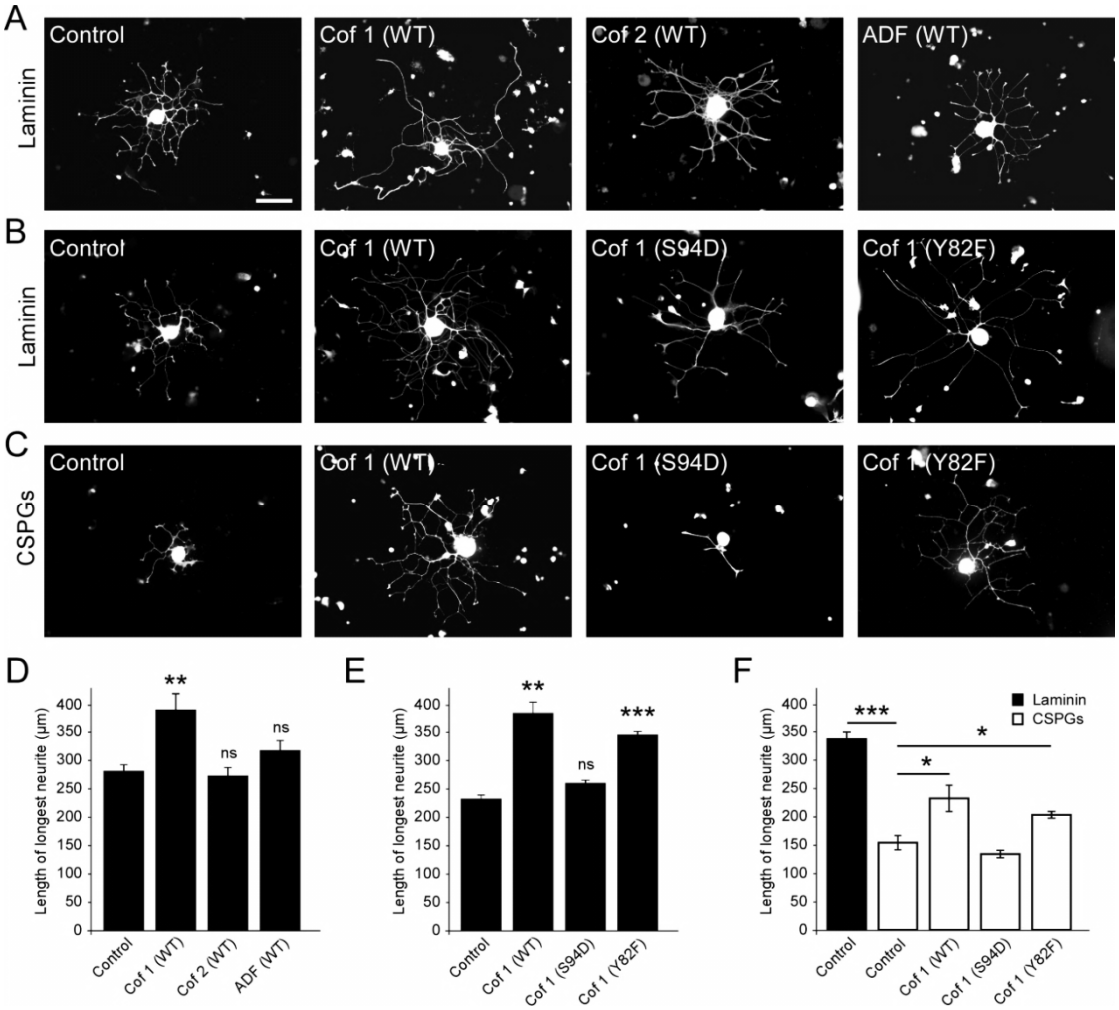

Figure 3.28. The severing activity of cofilin drives axon. (A-C) Representative fluorescence images of adult naïve dissociated rat DRG neurons electroporated with plasmids encoding red fluorescent protein (RFP), wild-type cofilin 1 (Cof1 WT), wild-type cofilin 2 (Cof2 WT), wild-type ADF (ADF WT), the severing mutant of cofilin 1 (CofY82F) or the depolymerizing mutant of cofilin 1 (CofS94D). Neurons were either plated on laminin (A+B) or CSPGs (C). (D-F) Quantification of (A-C), respectively (* $p < 0.05$; ** $p < 0.01$; *** $p < 0.001$; ns: not significant by t-test, $n > 90$ neurons from at least three independent experiments, mean ± SEM, scalebar 100 µm).

3.18 Cofilin - a potential target to promote axon regeneration following SCI?

In the preceding sections I provided evidence that AC proteins are necessary for axon growth both *in vitro* and *in vivo*. Furthermore, I showed that cofilin 1 is sufficient to promote axon outgrowth *in vitro* - albeit the effect not being as robust as a conditioning lesion. My results thus prompted the idea that increasing the activity of cofilin 1 may potentially promote regeneration of dorsal column axons following spinal cord injury *in vivo*. Thus, I successfully established two strategies to manipulate cofilin 1 expression *in vivo* and to test axon regeneration

thereafter: (1) an approach using virus-mediated transduction of cofilin and (2) an approach using *in vivo* DRG electroporation (Saijilafu et al., 2011).

(1) AAV-based approach: Custom-made adeno-associated viruses (AAVs) expressing red fluorescent protein (RFP) or wild-type cofilin 1 conjugated to RFP are co-injected into the sciatic nerves of adult C57BL/6J wild-type mice with an AAV vector expressing enhanced green fluorescent protein (GFP) in a 1:1 mixture to efficiently label axons of the spinal cord (**Figure 3.29**).

Co-injection of two viral vectors is a valid method, since the double transduction rate is high and approximately 60-80% of GFP positive neurons will also express RFP or CofWT-RFP (**Figure 3.15**; Fagoe et al., 2015). 2 weeks post-injection of the AAV mixture into the sciatic nerve, a dorsal column lesion (DCL) is performed at thoracic level (T) 12. Mice are terminated four weeks following spinal cord injury. Imaging of the unsectioned spinal cord is performed using two-photon microscopy.

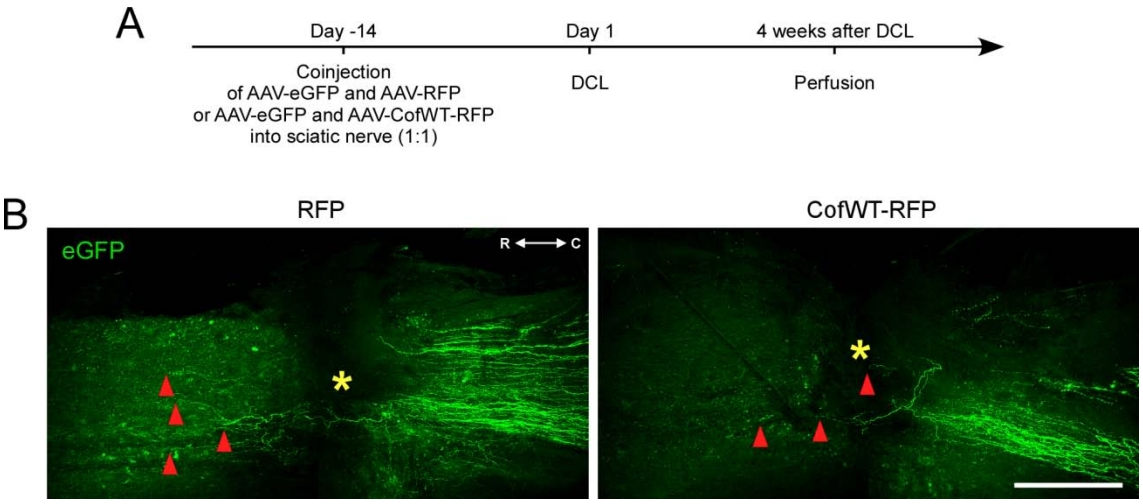

Figure 3.29. Overexpression of cofilin 1 in dorsal column axons using an adeno-associated-virus approach. (A) Timeline of the experiment to assess spinal cord regeneration. (B) Multiphoton scans of the unsectioned adult mouse spinal cords 4 weeks after SCI. DC axons were labeled by coinjecting AAV-eGFP and RFP or CofWT-RFP into the left sciatic nerve. Red arrowheads indicate regenerating axons. Yellow asterisks indicate the lesion site (LS). (R: rostral, C: caudal; scalebar 400 µm).

To date, acute virus-based gene delivery is often used to modulate gene expression, especially because of its high labeling efficiency. However, this method is expensive and involves labor-intensive production of the viruses. Moreover, viral particles may have undesired effects on the immune system of the host, which could potentially affect the experimental results and interpretation of data. Hence, I additionally tested a promising alternative tool to manipulate gene expression with high spatiotemporal control: *in vivo* electroporation of adult sensory neurons (Saijilafu et al., 2011). Using this novel approach, fluorescent constructs can be expressed in sensory neurons and the transfected genes start to be expressed within a few hours after electroporation in living animals.

(2) In vivo electroporation approach: L4 and L5 dorsal root ganglia of C57BL/6J wild-type mice are injected with plasmid DNAs expressing RFP or wild-type cofilin 1 conjugated to RFP and electroporated as described in the respective materials and methods section (**Figure 5.1**). 14 days following electroporation, the ipsilateral dorsal column is transected at level T12. 4 week post-injury animals are perfused and spinal cords analyzed.

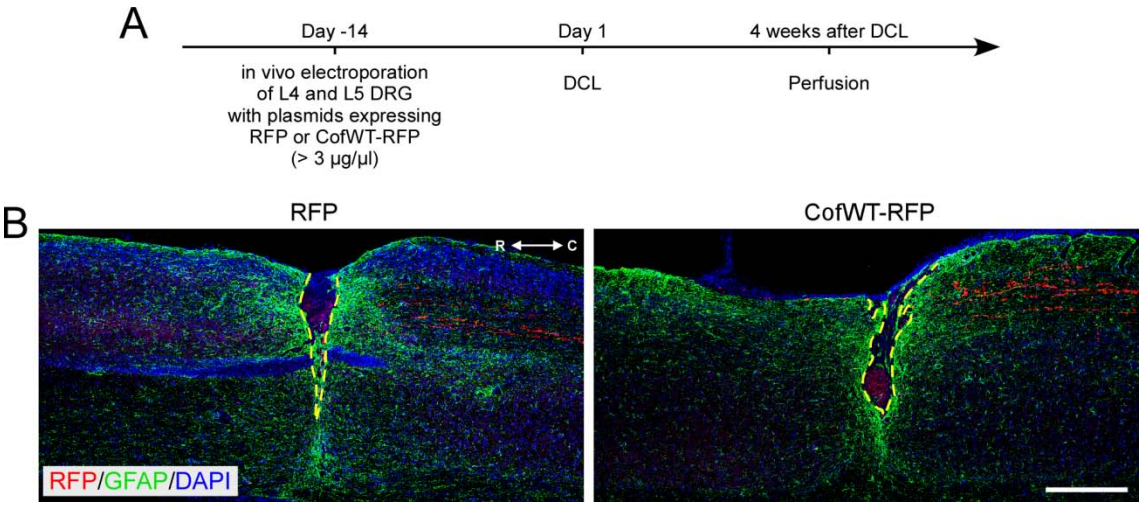

Figure 3.30. Overexpression of cofilin 1 in dorsal column axons using *in vivo* DRG electroporation. (A) Timeline of the experiment to assess spinal cord regeneration. (B) Sagittal sections of the injured spinal cord expressing RFP and stained for GFAP. DAPI stained nuclei. The yellow dashed line indicates the lesion border (R: rostral, C: caudal; scalebar 400 µm).

Even though the RFP signal is distributed evenly throughout the axons of the dorsal column (**Figure 3.30** and **Figure 5.1**), this technique still has a clear drawback: with only 10-20 RFP positive fibers per animal, the number of sensory axons labeled in the dorsal column at level T12 is fairly low. Despite these technical limitations, both the AAV- and the *in vivo* DRG electroporation-based approach are applicable and will be employed in future studies to test potential benefits of overexpressing cofilin 1 for spinal cord regeneration *in vivo*.

In conclusion, I report that high actin turnover is necessary for rapid axon growth and regeneration. My data indicate that a single family of actin regulatory proteins, ADF/cofilin, drives the conditioning regenerative response. In particular, the actin severing activity of cofilin is essential for axon elongation upon peripheral nerve lesion. Thus, my data reveal that cofilin mediated actin turnover is necessary for axon regeneration by recapitulating processes that occur during neurite initiation in development.

4 DISCUSSION

Axons in the central nervous system (CNS) generally do not regenerate after traumatic injury. Both a non-permissive environment and reduced intrinsic growth ability account for this regenerative failure (Liu et al., 2011). However, primary sensory neurons manifest a classical exception to this dogma. A primary "conditioning" lesion to the peripheral branch of dorsal root ganglion (DRG) neurons followed by a second lesion to the central branch of the same cells results in a robust regenerative response of the central axons (Richardson and Issa, 1984, Neumann and Woolf, 1999, Ylera et al., 2009). This "conditioning" phenomenon (McQuarrie et al., 1977) is able to reinitialize the intrinsic competence for an elongating growth-mode in adult primary sensory neurons (Smith and Skene, 1997). Despite its discovery over thirty years ago, the knowledge about the intracellular events underlying this transition in growth competence is still fragmentary.

Growth cones are highly motile structures at the tip of extending axons, which determine the rate and direction of axonal propagation during development and regeneration. Axon extension requires assembly and reorganization of the growth cone cytoskeleton, which is composed of two principle components: (1) actin filaments, the cytoskeletal element that maintains the growth cone shape and is essential for proper axon guidance. (2) And microtubules, essential for giving the axon structure and providing the substrate for intracellular transport (reviewed by (Dent and Gertler, 2003, Dent et al., 2011, Bradke et al., 2012).

Since a conditioning lesion results in a clear-cut transformation and reorganization of the neuronal morphology, I postulated that the cytoskeleton of DRG neurons should experience some form of rearrangement following peripheral nerve lesion (PNL). In my thesis project presented here, I thus wanted to analyze the intrinsic changes that occur at the level of the actin and microtubule cytoskeleton in primary sensory neurons after a peripheral nerve lesion.

4.1 Peripheral nerve lesion leads to enhanced axon extension

To study potential correlations between the cytoskeleton and enhanced axonal growth in primary sensory neurons, it was pivotal to establish the conditioning lesion model successfully. Therefore, my first objective was to successfully reproduce the conditioning effect *in vitro*. In fact, a unilateral peripheral nerve lesion one week prior to the dissection and culture of naïve and conditioned DRG neurons resulted in a clear-cut increase in axonal length and neurons extending axons, as well as a decrease in branching frequency (**Figure 3.1**). These findings are in accordance with previous studies where a preconditioning lesion resulted in the transition from an "arborizing" to an "elongating" growth-mode in dissociated adult DRG neurons (Smith and Skene, 1997).

In order to characterize the intracellular events leading to the increase in axonal length, I started out by characterizing the growth rate and dynamics of cultured primary sensory neurons using single-cell video live-microscopy. Growth cones of conditioned DRG neurons are characterized by a typical step-like growth curve: phases of rapid growth are correlated with rapid ejection of membrane and thin, filopodia-like structures, while phases of growth arrest are associated with the formation of bulbous structures at the tip of the axons (**Figure 3.2**). By contrast, growth cone advance of naïve DRG neurons is more homogeneous. In consequence, the average and maximal rate of advance is more than doubled upon PNL. Even though the absolute values might differ, our findings are consistent with previous observations where conditioned neurons reached peak velocities of up to 1.0 mm/hour, while naïve DRG neurons rarely exceeded 10 µm/hour (Hess et al., 1993, Smith and Skene, 1997). The deviant growth rates of the latter studies might be due to the use of a modified culturing medium containing up to 10% horse serum, promoting faster growth.

4.2 Peripheral nerve lesion results in restructuring of the actin cytoskeleton

Earlier studies in sympathetic neurons demonstrated that the rate of growth cone advance directly correlates with their size and dynamics (Argiro et al., 1984, 1985). In addition, Dent et al. (2003) showed that rapidly growing growth cones have the tendency to be small, while slow moving or paused growth cones are very large.

This was confirmed in a recent study showing that wider growth cones have a smaller tendency to take larger steps using principal components analysis in shape space (Goodhill et al., 2015). Subsequently, I hypothesized that a change of the growth cone morphology might be observed in primary sensory neurons following peripheral nerve lesion. In fact, I found that peripheral axotomy is correlated with a significant reduction in the complexity of growth cones and actin distribution in the growth cone periphery. Naïve DRG neurons on the other hand, feature a complex, fan-like growth cone morphology and have abundant actin sites at the leading edge (**Figure 3.3**). These findings are in accordance with a previous study (Smith and Skene, 1997), which showed that growth cones of conditioned DRG neurons were typically tapered and displayed few filopodia, while naïve DRG neurons more often terminated in larger, palmate growth cones with numerous short filopodia. Interestingly though, no other study so far reported the existence of the extremely thin and long filopodia-like actin based membrane protrusions from the typical bulbous growth cones of conditioned primary sensory neurons that I observed. Most likely, this is attributed to the use of improved technical equipment, better resolving microscopes and optimized culturing conditions compared to the other studies that were performed more than twenty years ago. Regardless, my findings suggest that a reduced morphological growth cone and actin complexity is associated with rapid elongation typical for conditioned DRG neurons. In this context it is interesting to note that chicken sensory neurons can regenerate in the absence of F-actin in the growth cones (Marsh and Letourneau, 1984, Letourneau et al., 1987, Jones et al., 2006) and localized actin network instability induced by cytochalasin D treatment supports axon elongation in hippocampal neurons (Bradke and Dotti, 1999). This is in accordance with the model of "steric-hindrance", which states that microtubule extension, and therefore axon elongation, is enhanced due to relief of physical restraints normally imposed by peripheral actin networks on microtubules (Forscher and Smith, 1988).

With these findings in mind I wanted to test whether loosening of the actin network may play a role in mediating the conditioning effect of DRG neurons. If there should be a causal relationship, pharmacologically induced destabilization of actin in naïve DRG neurons should result in similar neurite outgrowth to that found after PNL. In fact, cytochalasin D treatment led to an increase in axon length

of naïve DRG neurons, suggesting that loosening of the actin network is a potential mechanism underlying the conditioning effect (**Figure 3.4**). Nonetheless, the observed effect on axon extension was moderate and not comparable to the robust growth response after PNL. This can be explained by the fact that depolymerization of the actin cytoskeleton is probably not the only mechanism responsible for transducing the conditioning effect. In fact, as described in earlier sections, other regeneration associated genes and proteins were shown to be involved. The different temporal aspects may provide another way of interpreting the fact that pharmacological actin destabilization does not reach up to the effects on length observed after peripheral axotomy. Conditioned DRG neurons are exposed to the effects of a peripheral nerve lesion for approximately 7 days *in vivo* prior to culturing, and are then subjected to a further decrease in actin stability by cytochalasin D for 16-18 hours. In other words, alterations induced by a potential depolymerization of actin associated with a conditioning lesion have more time to become effective. Naïve DRG neurons, on the other hand, are only subjected to the pharmacological actin depolymerization for 16-18 hours *in vitro*. It is plausible, that this time frame is simply too short to lead to more significant effects on length.

4.3 Microtubules are more stable upon PNL

In addition to the actin cytoskeleton, microtubules and their dynamic rearrangements are essential for axon extension (Forscher and Smith, 1988, Sabry et al., 1991, Dent and Gertler, 2003). It was shown by our group, that disorganized microtubules underlie the formation of retraction bulbs after injury and the subsequent failure of axonal regeneration *in vivo* (Erturk et al., 2007). Furthermore, microtubule stabilization is sufficient to induce axon formation in hippocampal neurons *in vitro* (Witte et al., 2008) and to promote regeneration *in vivo* (Hellal et al., 2011, Ruschel et al., 2015). Thus, I postulated that in addition to the changes observed at the actin level, naïve and conditioned DRG neurons may also differ in the organization of microtubules. Neuronal microtubule subpopulations are composed of α-tubulins that can be distinguished by their post-translational modifications, such as tyrosination and acetylation (Burgoyne and Norman, 1986, Cambray-Deakin and Burgoyne, 1987). Acetylated α-tubulin is characterized by

slower turnover rates (Kreis, 1987, Schulze and Kirschner, 1987, Webster et al., 1987) and greater resistance to depolymerizing drugs (Piperno et al., 1987, Cambray-Deakin et al., 1988), and thus constitutes an ideal marker for stable microtubule assemblies. By contrast, tyrosinated α-tubulin is a typical marker for dynamic microtubule arrays. Typically, axons of cultured neurons display a gradation of stability from the axon base towards the growth cone. While the axon shaft is enriched in stable (acetylated) microtubules, the distal shaft and growth cone mainly contains a dynamic (tyrosinated) pool of microtubules (Robson and Burgoyne, 1989). To assess whether naïve and conditioned DRG neurons differ in the stability of their microtubules, I examined the ratio of acetylated to tyrosinated α-tubulin at four distinct locations along the longest axon. The analysis revealed that conditioned neurons show a significantly higher degree of microtubule acetylation at the axon base and in the medial part of the neurite shaft (**Figure 3.5**). However, in both naïve and conditioned DRG neurons, tyrosinated microtubules are the predominant form in the distal axon shaft and growth cone. This is in accordance with a study showing that dynamic microtubules in the growth cones are required for proper axon steering and elongation (Tanaka and Sabry, 1995). In addition, I showed previously that naïve DRG neurons are more sensitive to drug induced microtubule depolymerization than conditioned neurons (Laskowski, 2008), another piece of evidence supporting the hypothesis that conditioned DRG neurons show increased levels of stable microtubules. In summary, my results show that there is a clear correlation between increased microtubule stability and enhanced axonal length in conditioned primary sensory neurons.

Subsequently, I postulated that there might also be a causal relationship between enhanced microtubule stability and axon growth. To test this idea, I treated naïve DRG neurons with taxol (paclitaxel), an anti-neoplastic microtubule stabilizing agent (Schiff et al., 1979). If increased microtubule stability is partly responsible for mediating the conditioning effect, naïve DRG neurons should extend longer neurites upon taxol treatment. Surprisingly, the effect of pharmacological microtubule stabilization on axon length was only minor (**Figure 3.6**). However, there was a clear-cut reduction in axon branching, the second hallmark of the elongating growth mode typical for conditioned DRG neurons. This finding is in line with a study showing that taxol treatment reduces the incidence in growth

cone branching in cultured sensory and sympathetic neurons from chick embryos (Letourneau et al., 1986). A possible explanation for the moderate effect on axon length is the fact that maintenance of a population of unstable microtubules is a requirement for axon growth and turning (reviewed in Goold and Gordon-Weeks, 2004). In fact, excessive stability of microtubules can inhibit axonal outgrowth as shown in a study where treatment of dissociated cultures of rat sensory neurons with varying concentrations of taxol resulted in abnormal cell morphology and stunted axonal growth (Haque et al., 2004). Another explanation may also relate to the reduction in non-neuronal cells, which are vital for secreting growth factors, upon taxol treatment. Finally, it is feasible that moderate stabilization of microtubules alone might not be sufficient to enhance axon growth beyond a certain threshold, because naïve neurons are simply lacking the "building blocks" to boost axon growth. In fact, peripheral nerve lesion leads to the activation of a plethora of regeneration associated genes that supply the axon of conditioned DRG neurons with structural components (tubulin, actin and neurofilaments), synaptic and cytosolic proteins, vesicles, and organelles. This, in conjunction with microtubule stabilization, then enables conditioned DRG neurons to mount a robust growth response. In naïve DRG neurons however, the synthesis of these growth permissive prerequisites is not given. Nonetheless, I showed that moderate microtubule stabilization via taxol was able to decrease axonal branching in naïve DRG neurons and thus to mimic at least one of two key aspects of the elongating growth typical for conditioned DRG neurons.

4.4 Growth cones of conditioned DRG neurons are enriched in mitochondria and contain disorganized microtubules

Smith and Skene (1997) showed that growth cones of conditioned DRG neurons are typically tapered and display few filopodia, while naïve DRG neurons often terminate in larger, palmate growth cones with numerous short filopodia. In line with these observations, my own live-cell imaging and immunocytochemical analyses revealed that the most prominent feature of conditioned growth cones are torpedo-shaped, bulbous structures at the distal end of the axons (**Figures 3.2 and 3.3**). In phases of no growth the lamellipodia and filopodia are retracted from the leading edge and a bulbous ending is formed that gradually enlarges. After

varying time-periods (minutes to sometimes hours) thin filopodia-like membrane protrusions are rapidly ejected from these bulbous endings and a new growth cone starts to form, propelling the axon forward. To analyze the underlying ultrastructure of these prominent endbulbs, I performed electron microscopy. In electron micrographs, growth cones of conditioned DRG neurons were typically characterized by disorganized microtubules in their bulbous center (**Figure 3.7 - 3.9)** and by an accumulation of vesicles and mitochondria (**Figure 3.10**). From the mere appearance in culture these bulbous endings were similar to so-called dystrophic end bulbs (also called retraction bulbs or frustrated growth cones). When regenerating axons encounter a barrier in their environment like the glial scar, dystrophic end bulbs that were first described by Ramon y Cajal (1928) are formed. In general, they feature an accumulation of anterogradely transported vesicles, mitochondria and microtubules. The latter appear disoriented and extend in various directions, sometimes even turning around to point their plus-ends away from the leading edge (reviewed in Bradke et al., 2012). For many years it was thought that these endbulbs are sterile and therefore incapable of extending axons through the lesion. Later research implicated, however, that these endbulbs do not lose the ability to regenerate. Instead of dying back, they persist at the lesion site for lengthy time-periods and can even return to active growth states (reviewed in Miller, 2006). In fact, more recently, Tom et al. (2004) obtained evidence using a novel *in vitro* model of the glial scar that these endbulbs are highly active structures; they remain stationary, while their distal membrane and cytoskeleton is continuously turned over. These findings implicate, that adult sensory neurons use this form of "aberrant" growth cone to survive and maintain itself in a hostile environment. In the case of conditioned DRG neurons I am inclined to use the term "loading bulb" instead of dystrophic endbulb, as the bulbous growth cones are not permanently stalled but just transiently paused. As the growth cone propels itself forward, it may encounter an extracellular barrier or point of decision and reposes momentarily. From that moment all the raw material needed for further rapid growth, i.e. cytoskeletal components, organelles and a plethora of proteins, is transported anterogradely and collected at the distal tip, where a bulbous structure forms. Subsequently, growth is continued by rapid ejection of membrane protrusions, filopodia and lamellipodia. So far, the exact trigger and mechanism of reinitiating elongation

after the phase of growth arrest is not known. Future research should be invested in understanding this fascinating process in more detail.

4.5 Rapid axon extension upon PNL is correlated with enhanced growth cone and actin dynamics

A potential approach to explain the just described phenomenon may be found upon taking a closer look at the actin cytoskeleton. As described in earlier sections, the model of "steric-hindrance" states that microtubule extension is typically restrained by a physical barrier imposed by the dense peripheral actin network, therefore impeding axon extension (Forscher and Smith, 1988, Bradke and Dotti, 1999, Witte and Bradke, 2008). Loosening of this restraint allows microtubules to protrude farther into the periphery and thus to prompt axon elongation. Hence, to analyze whether this may also be a mechanisms underlying regenerative growth upon peripheral nerve lesion, I analyzed the growth cone and actin dynamics of naïve and conditioned DRG neurons using time-lapse microscopy. I showed that increased growth cone dynamics and actin turnover are correlated with rapid axon extension after a peripheral nerve lesion in adult DRG neurons (**Figure 3.11**). In addition, pharmacological inhibition of actin dynamics via jasplakinolide treatment abolished the conditioning effect and prevented rapid axonal growth (**Figure 3.12**), indicating that high actin turnover is a prerequisite for the conditioning effect. My finding is in line with recent results showing that wider growth cones have a smaller tendency to take larger steps and growth cones that are oscillating strongly and rapidly tend to make forward progress faster (Goodhill et al., 2015). Furthermore, a study by our group showed that augmented actin dynamics are typical for neurite-forming regions at the soma and that high actin turnover is essential for driving neuritogenesis (Flynn et al., 2012). The authors further provided unambiguous evidence that a single family of actin regulatory proteins, ADF/cofilin, provides the necessary control of actin dynamics to form neurites during development. I thus postulated that the same family of actin binding proteins may be involved in mediating the conditioning effect by reactivating the developmental program described by Flynn et al. (2012).

4.6 Cofilin activity is enhanced upon PNL

Actin filament dynamics and reorganization are key processes enabling growth cone motility, morphology, and extension (Mitchison and Kirschner, 1988, Tanaka and Sabry, 1995, Luo, 2000, Song and Poo, 2001). Since ADF/cofilin (AC) is an essential regulator of actin dynamics and highly expressed in growth cones, it likely plays a vital role in growth cone motility and extension (Bamburg and Bray, 1987, Kuhn et al., 2000, Meberg, 2000, Endo et al., 2003, Flynn et al., 2012). In my thesis project, using western blot analysis, I showed that AC activity is enhanced following peripheral nerve lesion, indicating that AC might be critically involved in transducing the conditioning response (**Figure 3.13**). The activity of AC proteins is reversibly regulated by pH, phosphoinositides and phosphorylation at Ser3 (reviewed in Meberg and Bamburg, 2000, Van Troys et al., 2008). Phosphorylation by LIM kinases (LIMK) and TES kinases (TESK) inactivates cofilin (Arber et al., 1998, Toshima et al., 2001a, Toshima et al., 2001b, Scott and Olson, 2007) and dephosphorylation by the phosphatases slingshot homolog (SSH) and chronophin (CIN) reactivates cofilin (Niwa et al., 2002, Huang et al., 2006). In a study by Endo et al. (2003), the authors obtained evidence that specifically LIMK1 and SSH1 play important roles in the control of growth cone motility and morphology and neurite extension, principally by regulating the activity of cofilin. Consistently, I show here that the phosphatase SSH1 is activated upon PNL. In contrast, the activity of LIMK1 was not altered upon PNL (**Figure 3.13)**. These data are in line with previous studies, showing that expression of human SSH homologs dampen both LIMK1 and TESK1 activity in mammalian cell lines (Niwa et al., 2002). Furthermore, overexpression of SSH increases growth cone motility and neurite extension in chick DRG neurons while expression of LIMK reduces these events (Endo et al., 2003). In contrast, suppression of LIMK1/2 expression or activity also significantly reduced NGF-induced neurite extension from PC12 cells or chick DRG neurons and reduced actin filament assembly in the peripheral region of the growth cone of chick DRG neurons (Endo et al., 2007). Despite apparent contradictions in the results obtained, all modifications of the activity levels of either ADF/cofilin kinases or phosphatases lead to reorganization of the actin cytoskeleton and to changes of growth cone motility, migration and axon extension. These results suggest that adequate regulation of AC activity through control of phosphorylation by the LIMK and SSH family members are critical for

proper neurite extension. Further studies are required to untangle the relative contribution of ADF/cofilin regulating kinases and phosphatases, lying special emphasis on their expression levels and tissue distributions, their activation pathways and activity levels and lastly their subcellular localization (reviewed in Van Troys et al., 2008). Here, I provided first evidence that the activity levels AC proteins and their upstream regulators are modulated following PNL and thus constitute potential candidates in transducing the conditioning response.

4.7 AC proteins are necessary for high actin turnover and axon extension

To test if AC mechanistically contributes to the conditioning phenomenon, we used loss-of-function manipulations *in vitro* and in vivo by genetically depleting ADF and cofilin 1 from adult mouse DRG neurons (AC1 knockout). During development, AC1 KO resulted in a remarkable immobilization of actin dynamics and complete abolishment of neuritogenesis in hippocampal and cortical neurons (Flynn et al., 2012). Surprisingly, depletion of both ADF and cofilin 1 in adult DRG neurons resulted in only moderate reduction of actin turnover, axon length and regeneration (**Figure 3.16 and 3.17**). This suggested that AC proteins might not be as critical for regenerative growth as opposed to axon growth during development. Alternatively, I postulated that another member of the AC family may compensate for the loss of ADF and cofilin 1 in adult DRG neurons. In fact, using western blot analysis, I showed that cofilin 2, the third AC isoform was up-regulated upon depletion of ADF and cofilin 1 in adult DRG neurons (**Figure 3.18**).

The exact biochemical and functional properties of the three isoforms are still unclear, with cofilin 2 being the least understood member of the AC family. Despite sharing a highly conserved genomic and amino-acid structure, all three AC isoforms differ considerably in their activities and expression patterns (Vartiainen et al., 2002, Gurniak et al., 2005, Nakashima et al., 2005, Gurniak et al., 2014, Kremneva et al., 2014). Thus it is not surprising that to date most studies suggested that AC isoforms cannot functionally compensate for each other *in vivo*. While *in vitro*, cofilin 1 downregulation could still be rescued by ADF expression and vice versa (Hotulainen et al., 2005), in more complex conditions *in vivo*, the AC isoforms seem to have divergent effects. In fact, cofilin 1 deficient mice display early embryonic lethality and defects in actin-dependent morphogenic processes

(Gurniak et al., 2005, Bellenchi et al., 2007). ADF inactivation leads to corneal defects and blinding (Ikeda et al., 2003), and cofilin 2 deficient mice show progressive disruption of the sarcomeric architecture and accumulation of F-actin in skeletal muscles and eventually die between postnatal day 10 and 12 (Agrawal et al., 2012, Gurniak et al., 2014). These studies showed that the different AC isoforms are not completely redundant, most likely because they have quantitatively different effects on actin dynamics. To a certain degree, all three AC proteins have F-actin binding and depolymerizing activities. However, ADF depolymerizes actin filaments better than cofilin 1, and cofilin 1 severs filaments better than ADF (Vartiainen et al., 2002, Bamburg and Bernstein, 2010). And cofilin 2 displays a much higher affinity for ATP-actin monomers and even promotes filament assembly rather than disassembly in steady-state assays (Vartiainen et al., 2002). Nonetheless, there is recent evidence suggesting that cofilin 2 can also bind and disassemble ADP-Pi F-actin filaments in muscles (Kremneva et al., 2014). Importantly, cofilin 2 is predominantly expressed in late development in differentiated muscle and only to a lesser extent in other tissues such as heart and brain (Vartiainen et al., 2002, Gurniak et al., 2005, Gurniak et al., 2014, Kremneva et al., 2014). On this account it is clear why cofilin 2 expression did not compensate for the severe AC1 knockout phenotype in embryonic neurons (Flynn et al., 2012).

The unexpected discovery of the functional compensation by cofilin 2 in adult AC1 DRG knockout neurons is intriguing and the precise mechanisms how cofilin 2 is able to dynamize the actin cytoskeleton in adult DRG neurons needs to be teased out in future studies. In summary my data support the notion that, despite having distinct biochemical properties, all three AC isoforms are able to functionally compensate for each other - at least in part - in adult DRG neurons. This hypothesis is supported by the results obtained in DRG neurons from ADF/cofilin 2 (AC2 KO) or cofilin 1/cofilin 2 (C1C2 KO) double knockout mice, where axon extension and branching was affected to a similar extent as in the AC1 KO mice (**Figure 3.18**).

Finally, deletion of all three isoforms of the AC family (AC1C2 knockout) resulted in severe disturbance of actin dynamics and axon extension *in vitro*, as well as axon regeneration *in vivo* (**Figures 3.19 - 3.21**). Interestingly though, not all aspects of

actin dynamics were perturbed upon ablation of ADF, cofilin 1 and 2. While retrograde flow and protrusion frequency were considerably decreased, the protrusion length was not significantly affected by the AC1C2 KO. Due to the reduced actin turnover in AC1C2 KO growth cones, the actin filaments potentially persist longer at the leading edge before they are disassembled and fragmented. Contradicting this hypothesis is the fact that long protrusions are characteristically found in conditioned wild-type DRG growth cones. Whether these protrusions are only correlated with the robust outgrowth observed after PNL, or whether there is a direct causal relationship needs to be deciphered in more detail in future studies. Overexpression of filopodial proteins like fascin in naïve DRG neurons and subsequent analysis of growth cone and actin dynamics as well as axon outgrowth may improve our understanding of this "filopodia phenomenon". Certainly though, retrograde flow and protrusion frequency seem to be the main determinants of axon growth, since reintroduction of wild-type cofilin 1 restored both parameters of actin dynamics as well as axon outgrowth to control levels. In the future, it should be tested whether ADF and cofilin 2 are also able to rescue the severe AC1C2 knockout phenotype to gather more evidence on the functional redundancy of AC proteins in adult sensory neurons.

In summary, my results show that AC proteins are necessary for regulating enhanced actin retrograde flow and actin dynamics associated with rapid axon growth following a peripheral nerve lesion, and are thus centrally involved in mediating the conditioning response.

4.8 The severing activity of AC proteins regulates actin turnover and axon extension

Actin filament dynamics and reorganization are central for motility, morphology, and directional movement of axonal growth cones (Mitchison and Kirschner, 1988, Tanaka and Sabry, 1995). Polarized growing and shrinking of actin filaments through polymerization at the leading edge and disassembly at the central domain, results in dynamic actin turnover and is fundamental for generation of protrusive forces in axons (Lin and Forscher, 1995). This actin turnover is augmented by either increasing the number of filament ends (through de novo nucleation of actin filaments or severing of existing filaments) or by enhancing the rate of monomer assembly and disassembly from pointed filament ends. In fact,

AC proteins are known to be involved in regulating actin dynamics via diverse but overlapping activities. AC accelerates spontaneous nucleation of actin monomers, increases the dissociation rate of actin subunits from the pointed end and severs actin filaments by binding to actin filaments, thereby inducing a conformational change in the filaments that eventually leads to their fragmentation (Van Troys et al., 2008).

To discern the relative contributions of each of these activities in dynamizing the actin cytoskeleton following peripheral nerve lesion, I tested the efficiency of the two activity mutants of cofilin, S94D and Y82F, in rescuing the profound AC1C2 triple knockout phenotype. The cofilin-S94D mutant cannot sever actin filaments but retains its depolymerizing activity, while cofilin-Y82F cannot depolymerize actin filaments but retains its severing activity (**Figure 3.22**) (Moriyama and Yahara, 1999, 2002). I showed that cofilin-Y82F, but not cofilin-S94D increased both actin retrograde flow and protrusion frequency of conditioned AC1C2 KO growth cones back to wild-type control levels (**Figure 3.23 and 3.24**), suggesting that the severing activity is pivotal for mediating the effects on the actin cytoskeleton following peripheral nerve lesion. Consistently, expression of cofilin-Y82F in naïve wild-type DRG neurons was sufficient to increase axon outgrowth on the permissive substrate laminin and even to rescue the growth inhibitory effects after plating the naïve wild-type neurons on two different inhibitory substrates (**Figure 3.28**). Analogous to my study, Endo et al. (2003) used the same mutants to investigate their ability to rescue the inhibitory effect on growth upon LIMK1 overexpression in chick DRG growth cones. Similarly, the filament severing activity of cofilin prevailed in exerting AC's effects (Endo et al., 2003). In addition, Flynn et al. (2012) showed that the severing activity of AC organizes space for the protrusion and bundling of microtubules during neuritogenesis and cofilin-Y82F rescued the severe AC1 double knockout phenotype in developing hippocampal and cortical neurons. Interestingly though, in my studies, protrusion length was decreased in cofilin-Y82F expressing and increased in cofilin-S94D expressing AC1C2 KO DRG neurons. As hypothesized in the previous section, a reduced severing activity of cofilin (as is the case in cofilin-S94D expressing neurons) may lead to longer persistence of actin filaments at the leading edge. Actin turnover is decreased and in consequence disassembly of filaments is slower. In contrast, expression of cofilin-Y82F leads to an increase in the severing activity and thus to

a fast fragmentation of filaments in the growth cone periphery, leading to decreased protrusion length as observed in cofilin-Y82F expressing DRG neurons. In conflict with this hypothesis, it has been suggested that AC activity regulates growth cone structure, at least partly by promoting filopodia dynamics (reviewed in Flynn et al., 2007). This idea was prompted by the observation that overexpression of constitutively active human cofilin S3A in chick DRG growth cones and direct loading of *Xenopus* ADF/cofilin S3A protein in chick RGC growth cones, resulted in augmented filopodia length (Endo et al., 2003, Gehler et al., 2004), a phenotype similar to what I observed after a conditioning lesion (**Figure 3.2**). In addition, filopodia branched more frequently and appeared tortuous in chick DRG growth cones expressing human cofilin S3A (Endo et al., 2003). As explanation the authors proposed that one activity of AC is to enhance local actin polymerization, thereby enabling filopodia elongation. However, growth cone morphology was perturbed, as they did not have the classical "fan-shape" (Endo et al., 2003, Gehler et al., 2004). In addition, the C-domain was lost and lamellar protrusions were reduced, suggesting that a second activity of AC is to depolymerize existing actin networks. In conclusion, these results support the notion that the principal role of AC is to stimulate rapid actin turnover by regulating both actin assembly and disassembly. Most likely, the effects of AC activity within growth cones cannot be defined in clear cut categories and are likely regulated in subtly different ways depending on the cells and the extracellular environment analyzed.

4.9 Overexpression of cofilin is sufficient to drive axon growth in vitro

An increasing body of evidence suggests that AC plays a role in regulating actin treadmilling, growth cone motility and extension. For example, ADF is essential for actin-based motility of *Listeria* (Carlier et al., 1997, Rosenblatt et al., 1997) and overexpression of cofilin enhanced *Dictyostelium* cell motility (Aizawa et al., 1996). In addition, the expression of wild-type *Xenopus* ADF/cofilin (XAC) and nonphosphorylatable, constitutively active *Xenopus* ADF/cofilin S3A, but not its S3E mutant that mimics the phosphorylated form of cofilin, increased the neurite length of primary cultured neurons (Meberg and Bamburg, 2000). Endo et al. (2003) further showed that expression of human wild-type cofilin and the S3A

mutant increased axon extension, growth cone motility and growth rate in chick DRG neurons. Similarly, exogenous expression of wild-type and S3A cofilin in embryonic hippocampal neurons only moderately increased the number of neurons extending multiple axons but greatly augmented axon length (Garvalov et al., 2007). Moreover, Flynn et al. (2012) showed that the family of ADF/cofilin provides the required control of actin retrograde flow and dynamics necessary to form neurites during development. In this study, finally, I proved that AC proteins are essential for mediating the effects on actin dynamics and axon growth following a peripheral nerve lesion.

To investigate whether AC proteins are not only necessary, but also sufficient for enhancing axon growth in adult primary sensory neurons, I overexpressed human wild-type and the S3A mutant of cofilin in dissociated naïve DRG neurons. The unphosphorylatable S3A mutant is considered to be "constitutively active", although regulation by other mechanisms (pH, PIP_2-binding, etc...) can still occur. Expression of cofilin-S3A increased axon length by approximately 20% and wild-type cofilin by 40% on the permissive substrate laminin (**Figure 3.25**). Faster actin disassembly through cofilin overexpression enhances actin turnover and may also accelerate polymerization by increasing the pool of polymerization competent actin monomers or oligomers. Overexpression of the other two AC isoforms, ADF and cofilin 2, however, did not lead to an increase of axonal length (**Figure 3.27**). This is consistent with the idea that the main function of ADF is to depolymerize actin, as opposed to cofilin 1, which predominantly severs F-actin filaments (Vartiainen et al., 2002). Cofilin 2, on the other hand, has a weaker actin filament depolymerization activity and displays a much higher affinity for ATP-actin monomers than ADF and cofilin 1 (Vartiainen et al., 2002). It was also shown recently that in contrast to other isoforms, cofilin 2 can bind and disassemble ADP-Pi F-actin filaments (Kremneva et al., 2014). Still, cofilin 2 is the least understood member of the AC family and its exact biochemical and functional properties remain unclear.

Although somewhat counterintuitive, the result that wild-type cofilin enhances axon growth to a larger extent than cofilin-S3A, is mirrored by other studies showing that overexpression of the XAC S3A mutant in rat cortical neurons resulted in an increase in average neurite length of 17%, while wild-type XAC increased neurite length by 60% (Meberg and Bamburg, 2000). Similarly,

overexpression of *Drosophila* wild-type twinstar (the *Drosophila* AC protein orthologue) rescued normal axon growth better than the twinstar S3A mutant in tsr^{null} mushroom body neurons (Ng and Luo, 2004). Moreover, my own preliminary data showed that pharmacological treatment of naïve wild-type DRG neurons with the actin severing drug swinholide A (Bubb et al., 1995) leads to a moderate increase in axon outgrowth (data not shown). Further titration of the drug may yield similar results as overexpression of wild-type cofilin. However, it is feasible that the higher potential of wild-type cofilin to enhance outgrowth compared to cofilin-S3A or swinholide A could be explained by the need for a coupled phosphocycling of AC activity to enhance F-actin turnover and to allow microtubules to penetrate efficiently into the P-domain to promote microtubule-dependent axon growth (see model of "steric hindrance"). A second possibility is that F-actin turnover may follow a bell-shaped dose-response curve for AC activity to function properly and that the S3A mutant potentially lowers this response because of its higher activity (reviewed in Flynn et al., 2007). On the other hand, when naïve neurons were plated on the growth inhibitory substrates Nogo-A or CSPGs, both wild-type cofilin and the S3A mutant of cofilin rescued the axonal growth equally well, suggesting that the ability of cofilin to promote axon growth might also depend on the cell culture substrate used (**Figure 3.26**). In fact, my own preliminary data have shown that overexpression of wild-type or constitutively active cofilin does not increase axon growth in naïve DRG neurons plated on poly-L-lysine. This implies that regulation of cofilin activity is dependent on the specific upstream signaling pathways, which are activated by diverse components contained in the extracelluar environment.

Independent of the substrate and the AC isoform used, though, the effect on axon growth upon overexpressing cofilin was not as great as the growth response obtained following a conditioning lesion. Most likely, this is explained by the fact that AC proteins are not the only players responsible for transducing the conditioning effect. Indeed, as described in the introduction, a plethora of regeneration associated genes and factors that are upregulated upon peripheral axotomy have been described. Temporal aspects may contribute further to the reduced effect observed. A conditioning lesion results in numerous intrinsic changes that can act en masse in the DRG neurons for 6-7 days *in vivo* prior to culturing of the neurons. Naïve DRG neurons, on the other hand, are only

subjected to overexpression of cofilin for 16-18 hours *in vitro*. It is thinkable, that this time frame is too short to lead to more drastic effects on axon length. In future studies, it should be tested whether overexpressing cofilin *in vivo* for several days prior to culturing could enhance axon outgrowth further. This could be achieved by electroporating or injecting dorsal root ganglia with cofilin expressing DNA plasmids or adeno-associated viruses, respectively. Moreover, the lower levels of exogenous cofilin need to compete with the abundantly expressed intracellular cofilin, masking potential effects of cofilin overexpression. In consequence, it might be more informative to perform overexpression studies in an AC free setting, as is the case in the AC1C2 knockouts or by fully inhibiting AC activity pharmacologically.

In addition, it needs to be considered that cofilin activity is a highly regulated process. In order to be activated and functional, cofilin needs to be phosporylated by the appropriate phosphatases. Hence, it is conceivable that introducing cofilin alone might not be sufficient. In fact, despite being necessary for actin dynamics (as shown in this thesis project), cofilin does not appear to be sufficient under normal conditions, and auxiliary factors appear to be required to help cofilin overcome intracellular obstacles otherwise inhibiting actin disassembly (reviewed in Brieher, 2013). Coexpression of cofilin and its positive upstream regulators such as SSH1 (Niwa et al., 2002), chronophin (Wiggan et al., 2005) or calcineurin (Wang et al., 2005) could be beneficial for axon outgrowth. In addition, it was recently shown that Aip1 (actin-interacting protein 1), a cofilin-dependent auxiliary factor, facilitates actin destabilization through faster severing and accelerated monomer loss from barbed and pointed ends (Nadkarni and Brieher, 2014, Gressin et al., 2015). Also, cyclase-associated protein (CAP) was found to accelerate cofilin-dependent severing, enabling it to sever actin across the range of physiological pHs (Normoyle and Brieher, 2012). Myosin II appears to be another promising candidate involved in regulating actin dynamics in the axon shaft and growth cone. In fact, down-regulation of myosin IIA and myosin IIB resulted in decrease of neurite outgrowth in N2A cells (Wylie and Chantler, 2001). And using fluorescent speckle microscopy (FSM) to assess actin dynamics, Medeiros et al. (2006) reported that inhibition of myosin II decreased retrograde flow by 51% in *Aplysia* bag cell neurons. In growth cones of myosin $IIB^{-/-}$ superior cervical ganglion neurons, however, retrograde flow of F-actin was enhanced (Brown and Bridgman,

2003). In addition, myosin II inhibition alone led to an increase in supernumerary axons in embryonic hippocampal neurons. And in conjunction with cofilin overexpression, low levels of myosin II inhibition led to a greater increase in axonogenesis than either treatment alone (Flynn, 2008). In fact, own preliminary data have also shown that inhibition of myosin II ATPase activity using blebbistatin or inhibiting myosin light chain (MLC) kinase using ML-7 led to an increase in axonal length of 40% in adult naïve DRG neurons. Hence, further elucidation of the mechanisms of actin turnover and all the involved players will be essential to future studies in understanding axon growth and regeneration.

4.10 Concluding remarks

To promote our understanding of the intracellular mechanisms governing the intrinsic growth competence of adult primary sensory neurons, this study focused on one of the most robust regeneration paradigms: the conditioning effect. My data provide evidence that growth cone dynamics and high actin turnover are necessary for rapid axon extension following a peripheral nerve lesion. The family of ADF/cofilin drives actin retrograde flow and thus regulates axon extension and regeneration in adult DRG neurons. The underlying mechanism entails dynamizing and restructuring of F-actin. Specifically, the severing activity of AC proteins is of central importance for actin dynamics and retrograde flow necessary for axon extension and regeneration. At the same time microtubules are stabilized in the axon shaft and mitochondria and vesicles transported into the periphery of the growth cones, providing the necessary substrates and material for rapid axon elongation. It is fascinating that a similar process transforms newly born neurons, which are spherical, into neurons containing neurites (Flynn et al., 2012). It thereby gives molecular support to the idea that the regeneration of axons relies on reactivation of the developmental program of axon formation, which is the initial process of neuronal polarization.

A model of the proposed action of ADF/cofilin following a peripheral nerve lesion and the major findings of my thesis project are summarized in **Figure 4.1**.

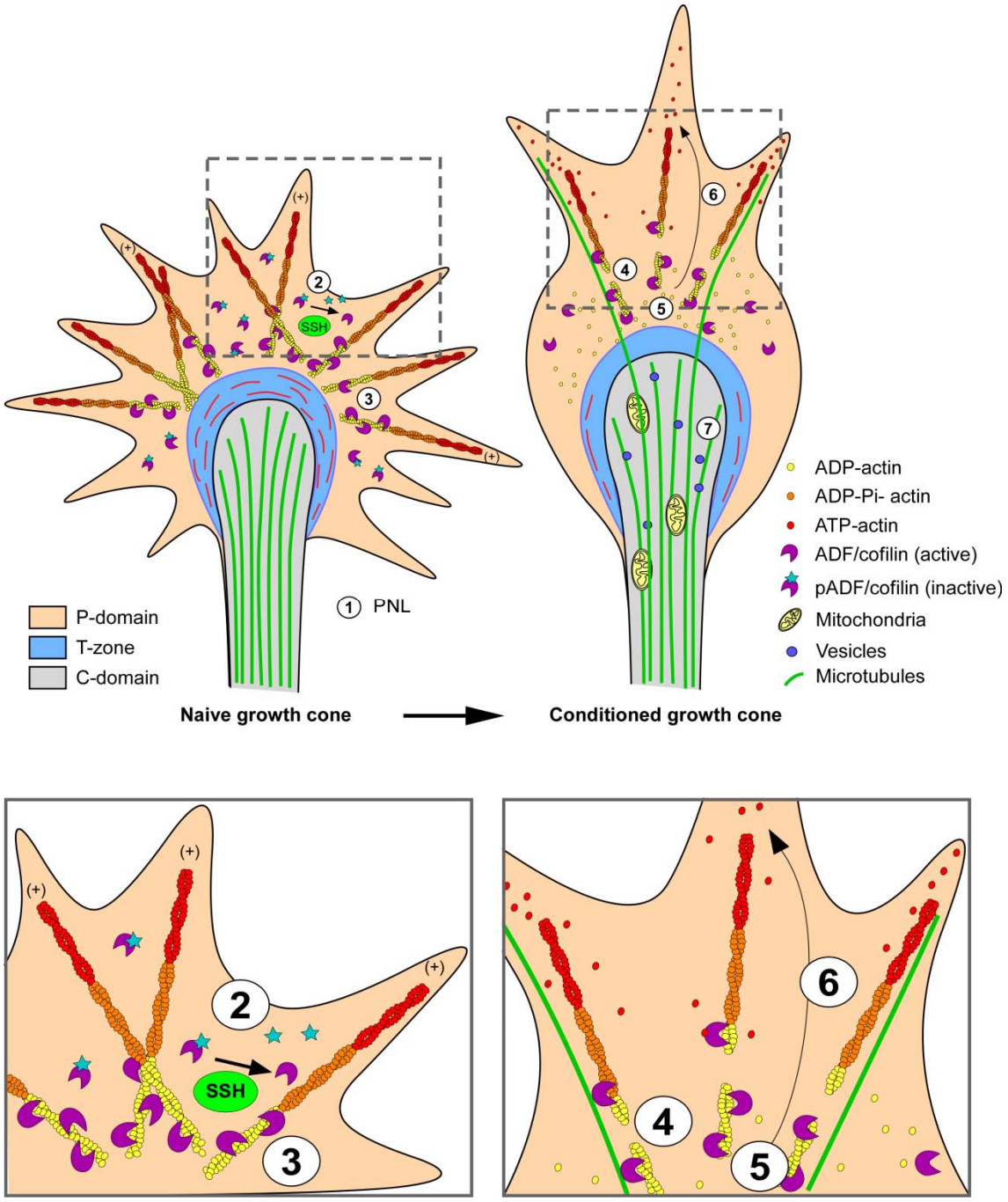

Figure 4.1. Proposed model of ADF/cofilin action upon PNL. 1) Upon peripheral nerve lesion, expression of RAGs induces the activation and synthesis of cytoskeleton associated proteins. 2) Among others, the phosphatase slingshot homolog 1 (SSH1) is activated and dephosphorylates ADF/cofilin, thereby activating it. 3) ADF/cofilin binds to ADP-actin subunits at the (-) end of the F-actin filaments. 4) The binding of ADF/cofilin induces a conformational twist in the filaments that propagates and finally leads to the severing of the filaments. 5) The resulting shorter ADP-actin oligomers are disassembled into ADP-actin monomers and recycled to ATP-actin. 6) The resulting ATP-actin monomers are added to the free G-actin pool and are available for further nucleation and polymerization of F-actin filaments at the leading edge. In consequence, actin turnover is increased and the dense actin meshwork is loosened. 7) In addition, microtubules are stabilized and can protrude from the C-domain into the P-domain of the growth cone. Mitochondria and vesicles are transported along microtubules into the periphery, supplying the growth cone with the necessary energy and material for rapid growth.

5 MATERIALS AND METHODS

5.1 Materials

5.1.1 Chemicals

Name	Supplier	Product no.
Agarose (Standard, low EEO)	Biomol GmbH	50402.100
Ammonium chloride	Merck	1.01145.0500
Ammonium persulfate (APS)	AppliChem	A2941,0100
B-27 supplement (50x)	Gibco – by life technologies	17504-044
Boric acid	Sigma	B6768
Borax	Sigma	71996
Bradford solution	Applichem	A6932,0250
Bromphenol blue	Merck	1.08122.0005
Bovine serum albumin (BSA)	Sigma	A7906
Collagenase Type I	Worthington	LS004196
Complete, Mini, EDTA-free protease inhibitor cocktail (10x)	Roche	11836170001
Chondroitin sulphate proteoglycans (CSPGs; 1mg/ml)	Millipore	CC117
D(+) Glucose monohydrate	Merck	104074
Deconex 11 Universal	Borer Chemie	500100.00-F10W
4',6-Diamidino-2-phenylindole (DAPI)	Invitrogen	D21490
Di-Sodium hydrogen phosphate (Na_2HPO_4)	Merck	1065861000
DMEM + GlutaMAX™-I	Gibco – by life technologies	31966-021
DNA ladder (100bp)	New England Biolabs	N3231S
dNTPs (set of dATP, dCTP, dGTP, dTTP)	Promega	U1240
Dimethyl sulfoxide (DMSO)	Sigma	D5879
Ethylene glycol-bis (2-aminoethylether)-N,N,N´,N´-tetraacetic acid (EGTA)	Sigma	E3889-100G
Ethanol, absolute	Merck	8.18760.1000
Ethanol, 70%	AppliChem	A0565,9010
Fast Green	Sigma	F7258-25G
Fluoromount mounting medium	Sigma	F4680-25ml
Foetal bovine serum (FBS)	Sigma	F7524
Gelatin, from cold water fish skin	Sigma	G7765
GelRed (10 000x in water)	Genaxxon bioscience	M3199.1010
Glutaraldehyde (25%) aqueous solution	MP Biomedicals	195199
Glutaraldehyde (50%) EM grade	Electron Microscopy	111-30-8

	Systems	
GoTaq® Green Master Mix	Promega	M7122
GoTaq® Flexi DNA Polymerase	Promega	M8305
Glycerol	Roth	7530.1
Glycine	Sigma	G8898-1KG
HBSS	Gibco – by life technologies	14025-100
Hepes buffer solution (1M)	Genaxxon bioscience	C4212.0100
Horse serum	PAN Biotech	P30-0702
Hydrochloric acid (HCl, 1N)	Roth	K025.1
Hydrochloric acid (≥37%)	Sigma	84418-1L
Hydrogen peroxide (H_2O_2, 30%)	Merck	1.07210.0250
I-Block (Tropix)	Applied Systems	T2015
Isopropanol	Roth	9866.1
Laminin (1mg/2ml)	Roche	11 243 217 001
L-Glutamine (200mM; 100x)	Gibco – by life technologies	25030-024
M1 embedding matrix (Shandon)	Thermo Scientific	1310
Magnesiumchloride (MgCl)	Sigma	M8266-100g
Marker (Page Ruler Plus Prestained)	Invitrogen	26619
ß-Mercaptoethanol	VWR	436024C
Methanol, 100%	Roth	CP43.2
Midori Green Advance	Nippon Genetics	MG04
Milk powder (nonfat, dried)	AppliChem	A0830,1000
Neurobasal-A Medium	Gibco – by life technologies	12349-015
Normal donkey serum	Sigma	D9663
Normal goat serum (NGS)	Sigma	G9023-10ML
rrNogo-A/Fc chimera	R&D Systems	3728-NG
PBS (10x) powder	AppliChem	A0965,9050
Paraformaldehyde	Merck	104005
Penicilline/Streptomycine	Gibco – by life technologies	15140-122
PhosSTOP phosphatase inhibitor cocktail (10x)	Roche	04906845001
Pipes (1,4-Piperazinediethanesulfonic acid)	Sigma	P-1851
Polyacrylamide (PAA) 40% (29:1)	AppliChem	A0385,0500
Poly-L-lysine	Sigma	P-2636
Ponceau S solution	AppliChem	A2935,0500
Potassium chloride (KCl)	AppliChem	A3980,0500
Potassium dihydrogen phosphate (KH_2PO_4)	Merck	1.04873.0250
Red Load Taq Master/high yield	Jena Bioscience	PCR-106L
Sodium dodecyl sulfate (SDS)	Sigma	L4509-500g

Sodium chloride (NaCl)	Merck	106404
Sodium hydroxide solution (NaOH; 1N)	Roth	K021.1
Sodium hydroxide pellets (NaOH)	Merck	1064821000
Sucrose	Fluka	84100-1Kg
Super Signal West Dura Extended Duration Substrate	Thermo Scientific	34076
Super Signal West Femto Maximum Sensitivity Substrate	Thermo Scientific	34095
Tris acetate (TAE) buffer (50x)	AppliChem	A1691,1000
TEMED	Sigma	T9281-25ml
Triton X-100	Sigma	X100-100ML
Trizma base	Sigma	T1503-1KG
Trypsin-EDTA (0.25%; 1x)	Gibco – by life technologies	25200-056
Tween 20	Merck	8.22184.0500

5.1.2 Drugs

Drug name	**Stock**	**solvent**	**Supplier**	**Function**
CSPGs	1mg/ml	PBS	Millipore	Inhibitory substrate
Cytochalasin D	10mM	DMSO	Sigma	Destabilization of F-actin
Jasplakinolide	1mM	DMSO	Molecular Probes	Actin stabilization
Nocodazole	6.67mM	DMSO	Sigma	Microtubule destabilization
Nogo-A	100µg/ml	PBS	R&D Systems	Inhibitory substrate
Taxol	5mM	DMSO	Sigma	Microtubule stabilization

Single-use aliquots of the drug stock solutions were kept at -20°C.

5.1.3 Commercial kits

Name	**Supplier**	**Product no.**
EndoFree Plasmid Maxi Kit	Qiagen	12362
Mouse Neuron Nucleofector® Kit	Lonza (Amaxa)	VPG-1001
Rat Neuron Nucleofector® Kit	Lonza (Amaxa)	VPG-1003
Red Load Taq Master / high yield	Jena Bioscience	PCR-106L
Slingshot-1L Phospho-Regulation Antibody Sampler Kit	ECM Biosciences	SK6410

5.1.4 Equipment

Name and application	Model	Supplier
General		
Scale	Scout Pro 400g	Scout
Fine scale	CPA 225D	Sartorius
pH meter	Seven Easy	METTLER Toledo
Magnetic stirrer	RH Basic 2	IKA
Primary Cell Culture		
Incubator	240i	HERAcell
Sterile hood	Mars safety class 2	Scanlaf
Stereomicroscope	Discovery.V8 SteREO	Zeiss
Cold light source	KL 1500 LCD	Schott
Centrifuge	5702	eppendorf
Nucleofector device	II	Lonza
Microscope	PrimoVert	Zeiss
Waterbath	1003	GFL
Metal racks	Custom made	MPI
Vacuum pump	BVC21	Vacuubrand
Vortex	VortexMixer	Corning LSE
Tabletop centrifuge	Mini Microcentrifuge	Corning LSE
Pipetting controller	Accu-jet® pro	Brand
Thermo oven	OGS60	HERA
PCR-Genotyping		
Thermomixer	Thermomixer Comfort	Eppendorf
Centrifuge	5424R	Eppendorf
Electrophoresis system	Blue Marine 100 and 200	Serva Electrophoresis
Power pack	P25	Biometra
Microwave	Grill – Hot Air	Sharp
Thermocycler	T3000	Biometra/ Analytik Jena
Imaging system	Uvsolo TS	Biometra/ Analytik Jena
Printer	P95	Biometra/ Mitsubishi
In vivo DRG injections/ electroporation		
Cold light source	KL 1500 LCD	Schott
Electro Square Porator	ECM 830	BTX Harvard Apparatus
Electrodes	Tweezertrodes flat 1.2mm	VWR
Hot bead sterilizer	18000-45	FST
Medium heating plate (15 x 25cm)	502196	WPI
Pneumatic picoPump	PV 820	WPI

Pipette puller	DMZ-Puller	Zeitz
Anesthesia system	931401	VetEquip Inc.
Rectal probe	RET-3	WPI
Scale	440-49A	Kern
Shaver	PG-6030	Remington
Stereomicroscope	M651	Leica
Temperature Controller	ATC 1000	WPI
Western Blotting		
Photometer	Biophotometer plus	Eppendorf
Shaker	Rocking Platform Shaker	VWR
Power pack	Power Pac basic	Bio-Rad
Blotting system	Mini-Protean®Tetra System	Bio-Rad
Mini-Cell Electrophoresis System	Xcell Sure Lock™	Bio-Rad
Gel imaging system	Chemidoc	Bio-Rad
Tabletop processor	Curix 60, Type 9462/160	AGFA
Developer cassettes	20x40cm	Okamoto
Plasmid preparation		
Shaker	Ecotron	Infors HT
Centrifuge	Multifuge X3R	Heraeus
Compact Incubator	B15	Heraeus
Nanodrop	2000C	ThermoScientific
Immunocytochemistry and histology		
Cryostat	CM3050S	Leica
Liquid nitrogen tanks	Dewar-Transport Typ B	VWR
Slide warmer	IKA® C-MAG HP10	IKA
Ice box	300 x 228 x 200 mm, 4L	Neolab
Vacuum Diaphragm Pump	MVP 070-3 C	Pfeiffer
Fluorescence Microscopy		
Fluorescence microscope	AxioObserver.D1	Zeiss
Illuminator	HXP 120C	Zeiss
Black and white camera	AxioCam MRm	Zeiss
Colour camera	AxioCam Icc1	Zeiss
Objectives	10- 100x Plan Neon/Apo	Zeiss
Gas Incubation System	For CO_2 and O_2, The brick	ibidi
Heating System	System 1, Universal Fit	ibidi

5.1.5 Consumables

Material	Type	Supplier
Cassettes for western blot	1.5mm	Invitrogen
Cell culture dishes	4 well dish, #10507591 P35G-1.5-14-C P35G-1.5-20-C 6 cm	NUNC, Fisher Scientific MatTek MatTeK NUNC, Fisher Scientific
Coverslips	Ø 13mm, #01-115 30 24 x 50 mm, no. 1.5	Marienfeld Marienfeld
Cuvettes	Semi-micro, #634-0678	VWR
Disposable base molds	15mmx15mmx5mm , #27147-2	Ted Pella Inc.
Eppendorf tubes	1.5ml, 2ml	Eppendorf
Filter bottle system	150ml	Corning
PVDF membrane	Immobilon-P^{SQ}, pore size 0.2µm	Millipore
Falcon tubes (general)	50ml, 15ml	nerbeplus
Falcon tubes (cell culture)	15ml	Corning
Immersion oils	Immersol 518 F Immersol W 2010	Zeiss Zeiss
Micropistille (10x)	0030 120 973	Eppendorf
Microscope slides (immunocytochemistry)	Mattrand, 76x20x1mm, #11699938	ThermoScientific
Microscope slides (histology)	Superfrost Plus, #J1800AMNZ	ThermoScientific
Microtome-blades	819	Leica
PCR 8er-SoftStrips	0.2ml, transparent, high profile, 710990	Biozym
Pipette tips (non-sterile)	1000µl, 200µl, 20µl, 10µl	nerbeplus
Pipette filter tips (sterile)	1000µl, 200µl, 20µl, 10µl	nerbeplus
Soft nitrile gloves	Size M (7-8)	Th. Geyer
Semperguard® latex gloves	Semperit, powderfree	Semperguard
Supported nitrocellulose membrane	0.45 µm, 30 cm x 3 m	Bio-Rad
Syringes (luer lock, without needle)	50ml, 20ml	Terumo
Syringe driven filter unit	0.22µm PES express	Millex-GP
Western Blot films	CL-X PosureTM Film	ThermoScientific
Western Blot films	Carestream Bio Max Light Film	Kodak
Whatman™ paper	46x57cm, 2300916	Whatman

5.1.6 Surgical instruments, drugs and supplies

Name	Supplier	Product no.
Adson forceps – serrated straight 12cm	Fine Science Tools	11006-12
Adson forceps – 1x2 teeth 12cm	Fine Science Tools	11027-12
Askina gauze compress 10x10cm	B. Braun Melsungen AG	9031324
Agricola retractor – 3.5cm spread	Fine Science Tools	17005-04
Baytril 2.5% Vet injection solution (active reagent: Enrofloxacin)	Bayer Vital GmbH -Animal Health-	PZN 3543238
Bepanthen® Eye- and nose ointment	Bayer Vital GmbH	1578681
Borosilicate glass capillaries	World Precision Instruments	TW-100-4
Braunol® povidon iodine solution	B. Braun Melsungen AG	9322531
Cotton tipped applicators	Stoelting	50975
Crile hemostat curved 14cm	Fine Science Tools	13005-14
Dumont #2 laminectomy forceps – Inox	Fine Science Tools	11223-20
Dumont #5 forceps – Dumoxel	Fine Science Tools	11251-30
Feeding needle – 20 gauge, 3cm	Fine Science Tools	18060-20
Fine iris scissors – Large loops, straight	Fine Science Tools	14106-09
Forene (active reagent isoflurane)	Abbott GmbH	PZN 4831850
Friedman rongeur – 2.5mm cup curved	Fine Science Tools	16000-14
Friedman-Pearson rongeur – 0.5mm cup curved	Fine Science Tools	16221-14
Gelita tampon	B. Braun Melsungen AG	2070154
Glucose 5% (G5) solution – 100ml	B. Braun Melsungen AG	3154910
Graefe forceps – 1x2 teeth 0.8mm tips straight	Fine Science Tools	11053-10
Hartman hemostat curved 10cm	Fine Science Tools	13003-10
Heparin-natrium "Multi" 10.000iU	B. Braun Melsungen AG	PZN 3212010
Iris scissors – ToughCut straight 9cm	Fine Science Tools	14058-09
Isotonic 0.9% NaCl solution – 100ml	B. Braun Melsungen AG	3200905
Isotonic 0.9% NaCl solution – 1000ml	B. Braun Melsungen AG	3200970
Ketamine 10% Vet injection solution (active reagent: ketamine-hydrochlor.)	Medistar	/
Lidocain 2% injection solution (active reagent: lidocaine hydrochloride)	RotexMedica	PZN 3346176
Malleus nipper straight	Fine Science Tools	16140-11
Mayo scissors – ToughCut straight, 15cm	Fine Science Tools	14110-15
MicroFil – 28ga, 67mm	World Precision Instruments	MF28G67-5

Moria iris forceps – 0.5mm tip curved	Fine Science Tools	11373-12
Olsen-Hegar needle holder 12cm	Fine Science Tools	12002-12
Omnican® 50 syringe	B. Braun Melsungen AG	9151117
Reflex wound clip applicator, 7mm (mice)	Fine Science Tools	12031-07
Reflex wound clip applicator, 9mm (rats)	Fine Science Tools	12031-09
Reflex wound clips, 7mm (mice)	Fine Science Tools	12032-07
Reflex wound clips, 9mm (rats)	Fine Science Tools	12032-09
Rompun 2% (active reagent: Xylasine hydrochloride)	Bayer Vital GmbH -Animal Health-	PZN 1320422
Scalpel handle #3 – 12cm	Fine Science Tools	10003-12
Scalpel blades #10	Fine Science Tools	10010-00
Scalpel blades #15	Fine Science Tools	10015-00
Scissors – ToughCut sharp/blunt, 13cm	Fine Science Tools	14054-13
Sofsilk 4.0 suture material	Himed	S-1174
Sofsilk 5.0 suture material	Himed	S-1173
Spring scissors angled to side	Fine Science Tools	15006-09
Sugi® – Sterile Absorption Spears	Kettenbach Medical	30601
Temgesic (active reagent: Buprenorphine)	Essex Pharma	PZN 345928
Tissue forceps slim – 1x2 teeth, 12cm	Fine Science Tools	11023-12
Wire knife carrier	McHugh Milieux	M120
Wire knife (retractable – 1.5mm curvature)	McHugh Milieux	M121

5.1.7 Media, buffers and standard solutions

Name	Ingredients	Preparation and storage
Ammonium chloride (50mM)	1.34 g ammonium chloride in 500 ml PBS	Store at RT
Ammonium persulfate solution (10%)	10g APS Ad 100ml H_2O	Aliqout and store at -20°C
Blocking solution	2% fetal bovine serum 2% bovine serum albumin 0.2% fish gelatin in PBS	Aliquot and store at -20°C
Borate buffer	1.24g boric acid 1.9g Borax (Sodium borate) in 400 ml H2O	Adjust to pH 8.5
BSA (5%)	5g BSA Ad 100ml TBS-T (1x)	Store at 4°C
Collagenase solution (3000 U/ml)	1 g collagenase I (191 U/mg) 63ml Hepes buffered (10mM) HBSS	Filter sterilize with 0.22µm filter and store at -20°C
Complete neurobasal (NB) medium	48ml NB-A 0.5ml Pen/Strep (100x) 0.5ml L-Glutamine (100x) 1ml B-27 supplement	Filter sterilize with 0.22µm filter and store at 4°C for up to 2 weeks
Complete neurobasal (NB) medium containing 5% horse serum	45.5ml NB-A 0.5ml Pen/Strep (100x) 0.5ml L-Glutamine (100x) 1ml B-27 supplement 2.5ml horse serum (heat inactivated)	Filter sterilize with 0.22µm filter and store at 4°C for up to 2 weeks
DMEM containing 10% horse serum	45ml DMEM (High Glucose, GlutaMAX™) 5ml horse serum (heat-inact.)	Filter sterilize with 0.22µm filter and store at 4°C for up to 1 week
EDTA (0.5M)	93,5g EDTA*2H_2O 400ml H_2O NaOH (1M) solution or NaOH pellets	Stir vigorously and adjust the pH to 8.0 using NaOH. Dilute the solution to 500ml with H_2O and filter it. Store at RT
EGTA (0.5M)	19.02g EGTA 60ml H_2O NaOH (1M) solution or NaOH	Stir and adjust the pH to 8.0 using NaOH. Dilute the solution to 100ml with H_2O

	pellets	and filter it. Store at RT
Gel buffer (2x)	0.25M Tris-HCl pH 6.8 (7.6g) 0.2% SDS (5ml of 10% SDS sol.) Ad 250ml H_2O	Store at RT
Gel buffer (4x)	1.5M Tris-HCl pH 6.8 (45.4g) 0.4% SDS (10ml of 10% SDS sol.) Ad 250ml H2O	Store at RT
Glycine (0.1M) in TBS	3,75g Glycine in 500ml TBS (1x)	Store at RT
Hepes (1M)	23,8 g Hepes in 100 ml H_2O	Adjust to pH 7.25 and autoclave
Hepes buffered HBSS (10mM)	5 ml Hepes (1M, pH 7.25) in 500 ml HBSS	Store at 4°C
Laminin solution	Laminin (1mg/2ml) Complete NB medium	Laminin is diluted 1:100 in complete NB medium and added to the glass coverslips 2h prior to culturing the cells
Laemmli buffer (5x)	60mM Tris-HCl pH 6.8 2% SDS 10% Glycerol 5% β-mercaptoethanol 0.01% bromophenol blue	Store at RT
Loading buffer (6x)	<u>for 15ml</u> 300mM Tris pH 6.8 (3ml of 1.5M sol.) 600mM ß-Mercaptoethanol (0.63ml) 6% SDS (0.9g) 60% glycerol (9ml) 0.1% bromphenolblue (0.015g)	Aliquot and store at -20°C
Lysis buffer (for WB)	<u>for 100ml</u> 50mM Tris pH 7.4 (5ml of 1M sol.) 150mM NaCl (0.88g) 1mM EDTA (200µl of 0.5M sol.) 1% Triton-X 100 (1ml)	Store at 4°C, add 100µl PhosSTOP and 100µl Complete Mini to 800µl Lysis buffer immediately before using
Lysis buffer (for PCR)	<u>For 500ml</u> 50ml 1M Tris-HCl pH 8.0 5ml 0,5M EDTA 5ml 20% SDS	Store at RT

	20ml 5M NaCl Ad 500ml with H_2O	
$MgCl_2$ (1M)	20.33 g MgCl2*6 H_2O Ad 100ml with H_2O	Dissolve $MgCl_2$ in 100ml H_2O, filter sterilize and store at RT
Milk (5%)	5g milk powder Ad 100ml with TBS-T (1x)	Store at 4°C
NaCl (5M)	for 500ml 146,1g Nacl Ad 500ml with H_2O	Autoclave and store at RT
NaOH solution (50mM)	250µl NaOH (1M) 5ml H_2O	Always prepare fresh before using
Na_2HPO_4 (0.2 M)	28.2g Na_2HPO_4 (anhydrous) Ad 1000ml with H_2O	Store at RT
NaH_2PO_4 (0.2 M)	27.4g NaH_2PO_4 monohydrate Ad 1000ml with H_2O	Store at RT
Paraformaldehyde/sucrose (16%) →for ICC	16 g Paraformaldehyde 16 g sucrose in 100 ml PBS	Adjust to pH 7.4, filter sterilize, aliquot and store at -20°C → 4% dilutions are prepared from this stock in PBS
Paraformaldehyde (16%) → for histology/EM	800ml H_2O 800ml PBS (1M) 320g Paraformaldehyde 15-20 NaOH pellets	320g Paraformaldehyde are added to preheated 800ml H_2O (60°C), mixed and stirred for 15 minutes. Then, NaOH pellets are added until solution is clear, 800ml 1M PBS are added and the solution allowed cooling. The solution is filtered, adjusted to pH to 7.4 and stored at 4°C
PB buffer (0.1M) pH 7.4	405ml 0.2M Na_2HPO_4 95ml 0.2M NaH_2PO_4 Ad 1000ml with H_2O	Store at RT
PB buffer (0.1M) pH 6.0	61.5ml 0.2M Na_2HPO_4 438.5ml 0.2M NaH_2PO_4 Ad 1000ml with H_2O	Store at RT
PBS (1M)	114,9g Na_2HPO_4 26,41g NaH_2PO_4 90g NaCl Ad 1000ml with H_2O	Add ingredients and preheat to 50°C until solution is clear, adjust pH to 7.4 with HCl or NaOH, store at RT

0.1M PBS/Sucrose (30%)	300g Sucrose 10ml PBS (1M) Ad 100ml with H_2O	Filter sterilize and store at 4°C
PHEM buffer (5x)	<u>for 250 ml</u> 300 mM PIPES (4.54 g) 125 mM Hepes (1.49g) 50 mM EGTA (5ml EGTA [500mM]) 10 mM MgCl2 (0.5ml MgCl2 [1M]) in H_2O	Adjust to pH 6.9 and store at RT → For fixation 4% PFA/sucrose, 0.25 % glutaraldehyde and 0.1 % triton X-100 are added
Phosphate buffered saline (PBS)	0.2g KCl 0.2g KH_2PO_4 1.15g Na_2HPO_4 8g NaCl in 1L H_2O	Autoclave and store at RT
Poly-L-lysine solution	1mg/ml poly-L-lysine hydrobromide in borate buffer	solution is sterile filtered and stored at 4°C for up to 1 week → Glass coverslips and culture dishes are incubated with the solution overnight and then washed 3x with sterile H_2O
RIPA buffer (10x) + Inhibitors	0.5M Tris-HCl pH 8.0 1.5M NaCl 10% Triton-X100 2.5% deoxycholic acid 1% SDS 10x PhosphoSTOP 10x Complete Mini	The 10x solution is stored at -20°C A 5x RIPA solution is prepared by adding 100µl of sterile water to 100µl 10x RIPA
Running buffer (1x)	100ml transfer buffer (10x) 10ml SDS (10%) Ad 1000ml with H_2O	Store at RT and use up to 5 times
SDS (10%)	10g SDS Ad 100ml with H_2O	Store at RT
SDS (20%)	20g SDS Ad 100ml with H_2O	Store at RT
SDS-PAGE gel (10% separation gel)	10ml H2O 5ml 4x Gelpuffer 5ml 40% acrylamide 200µl 10% SDS 100ul 10% APS	Pour gel into cassettes and add 1-2ml isopropanol, allow to polymerize for 15 minutes, remove isopropanol, pour collection gel solution and

	15ul TEMED	add comb
SDS-PAGE gel (collection gel)	3,9ml H2O 5ml 2x Gelpuffer 1ml 40% acrylamide 100µl 10% SDS 50ul 10% APS 10ul TEMED	Allow to polymerize for 15 minutes, wrap in wet paper and store in a plastic bag at 4°C until further use
TAE buffer	20ml TAE buffer (50x) Ad 1000ml with H_2O	Store at RT
TBS (10x)	0.2M Tris (24.2g) 1.37M NaCl (80g) Ad 1000ml with H_2O	Adjust to pH 7.6 and store at RT
TBS-T (1x)	100ml TBS (10x) 1ml Tween20 Ad 1000ml with H_2O	Store at RT
Transfer buffer (10x)	1.92M Glycine (144g) 0.25M Tris pH 8.3 (30g) Ad 1000ml with H_2O	Adjust to pH 8.3 and store at RT
Transfer buffer (1x)	200ml Methanol 720ml H_2O 80ml transfer buffer (10x)	Cool at 4°C until use
Tris-HCl (1M)	121.1g Trizma base Ad 1000ml with H_2O	Adjust to pH 8.8 with HCl (37%), autoclave and store at RT
Tris-HCl (1.5M)	54.513g Trizma base Ad 300ml with H_2O	Add Trizma base to 200ml H_2O, adjust to pH 8.8 with HCl (37%), fill up to 300ml and store at RT
Triton (10%)	10% (v/v) Triton X-100 in PBS	Store at RT
Trypsin (0.25%)	1ml Hepes (1M, pH 7.25) 99ml 0.25% Trypsin-EDTA solution	Aliquot and store at -20°C

5.1.8 Antibodies

5.1.8.1 Primary antibodies

Name and application	Dilution	Type	Supplier	Product no.
anti-acetylated tubulin (clone 6-11B-1) for ICC	1:500	Mouse monoclonal, ascites fluid	Sigma	T-6793
anti-tyrosinated tubulin (YL1/2) for ICC	1:300	Rat monoclonal	Abcam	ab6160 (purified)
anti-ßIII tubulin (Tuj1) for ICC	1:1000	Mouse monoclonal	Covance	MMS-435P
anti-ßIII tubulin (Tuj1) for WB	1:10000	Rabbit polyclonal	Sigma	T2200
anti-tcofilin (D3F9) for WB	1:3000	Rabbit monoclonal	Cell Signaling	#5175
anti-tcofilin for IHC	1:200	Rabbit polyclonal	Abcam	ab42824
anti-cofilin 1 for WB	1:2000	Rabbit polyclonal	W. Witke	Custom-made
anti-cofilin 2 for WB	1:2000	Rabbit polyclonal	W. Witke	Custom-made
Anti-ADF for WB	1:5	Mouse monoclonal	W. Witke	(raw supernatant from hybridoma)
anti-pCofilin 1 (Ser3) for WB and IHC	1:1500	Rabbit monoclonal	Cell Signaling	#3313
anti-GAPDH for WB	1:20000	Mouse monoclonal	Acris	ACR001P
anti-GFAP for IHC	1:500	Rabbit polyclonal	Dako	Z0334
Anti-SSH1L for WB	1:500	Rabbit polyclonal	ECM biosciences	SP1711
Anti-pSSH1L for WB	1:500	Rabbit polyclonal	ECM biosciences	SP3901
Anti-LIMK1 for WB	1:250	Mouse monoclonal	BD	611748
Anti-pLIMK1/2 [pYpT$^{507/508}$] for WB	1:400	Rabbit polyclonal	Invitrogen	44-1076G

5.1.8.2 Secondary antibodies

Specificity	Dilution	Host	Fluorochrome	Supplier
anti-mouse	1:500	Goat	Alexa Fluor 488	Invitrogen
	1:500	Goat	Alexa Fluor 555	Invitrogen
	1:5000	Sheep	HRP labelled	GE Healthcare
anti-rat	1:500	Goat	Alexa Fluor 568	Invitrogen
anti-rabbit	1:500	Goat	Alexa Fluor 350	Invitrogen
	1:400	Goat	Alexa Fluor 488	Invitrogen
	1:500	Donkey	Alexa Fluor 488	Invitrogen
	1:500	Donkey	Alexa Fluor 568	Invitrogen
	1:5000	Donkey	HRP labeled	GE Healthcare
Other dyes				
Rhodamine-Phalloidin	1:75	/	TRITC (red)	Invitrogen
DAPI	1:10000	/	/ (blue)	Invitrogen

5.1.9 Plasmids

Name	Selection marker	Description	Reference
Lifeact-RFP	Kan	17-amino-acid peptide staining F-actin structures bound to RFP	Riedl et al., 2008
Lifeact-pEGFP-N1	Kan	17-amino-acid peptide staining F-actin structures bound to eGFP	Riedl et al., 2008
pmRFP-N1	Kan	Control vector encoding red fluorescent protein (RFP)	Flynn et al., 2012
hCofilinWT-mRFP-N1	Kan	Human cofilin (wild-type) bound to RFP	Flynn et al., 2012
hCofilinS3A-mRFP-N1	Kan	Human cofilin S3A mutant bound to RFP, (nonphosphorylatable - constitutively active)	Flynn et al., 2012
hCofilinS94D-mRFP-N1	Kan	Human cofilin S94D mutant bound to RFP (nonsevering - can only depolymerize actin)	Flynn et al., 2012
hCofilinY82F-mRFP-N1	Kan	Human cofilin Y82F mutant bound to RFP (nondepolymerizing - can only sever actin)	Flynn et al., 2012
hADF WT-mRFP-N1	Kan	Human ADF (wild-type) bound to red fluorescent protein (RFP)	J. Bamburg
eGFP-mCof2	Kan	Mouse cofilin 2 (wild-type) bound to eGFP	W. Witke

5.1.10 Primers

Name	Sequence	Supplier
ADF A: Lac-3	5'- GAT TAA GTT GGG TAA CGC C -3'	Sigma
ADF B: ADF-150-3	5'- GAA GAA GGC AAA GAG ATC TT -3'	Sigma
ADF C: ADF-INT2-5	5'- CTA CCT AAA GGG CAT CCT TC -3'	Sigma
Cofilin A	5'- CGC TGG ACC AGA GCA CGC GGC ATC -3'	Sigma
Cofilin B	5'- CTG GAA GGG TTG TTA CAA CCC TGG -3'	Sigma
Cofilin C	5'- CAT GAA GGT TCG CAA GTC CTC AAC -3'	Sigma
Rosa-1	5'- AAG GGA GCT GCA GTG GAG TA -3'	Sigma
Rosa-2	5'- CCG AAA ATC TGT GGG AAG TC -3'	Sigma
Rosa-3	5'- GGC ATT AAA GCA GCG TAT CC -3'	Sigma
Rosa-4	5'- CTG TTC CTG TAC GGC ATG G -3'	Sigma

5.1.11 Adeno-associated-viruses (AAVs)

Name	Order no.	Supplier	Titer (GC/ml)
AAV1.CMV.PI.Cre.rBG	AV-1-PV1090	UPenn VectorCore	1.03e13
AAV1.CMV.HI.GFP-Cre.WPRE.SV40	AV-1-PV2004	UPenn VectorCore	2.35e13
AAV1.CMV.PI.EGFP.WPRE.bGH	AV-1-PV0101	UPenn VectorCore	2.36e13
AAV1.CMV.PI.RFP.WPRE.bGH	Custom-made	UPenn VectorCore	4.73e12
AAV1.CMV.PI.hCofWT-RFP.WPRE.bGH	Custom-made	UPenn VectorCore	2.14e13
AAV1.CMV.PI.hCofY82F-RFP.WPRE.bGH	Custom-made	UPenn VectorCore	8.85e12
AAV1.CMV.PI.hCofS94D-RFP.WPRE.bGH	Custom-made	UPenn VectorCore	1.14e13

5.1.12 Animals

All experiments were conducted on adult rats and mice (2 - 4 months) of both genders. All animal experiments were performed in accordance with the animal handling laws of the government (Aktenzeichen 87-51.04 2011.A045, 84-02.04.2014.A060 and 84-02.04 2013.A316). Sprague Dawley wild-type rats and C57BL/6J wild-type mice were purchased from Charles River Laboratories or Harlan. The Cre reporter strain Gt(ROSA)26Sor $^{tm9\ (CAG\text{-}tdTomato)Hze}$/J mice were purchased from Jackson laboratories (strain #7909). The mice express a targeted mutation of the Gt(ROSA)26Sor locus with a loxP-flanked STOP cassette preventing transcription of a CAG promoter-driven red fluorescent protein variant (tdTomato).

Double knockout experiments were performed on ADF$^{-/-}$Cofilin1$^{flox/flox}$ mice with genomic ablation of ADF and expressing floxed cofilin 1 alleles (Gurniak et al., 2005, Bellenchi et al., 2007, Flynn et al., 2012). Triple knockout experiments were performed on ADF$^{-/-}$Cofilin1$^{flox/flox}$ Cofilin2$^{flox/flox}$ mice with genomic ablation of ADF and expressing floxed cofilin 1 and cofilin 2 alleles (Gurniak et al., 2005, Bellenchi et al., 2007, Flynn et al., 2012, Gurniak et al., 2014). These mice were originally generated by the laboratory of Prof. Dr. Walter Witke and kindly donated to us for these experiments.

5.2 Methods

5.2.1 Cell culture of primary DRG neurons

DRG neurons were dissected as previously described by Neumann et al. (2002). In brief, the animals were sacrificed and the lumbar spinal cord was exposed. Dorsal root ganglia were isolated from L4 and L5 spinal levels and transferred to ice cold Hank´s buffered salt solution (HBSS). Ganglia were cleaned of superfluous connective tissue and blood to minimize contamination of the culture by other cell types. Ganglia were enzymatically digested in collagenase (3000 U/ml) for 80 minutes at 37°C and washed once in pre-warmed HBSS. After centrifugation at low speed (630 rpm) for 5 minutes the supernatant was discarded, the cells were resuspended in Hepes buffered 0.25% trypsin-EDTA and incubated for another 15

minutes at 37°C. Enzymatic digestion was stopped by addition of complete NB medium containing 5 % horse serum. Neurons were then recovered by centrifugation at 630 rpm for 5 minutes. Dissociated neurons were cultured on poly-L-lysine (1 mg/ml in borate buffer) and laminin coated dishes (5 µg/ml) in complete NB medium complemented. Cells were incubated at 36.5 °C in a humidified atmosphere containing 5% CO_2 for 16, 19, 24 or 48 hours respectively. For live imaging neurons were grown on glass bottom dishes. For immunocytochemistry cells were cultured on glass coverslips contained in 4-well dishes.

5.2.2 In vitro electroporation of DRG neurons

For *in vitro* transfection of DRG neurons the L4-L6 ganglia from three individual animals were collected and pooled. In total, 8-12 DRGs were used per transfection reaction. The DRG neurons were dissected and dissociated as described above with minor alterations to the general protocol: After digestion of the cells in trypsin-EDTA, the cells were washed once in NB medium containing 5% horse serum. Subsequently, the cells were washed in 1 ml pre-warmed Hepes buffered HBSS to remove the serum. Finally, the cells were resuspended in 100 µl rat or mouse nucleofector solution respectively and approximately 12-17 µg of the appropriate DNA plasmid was added. The DNA-cell suspension was transferred to a disposable cuvette and placed into the nucleofector device. Program G-013 (alternative program DRG neurons, rat) was chosen from the menu and the cells were electroporated. Immediately upon electroporation 1 ml of DMEM medium containing 10% horse serum was added to the cells. The cells were allowed to recover in the water bath at 37°C for 10 minutes before plating. 2-3 hours after plating the medium of the cells was exchanged to complete NB medium.

5.2.3 Drug treatment

DRG neurons were dissected and cultured as described above. Approximately 2-4 hours after plating - when DRG neurons firmly attached to the substrate - they were treated with the respective drugs. As negative control neurons were treated with ≤0.2% DMSO. After treatment neurons were immediately returned to the humidified incubators (36.5°C and 5% CO_2).

5.2.4 Image acquisition

Fluorescence microscopy. Fixed cells were imaged using the AxioObserver.D1 inverted microscope (Zeiss). 25x NA 0.8, 40x NA 1.3, 63x NA 1.4 or 100x NA 1.4 oil immersion objectives (Zeiss) were used. Cells were illuminated with the Illuminator HXP 120 C (Zeiss) and imaged using the AxioCam MRm (black and white) or AxioCam Icc1 (colour) cameras (Zeiss). Pictures were recorded using the AxioVision software (Zeiss).

Live cell imaging (growth cone dynamics). A heating system combined with an active gas mixer for live cell imaging and video microscopy (ibidi) was used to image neurons under optimal conditions for growth (36.5°C and 5% CO_2). Living cells were kept on the stage of a fluorescence microscope (AxioObserver.D1; Zeiss) in 35 mm glass bottom dishes filled with complete NB medium without phenol red. A Plan-Apochromat 100x NA 1.4 objective (Zeiss) was used. Cells were illuminated with the Illuminator HXP 120 C (Zeiss). Halogen light was set to minimal intensity to avoid phototoxicity. Images were captured using a CCD camera (AxioCam MRm, Zeiss). Pictures were recorded using the AxioVision software (Zeiss). At least 20-30 cells per condition (naïve and pre-axotomized) were observed and imaged.

Live cell imaging (actin dynamics). Neurons were seeded on glass-bottom 35 mm dishes. Imaging was performed using a 60x NA 1.6 objective (Olympus) on a DeltaVision RT (Applied Precision) live-cell imaging setup based on an Olympus IX71 inverted microscope, with a CO_2 regulated incubation chamber maintained at 36°C (Solent Scientific). Images were acquired with a Photometrics CoolSnap HQ camera (Roper Scientific) using SoftWoRx 3.5.0 imaging software (Applied Precision). Images were acquired for 5 minutes at 3-5 second intervals depending on the experiment.

Image acquisition and quantification of actin dynamics were conducted with the help of Dr. Kevin Flynn and Telma da Silva Santos, members of the Axon Growth and Regeneration Group at the DZNE, Bonn.

5.2.5 Image analysis and quantification

Axonal length and branching. Length measurements were performed using the ImageJ analysis software (NIH, USA). The average length per condition was calculated by imaging and measuring the longest neurite of each cell. For quantification of the branching frequency, all primary branches were counted along the longest axon and expressed as number of branching points/100µm. A minimum of 90 cells per condition from three different experiments were imaged using a fluorescent microscope (AxioObserver.D1; Zeiss) and a 25x NA 0.8 objective (Zeiss).

Growth cone dynamics. The growth rate of naïve and conditioned DRG neurons was measured using the ImageJ analysis software (NIH, USA). The rate of advance of individual growth cones was measured every minute over a time period of 1-2 hours. Growth cone dynamics were quantified for a time period of 2 minutes by measuring changes of growth cone area every 10 seconds. Growth cones were outlined manually using Metamorph software. Growth-cone outlines were pasted onto the following images and changes of growth cone area between the single images were added together for a total growth cone area change over time.

Actin dynamics. The analysis of various parameters for actin dynamics was performed using Metamorph imaging software. All analysis was performed on neurons imaged at 3-5 second intervals for 3-5 minutes. Linescans around the perimeter of growth cones of naïve and conditioned neurons were used to measure retrograde flow, protrusion frequency and protrusion distances. Retrograde flow was measured as the slope of diagonal lines in kymographs that were acquired by using Metamorph software. Only the longest protrusion per 5 minutes was measured for the protrusion distance quantifications. For Protrusion frequency, all protrusions ≥1µm were counted.

Fluorescence intensity. Intensity measurements of acetylated and tyrosinated microtubule ratios were performed using Image Beta 4.0.2 for Microsoft Windows. A suited macro (03_Intensity or ratio_Claudia) was developed by Harald Witte (PhD, Axonal Growth and Regeneration Group, MPI for Neurobiology). Prior to intensity analyses a background correction was performed for all images using Adobe Photoshop. The ratio of acetylated versus tyrosinated α-tubulin was

determined from the mean fluorescence intensity of both channels in a square of 3x3 pixels in four separate regions of each cell. One measurement was carried out close to the soma of the DRG neuron, the second measurement in the medial part of each process; the third measurement approximately 100 µm away from the axonal tip and the last measurement was performed directly at the axonal tip.

Axon Regeneration. The number of regenerating axons at different distances from the lesion epicenter was normalized to the number of labeled axons caudal (200-400 µm) to the lesion. The lesion epicenter was identified based on axon morphology and GFAP staining. Presence of infiltrating macrophages containing autofluorescent phagocytic material was used as additional confirmation when quantifying 2-photon images. Samples with incomplete lesion or poor tracing were excluded from the analysis.

Quantifications of axon regeneration were conducted by Dr. Andrea Tedeschi, member of the Axon Growth and Regeneration Group at the DZNE, Bonn

Electron microscopy. Prior to quantification of angle deviations microtubules were pseudocoloured in black using Photoshop (Adobe Systems). Angle deviations, number of mitochondria were then quantified with the Analysis FIVE software (Olympus).

Statistical analyses. All results are depicted as average with error bars denoting standard error of mean (SEM) values. Mean values and standard errors were computed using Microsoft Office Excel 2010. Unpaired two-tailed, assuming unequal variance (heteroscedastic) student´s t-tests were performed using Microsoft Office Excel 2010 unless indicated otherwise. For figure 3.21 permutation tests to test the significance of mean differences T between three different animal groups ($T = \bar{X}_v - \bar{X}_d$) were performed by Christoph Möhl (Image and Data Facility, DZNE, Bonn) as previously described (Fisher, 1935, Ernst, 2004).

Diagrams and illustrations were drawn using Microsoft PowerPoint 2010 or Canvas (ACD systems). All figures were assembled using Canvas (ACD Systems).

5.2.6 Immunocytochemistry

Prior to fixation the DRG neurons were rinsed one time with pre-warmed PBS. Then two different fixation methods were applied. To stain for neuronal ßIII tubulin (Tuj1) and actin, 4% paraformaldehyde was used as fixative. Cells were incubated in pre-warmed 4% paraformaldehyde solution for 15 minutes and washed three times with PBS. Subsequently, free aldehyde groups were quenched in 50mM ammonium chloride for 10 minutes and washed repeatedly. After permeabilization with 0.1 % triton X-100 for 5 minutes, cells were again washed three times with PBS.

In the second approach, used to assess acetylated and tyrosinated and total tubulin integrated in microtubules (MTs) without non-polymerized tubulin subunits, cells were simultaneously fixed and permeabilized in PHEM buffer containing 3.7% paraformaldehyde, 3.7% sucrose, 0.25% glutaraldehyde and 0.1% triton X-100 (adapted from Smith, 1994). After washing the cells three times with PBS, aldehyde groups were quenched in 50mM ammonium chloride for 30 minutes.

For both approaches, the neurons were then incubated in blocking solution for 30-60 minutes at room temperature. Subsequently, cells were incubated with primary antibodies diluted in 10 % blocking solution at 4°C overnight or for 1-2 hours at room temperature. Cells were incubated with secondary antibodies for 30 minutes after washing the cells 3-5 times with PBS. For visualization of F-actin rhodamine-coupled phalloidin was applied at the same time as the secondary antibodies. After staining, the cells were washed thoroughly with PBS and mounted on microscope slides.

5.2.7 Molecular Biology

E. coli was cultivated at 37°C under aerobic conditions either in liquid TB-media under vigorous shaking (220 rpm) or on LB-plates. Cultures were inoculated from single colonies. For plasmid selection, media or plates containing appropriate antibiotics were used.

Transformation of competent E. coli cells. 10 to 100µl of Subcloning Efficiency™ DH5α™ Competent Cells competent bacteria were gently thawed on ice and mixed with the plasmid to be transformed in an 1.5ml eppendorf tube. The tube was incubated on ice for 10 minutes. Bacteria were heat-shocked by incubation at 42°C for 1 minute and then chilled on ice for 2 minutes. 1ml of plain TB medium (pre-warmed to 37°C) was added to the cells, incubated at 37°C for 60 minutes with shaking at 225-250 rpm. 50 to 100 µl of the transformation solution were plated on LB agar plates containing the appropriate antibiotic for plasmid selection and incubated at 37°C overnight.

Preparation of plasmid DNA. Plasmid DNA was purified from small-scale (3ml, mini-preparation) or from large-scale (100ml, maxi-preparation) bacterial cultures. LB medium containing 100 µg/ml ampicillin or 50 µg/ml kanamycin was inoculated from single colonies of transformed bacteria, starter cultures or bacterial glycerol stocks and incubated overnight at 37°C with vigorous shaking. The bacterial suspension was pelleted by centrifugation at 6.000g for 5 minutes at RT and then resuspended in buffer P1 (Qiagen; 50 mM Tris-Cl, pH 8.0; 10 mM EDTA; 100 µg/ml RNase A). Mini- and EndoFree® Maxipreparation of plasmid DNA were carried out according to the Qiagen protocol employing alkaline lysis of the cells and binding of the plasmid DNA to an anion exchange resin. After washing, elution and precipitation the plasmid DNA was re-dissolved in a suitable volume of PCR grade water. DNA concentration was analyzed using the Nanodrop System.

5.2.8 Protein extraction and western blotting

Dorsal root ganglia were dissected from rats and mice, rinsed shortly in ice-cold Hepes buffered HBSS, transferred to 2ml eppendorf tubes, snap frozen in liquid nitrogen and finally stored at -80°C until further use. For protein extraction, the DRGs were spun down to the bottom of the eppendorf tube and 500 µl of liquid nitrogen were added. The samples were mechanically ground with a micropistille and the procedure repeated 2-3 times, until the DRGs were powdery. 80 µl of distilled water were added and the samples lysed further by pipetting the solution up and down using a 1ml syringe with an 18 gauge needle. 20 µl of a 5x RIPA solution or lysis buffer containing protease and phosphatase inhibitors were then added and the samples left on ice for 10-15 minutes. Finally, the samples were centrifuged at 10000 rpm and 4°C for 5 minutes, the supernatant transferred to a fresh 1.5 ml eppendorf tube and the pellet discarded. 5µl of the solution was used for assessing protein amounts in the respective samples. To the remaining protein solution approximately 20 µl of 5x Laemmli solution were added and the samples stored at -20°C until further use. The protein concentration was determined applying the Precision Red protein assay (Cytoskeleton). Therefore, 1 ml of 1x protein assay reagent was added to semi-micro cuvettes. For the blank probe 5 µl of 1x RIPA buffer containing inhibitors and for the samples 5 µl of the protein solution were added. The solutions were thoroughly mixed and left at RT for 1 minute before measuring the absorbance at 595 nm on a photometer. The measured value was multiplied by 20 to obtain the protein concentration in µg/µl. Prior to SDS-PAGE protein extracts were boiled at 95°C in a thermomixer for 5 minutes. Approximately 15-20µg of protein solution was loaded on 10% polyacrylamide gels and run at 50 V for 20 minutes and 150V for 1.5 hours (300 mA). Proteins were transferred on polyvinylidene difluoride (PVDF) membranes using a wet transfer system (150 V and 300 mA for 2.5 hours). Membranes were blocked for 30-60 minutes at RT, incubated with primary antibodies overnight at 4°C, washed in 1x TBS-T and afterwards incubated with horse radish peroxide-linked secondary antibodies for 1 hour at RT. For protein detection, the membrane was incubated with enhanced chemiluminescence (ECL) solution.

All biochemical analyses were conducted with the help of Dr. Sebastian Dupraz, member of the Axon Growth and Regeneration Group at the DZNE, Bonn.

5.2.9 Electron microscopy

Cultured DRG neurons were fixed by adding glutaraldehyde to the medium to a final concentration of 2%. Neurons were postfixed with 1% osmium tetroxide. Cells were then dehydrated and embedded in Epon, cut by an ultramicrotome (Leica EM UC6) at 70 nm and post-stained with lead citrate and uranyl acetate by an ultrastainer (LKB). Electron microscopy images of the sections were acquired using a Zeiss EM10 (Kodak 4489) and a JEOL JEM-1230 electron microscope with a CCD-camera (Gatan Orius SC1000). The neuronal identity of the analyzed cells was confirmed by immunofluorescence and by morphology.

Electron microscopy was conducted with the help of Marianne Braun from the EM and histology facility of the MPI for Neurobiology, Martinsried.

5.2.10 Polymerase chain reaction (PCR) for genotyping of transgenic mice

ADF. After weaning, 1-2 mm long tail biopsies were collected from the mice and stored at -20°C in an 1.5 ml eppendorf tube. To extract the DNA from the tails, 500 µl lysis buffer and 7.5 µl Proteinase K solution were added and lysed for a minimum of 4 hours or overnight at 55°C and 1300 rpm in a thermomixer. Samples were then centrifuged for 20 minutes at 13000rpm. The supernatant was collected and transferred to a fresh eppendorf tube. 500 µl isopropanol were added and the tubes shaken briefly. The samples were centrifuged again for 20 minutes at 13000rpm. The supernatant was discarded and 200 µl of 70% ethanol added to the pellet. Then, the samples were once more centrifuged for 20 minutes at 13000 rpm and the supernatant discarded. The eppendorf tubes were dried overhead for 5 minutes at RT, followed by 20 minutes at 37°C. Finally, 50 µl PCR grade water was added and the samples left at 37°C for 1 hour.

Cofilin 1 and Gt(Rosa). After weaning, 1-2 mm long tail biopsies were collected from the mice and stored at -20°C in an 1.5 ml eppendorf tube. To extract the DNA from the tails, 100 µl NaOH (50 mM) solution were added and shaken at 95°C for 45 minutes in a thermomixer. Then, 10 µl 1.5 Tris-HCl (pH 8.8) were added and

the samples centrifuged for 5 minutes at 4°C and 15000 rpm. The supernatant containing the plasmid DNA was collected and transferred to a fresh tube.

ADF	**Cofilin**	**Gt(ROSA)26Sor**
Master Mix 9.17 µl PCR grade water 4.0 µl Green GoTaq® Flexi buffer 1.2 µl $MgCl_2$ (25 mM) 1.5 µl dNTPs (2.5 mM) 0.5 µl Primer 5 µM ADF A 1.5 µl Primer 5 µM ADF B 1.0 µl Primer 5 µM ADF C 0.13 µl GoTaq® DNA Polymerase (5U/µl) + 1 µl DNA template	8.0 µl PCR grade water 12.5 µl GoTaq® Green Master Mix 0.5 µl Primer 5µM Cofilin A 1.5 µl Primer 5µM Cofilin B 0.5 µl Primer 5µM Cofilin C + 2 µl DNA template	36 µl PCR grade water 10 µl Red Load Taq Master 0.5 µl Primer 10 µM Rosa-1 0.5 µl Primer 10 µM Rosa-2 0.5 µl Primer 10 µM Rosa-3 0.5 µl Primer 10 µM Rosa-4 + 2 µl DNA template
PCR cycler program Lid temperature: 99°C Preheating: on 1. 94°C - 2 min 2. 94°C - 30 sec 3. 58°C - 30 sec 4. 68°C - 40 sec repeat steps 2.-4. for 33x 5. 68°C - 5 min 6. 10°C - Pause	Lid temperature: 99°C Preheating: on 1. 94°C - 2 min 2. 94°C - 30 sec 3. 58°C - 30 sec 4. 68°C - 40 sec repeat steps 2.- 4. for 35x 5. 68°C - 5 min 6. 10°C - Pause	Lid temperature: 99°C Preheating: on 1. 94°C - 3 min 2. 94°C - 20 sec 3. 61°C - 30 sec 4. 72°C - 30 sec repeat steps 2.-4. for 35x 5. 72°C - 2 min 6. 10°C - Pause
Gelelectrophoresis 1.5% agarose in 1x TAE-Buffer add Midori Green (1.5µl/100ml TAE); run gel at 120V for 30 min	1.5% agarose in 1x TAE-Buffer add Midori Green (1.5µl/100ml TAE); run gel at 120V for 30 min	1.5% agarose in 1x TAE-Buffer; add Midori Green (1.5µl/100ml TAE); run gel at 120V for 30 min
Expected bands wt 420bp ko 180bp	fl 420bp wt 380bp ko 170bp	fl 196 bp wt 297 bp het 297 bp and 196 bp

5.2.11 Animal surgeries

5.2.11.1 Peripheral nerve lesion and sciatic nerve crush

The rats and mice were anesthetized with 2% isoflurane inhalation anesthesia or alternatively with a 1:1 mixture (1µl/1g body weight) of 10% ketamine and 2% xylasine injected intraperitoneally. The eyes of the animals were covered with eye- and nose cream to avoid drying out. The femoral region (thigh) was shaved and treated with iodine solution to keep the surgical area aseptic. During the surgery the animals were kept on a heating pad. After exposing the sciatic nerve approximately 2.5 cm (mice: 1 cm) from the L4/5 DRG cell bodies by a small incision, the nerve was either crushed using a #5 forceps for 10 seconds (crush) or ligated tightly and then cut distally to the ligation (PNL). Subsequently the muscle and the skin were sutured. To counteract the loss of fluid during anesthesia, animals were injected with 10 ml (mice: 1 ml) isotonic salt solution subcutaneously. Animals were kept on a heating pad until regaining consciousness.

5.2.11.2 In vivo DRG electroporation

The surgery was performed according to Saijilafu et al. (2011). The mice were anesthetized with 2% isoflurane or by intraperitoneal injection of a mixture of 10% ketamine and 2% xylasine (1 µl/g bodyweight, stock solution: 1 ml Ketamine and 0.5 ml xylasine in 8.5 ml NaCl). Eyes were covered by a thin layer of eye- and nose cream. The lower back of the animals was shaved (and optionally: treated with Veet hair removal gel for 5 min), wiped successively with 70% ethanol (EtOH), iodine solution and 70% EtOH again. Antibiotic and analgesic (1:10 dilutions of Baytryl and Temgesic respectively) were administered before the surgery. During the surgery the animals were kept on a heating pad. An incision of the skin (approximately 2 cm in length) was performed at the midline of the lower back rostral to the hip bone. An incision of the muscles was made on either side of the spinal cord to enable insertion of a retractor. The overlying muscles of laminae L3-5 were removed. Using a laminectomy forceps all the muscles and connective tissue on the lateral processes of L4 and/or L5 were removed. A small dorsolateral laminectomy was performed by removing the processus accessorius and parts of

the processus transversus until the DRG was exposed fully. By 3-5 injection points approximately 1-2 µl of DNA solution (containing > 3 µg/µl DNA and 5% Fast green) were injected into the DRG using a picospritzer (pressure: 30 psi; pulse duration: 8 ms) until the solution was uniformly distributed. The electrode was moistened by dipping it into isotonic salt solution (0.9% NaCl). Electroporation was performed immediately after the injection using a custom-made tweezer-like electrode and an electro square porator (five 15 ms pulses at 35 V with 950 ms interval). After application of the pulses, the electrode was immediately rinsed with 0.9% NaCl. Finally, the wound was closed by suturing the muscles and the skin. 1 ml of 5% glucose solution was injected and the animal kept on a heating pad until it regained consciousness. After 5-7 days the construct was expressed in approximately 10-30% of all DRG neurons (while efficiency strongly depended on the construct).

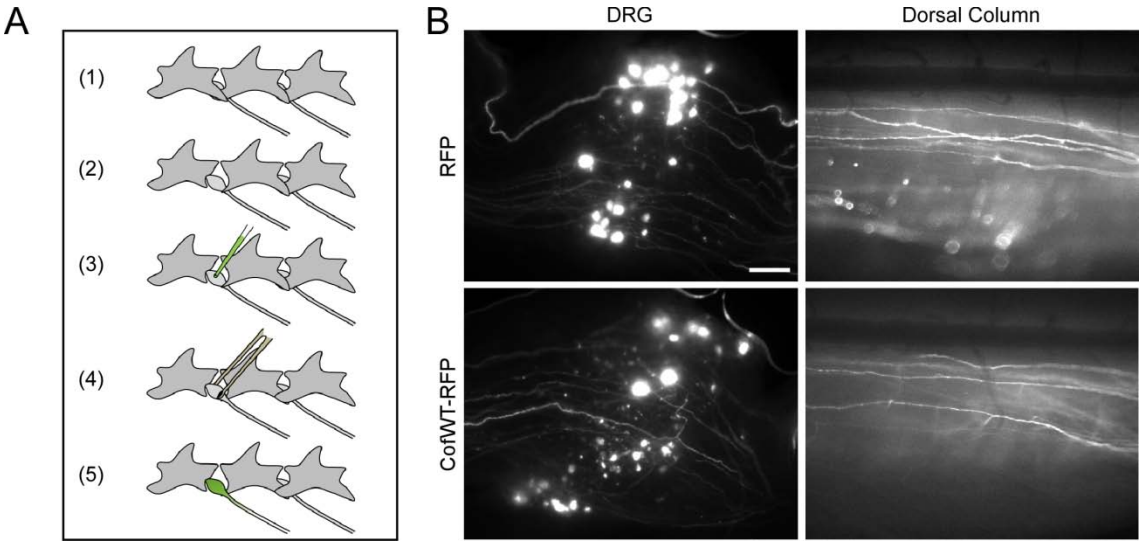

Figure 5.1. In vivo electroporation of adult mouse DRG neurons. (A) Image panel depicting the principal surgical steps to perform *in vivo* DRG electroporation. (1) The overlaying muscles of the lumbar spinal cord are dissected and removed from the L4 and L5 spinous processes. (2) To expose the L4 or L5 DRG, a small dorsolateral laminectomy is performed by removing the processus accessorius and part of the processus transversus. (3) The DNA constructs are injected into the DRG via a capillary glass tube and a picospritzer. (4) Electroporation is performed immediately after the injection using a custom-made tweezer-like electrode and an electro square porator. (5) Approximately 5-7 days after electroporation, the animals express the fluorophore in ~10% of neurons of the electroporated DRG. (B) Representative fluorescent images of DRGs (left panel) and axons in the dorsal column (right panel) that were electroporated with plasmids expressing red fluorescent protein (RFP) or wild-type cofilin 1 conjugated to RFP (CofWT-RFP) and imaged using an *in vivo* imaging setup, scalebar 200 µm.

5.2.11.3 Adeno-associated virus (AAV) transduction

For virus injections into the L4/5 dorsal root ganglia the same surgical procedure as described in the previous section was followed. The DRG was exposed and approximately 1-2 µl of AAV solution (containing 5% Fast Green) was injected. After injection, the animal was sutured and the wound closed immediately. Alternatively, 2 µl of AAV solution were injected into the sciatic nerve. Approximately after 5-7 days (injection into DRG) or 2 weeks (injection into sciatic nerve) roughly 70-90% of all DRG neurons were transduced with the virus.

5.2.11.4 In vivo imaging

In vivo imaging was performed according to Kerschensteiner et al. (2005) and Laskowski and Bradke (2013). Adult C57BL/6J wild-type mice (8-16 weeks) were electroprated *in vivo* using plasmid constructs expressing red fluorescent protein (RFP) or wild-type cofilin 1 conjugated to RFP. After *in vivo* electroporation, single axons at the surface of the surgically exposed dorsal column could be directly observed after SCI using simple wide-field epifluorescence microscopy. After induction of anesthesia, the mice were kept on a heating pad to maintain a constant body temperature. Efficient ventilation, anesthesia and analgesia were monitored constantly. Next, the dorsal lamina was removed at thoracic level 12 (T12) of the spinal cord to expose the dorsal column, i.e. the central axons of dorsal root ganglion (DRG) neurons that have their peripheral axons bundled within the sciatic nerve. In short, a 2 cm cut to the skin was performed at the midline of the animals back. The overlying muscles on the left and right side of the T11-L1 vertebra were cut and removed. Remaining connective and muscle tissue between the target (T12) and neighboring vertebrae was removed using a rongeur to create an entry point for the spring scissors. The tip of the scissors was then inserted on either side of the dorsal lamina and the bone was cut. The dorsal aspect of T12 was removed by lifting it up with a forceps so that the spinal cord was exposed fully. The imaging area was widened by taking small bites with a rongeur on either side of the opening. To obtain the optimal fluorescence signal the layer of dura mater covering the spinal cord was removed at the site of laminectomy. Special care was taken to avoid non-specific injury to the spinal cord. Due to leakage of cerebrospinal fluid (CSF), pre-warmed saline was applied

to the spinal cord. A fine iridectomy scissor was then used to carefully transect single or groups of superficial axons in the dorsal columns on either side of the prominent dorsal vein. Before and after induction of an injury the transected axons were imaged. Most dorsal column axons, which originate from the DRGs, run in parallel to the dorsal spinal cord surface. The superficial fraction of sensory axons could thus easily be imaged using a conventional wide-field epifluorescence microscope. A fast series of images were captured to circumvent artefacts caused by breathing of the animals. The best image of the series was chosen for illustration. After imaging, the lamina was closed with surrounding muscle tissue and the skin stapled until the next imaging time point. Post-surgery, the animals were revived and kept in their home cages. They were further supplemented with physiological saline or glucose solution to prevent dehydration and treated with antibiotics and analgesics for the following week.

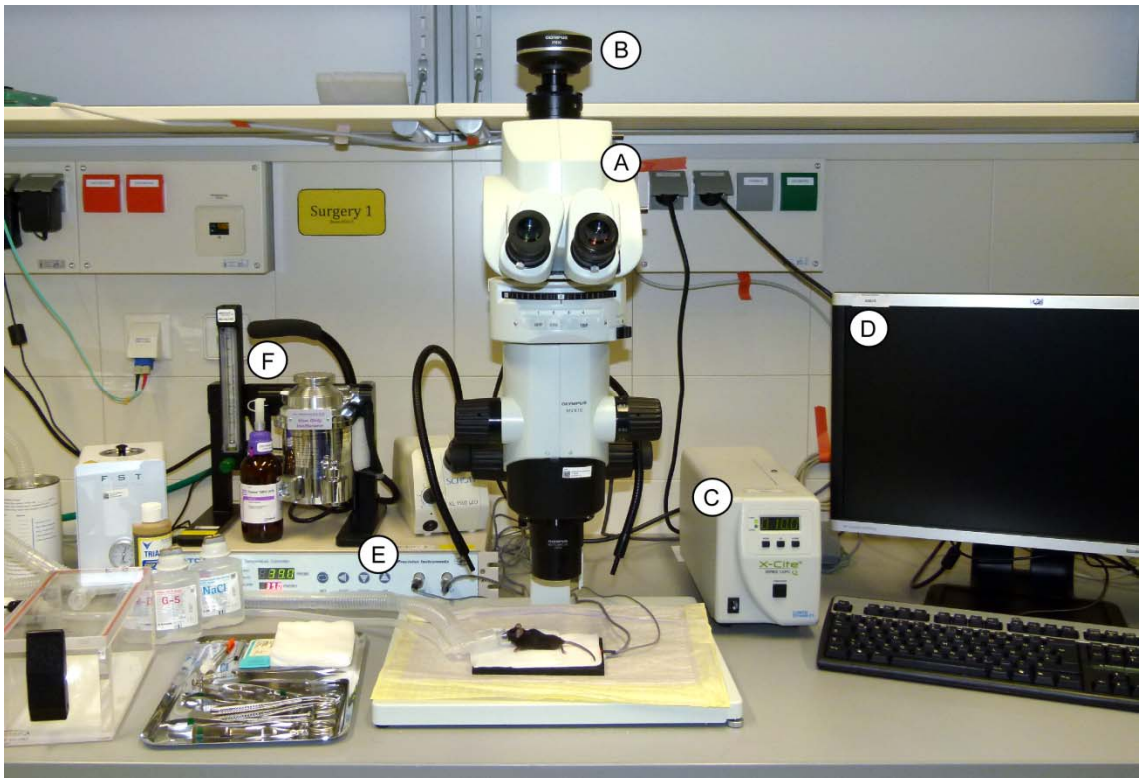

Figure 5.2. The basic experimental setup for in vivo imaging. The imaging setup consists of (A) an upright wide-field epifluorescence microscope (MVX10 Macroview, Olympus), (B) a black and white CCD camera (XM-10, Olympus), (C) a computer controlled fluorescence microscope light source (X-Cite 120PC Q) and (D) the corresponding digital imaging software (Cellsens®, Olympus). (E) A temperature controller and heating pad are required to monitor the animal´s body temperature (ATC 1000, World Precision Instruments). (F) A table top laboratory animal anesthesia system (VetEquip) is used to induce and maintain the anesthesia (Figure taken from Laskowski and Bradke, 2013)

5.2.11.4 Dorsal column lesion

The mice were anesthetized with a 2% isoflurane inhalation anesthesia or alternatively with a 1:1 mixture (1 µl/1g body weight) of 10% ketamine and 2% xylasine injected intraperitoneally. The eyes of the animals were covered with eye- and nose cream to avoid drying out. After induction of anesthesia, the mice were kept on a heating pad to maintain a constant body temperature. Efficient ventilation, anesthesia and analgesia were monitored constantly. In short, a 2 cm cut to the skin was performed at the midline of the animals back. The overlying muscles on the left and right side of the T11-L1 vertebra were cut and removed. Remaining connective and muscle tissue between the target (T12) and neighboring vertebrae was removed using a rongeur to create an entry point for the spring scissors. The tip of the scissors was then inserted on either side of the dorsal lamina and the bone was cut. The dorsal aspect of T12 was removed by lifting it up with a forceps so that the spinal cord was exposed fully. The surgical area was widened by taking small bites with a rongeur on either side of the opening. As a consequence, the dorsal columns - the central axons of dorsal root ganglion (DRG) neurons that have their peripheral axons bundled within the sciatic nerve - were exposed. Using #5 modified forceps a dorsal column lesion was performed. After lesioning the spinal cord, the muscle was sutured and the skin stapled. Post-surgery, the animals were revived and kept in their home cages. They were further supplemented with physiological saline or glucose solution to prevent dehydration and treated with antibiotics and analgesics for the following week.

All spinal cord injuries were conducted by Dr. Andrea Tedeschi, member of the Axon Growth and Regeneration Group at the DZNE, Bonn.

5.2.12 Intracardial perfusion

Animals were sacrificed and perfused at defined end points. In brief, animals were anesthetized by injecting an overdose of a 1:1 mixture of 10% ketamine and 2% xylasine intraperitoneally. The thorax was opened and the heart exposed. The animals were then perfused transcardially by flushing the blood out with

physiological saline solution containing Heparin-EDTA (100.000 iU/L 0.9% NaCl) immediately followed by 4% PFA (in 0.1 M PBS). Mice were perfused with approximately 30-50 ml and rats with 200ml. The spinal cords and DRGs were then carefully dissected and post-fixed in 4% PFA at 4°C overnight or 20 minutes at room temperature respectively. The tissue was then transferred to 30% sucrose in 0.1 M PBS for 3 days. The tissue was embedded in Shandon M1 embedding matrix and sectioned using a cryostat at 14 µm.

5.2.13 Immunohistochemistry

Dorsal root ganglia. 14 µm DRG sections were warmed at 37°C for 30 minutes on a slide warmer. The embedding matrix was washed out twice with PBS for 10 minutes each at RT. The sections were post-fixed for 5 minutes in -20°C methanol. Subsequently, the aldehydes were quenched with 0.1M Glycine in TBS for 30 minutes at RT. The sections were blocked in 10% normal goat serum (NGS) containing 0.5% Triton in TBS for 1 hour at RT. Then, the primary antibody (rabbit polyclonal anti-Cofilin) was diluted at 1:200 in 1% NGS (in TBS) and incubated at 4°C overnight. Subsequently, the sections were washed 3 times with TBS for 6-10 minutes each at RT. The secondary antibody (goat anti-rabbit Alexa 568 conjugated) was diluted at 1:400 in 1% NGS (in TBS) and incubated for 2 hours at RT. Once more, the sections were washed 3 times with TBS for 6-10 minutes each at RT. Finally, DAPI (diluted 1:10000 in TBS) was added to the sections, washed 2 times with TBS for 5 minutes each, and the sections mounted using Fluoromount.

Spinal Cord. 14 µm spinal cord sections were warmed at 37°C for 30 minutes on a slide warmer. The embedding matrix was washed out twice with PBS for 10 minutes each at RT. The sections were blocked in 10% normal goat serum (NGS) containing 0.2% Triton in PBS for 1 hour at RT. Then, the primary antibody (rabbit polyclonal anti-GFAP) was diluted at 1:500 in 1% NGS (in PBS) and incubated at 4°C overnight. Subsequently, the sections were washed 3 times with PBS for 6-10 minutes each at RT. The secondary antibody (goat anti-rabbit Alexa 488 conjugated) was diluted at 1:400 in 1% NGS (in PBS) and incubated for 1 hour at RT. Once more, the sections were washed 3 times with PBS for 6-10 minutes each at RT. Finally, DAPI (diluted 1:10000 in PBS) was added to the sections before mounting them using Fluoromount.

6 REFERENCES

Abe N, Cavalli V (2008) Nerve injury signaling. Current opinion in neurobiology 18:276-283.

Agrawal PB, Joshi M, Savic T, Chen Z, Beggs AH (2012) Normal myofibrillar development followed by progressive sarcomeric disruption with actin accumulations in a mouse Cfl2 knockout demonstrates requirement of cofilin-2 for muscle maintenance. Human molecular genetics 21:2341-2356.

Aizawa H, Sutoh K, Yahara I (1996) Overexpression of cofilin stimulates bundling of actin filaments, membrane ruffling, and cell movement in Dictyostelium. The Journal of cell biology 132:335-344.

Akhmanova A, Steinmetz MO (2008) Tracking the ends: a dynamic protein network controls the fate of microtubule tips. Nature reviews Molecular cell biology 9:309-322.

Al-Majed AA, Tam SL, Gordon T (2004) Electrical stimulation accelerates and enhances expression of regeneration-associated genes in regenerating rat femoral motoneurons. Cellular and molecular neurobiology 24:379-402.

Allen C, Borisy GG (1974) Structural polarity and directional growth of microtubules of Chlamydomonas flagella. Journal of molecular biology 90:381-402.

Ambron RT, Walters ET (1996) Priming events and retrograde injury signals. A new perspective on the cellular and molecular biology of nerve regeneration. Molecular neurobiology 13:61-79.

Amos L, Klug A (1974) Arrangement of subunits in flagellar microtubules. Journal of cell science 14:523-549.

Andrianantoandro E, Pollard TD (2006) Mechanism of actin filament turnover by severing and nucleation at different concentrations of ADF/cofilin. Molecular cell 24:13-23.

Arber S, Barbayannis FA, Hanser H, Schneider C, Stanyon CA, Bernard O, Caroni P (1998) Regulation of actin dynamics through phosphorylation of cofilin by LIM-kinase. Nature 393:805-809.

Argiro V, Bunge MB, Johnson MI (1984) Correlation between growth form and movement and their dependence on neuronal age. The Journal of neuroscience : the official journal of the Society for Neuroscience 4:3051-3062.

Argiro V, Bunge MB, Johnson MI (1985) A quantitative study of growth cone filopodial extension. Journal of neuroscience research 13:149-162.

Baas PW (1998) The role of motor proteins in establishing the microtubule arrays of axons and dendrites. Journal of chemical neuroanatomy 14:175-180.

Baas PW, Deitch JS, Black MM, Banker GA (1988) Polarity orientation of microtubules in hippocampal neurons: uniformity in the axon and nonuniformity in the dendrite. Proceedings of the National Academy of Sciences of the United States of America 85:8335-8339.

Bamburg JR, Bernstein BW (2010) Roles of ADF/cofilin in actin polymerization and beyond. F1000 biology reports 2:62.

Bamburg JR, Bray D (1987) Distribution and cellular localization of actin depolymerizing factor. The Journal of cell biology 105:2817-2825.

Bareyre FM, Garzorz N, Lang C, Misgeld T, Buning H, Kerschensteiner M (2011) In vivo imaging reveals a phase-specific role of STAT3 during central and peripheral nervous system axon regeneration. Proceedings of the National Academy of Sciences of the United States of America 108:6282-6287.

Bashaw GJ, Klein R (2010) Signaling from axon guidance receptors. Cold Spring Harbor perspectives in biology 2:a001941.

Bellenchi GC, Gurniak CB, Perlas E, Middei S, Ammassari-Teule M, Witke W (2007) N-cofilin is associated with neuronal migration disorders and cell cycle control in the cerebral cortex. Genes & development 21:2347-2357.

Bernstein BW, Bamburg JR (2010) ADF/cofilin: a functional node in cell biology. Trends in cell biology 20:187-195.

Blesch A, Lu P, Tsukada S, Alto LT, Roet K, Coppola G, Geschwind D, Tuszynski MH (2012) Conditioning lesions before or after spinal cord injury recruit broad genetic mechanisms that sustain axonal regeneration: superiority to camp-mediated effects. Experimental neurology 235:162-173.

Bollag DM, McQueney PA, Zhu J, Hensens O, Koupal L, Liesch J, Goetz M, Lazarides E, Woods CM (1995) Epothilones, a new class of microtubule-stabilizing agents with a taxol-like mechanism of action. Cancer research 55:2325-2333.

Bomze HM, Bulsara KR, Iskandar BJ, Caroni P, Skene JH (2001) Spinal axon regeneration evoked by replacing two growth cone proteins in adult neurons. Nature neuroscience 4:38-43.

Bonilla IE, Tanabe K, Strittmatter SM (2002) Small proline-rich repeat protein 1A is expressed by axotomized neurons and promotes axonal outgrowth. The Journal of neuroscience : the official journal of the Society for Neuroscience 22:1303-1315.

Bradbury EJ, McMahon SB (2006) Spinal cord repair strategies: why do they work? Nature reviews Neuroscience 7:644-653.

Bradbury EJ, Moon LD, Popat RJ, King VR, Bennett GS, Patel PN, Fawcett JW, McMahon SB (2002) Chondroitinase ABC promotes functional recovery after spinal cord injury. Nature 416:636-640.

Bradke F, Dotti CG (1999) The role of local actin instability in axon formation. Science 283:1931-1934.

Bradke F, Fawcett JW, Spira ME (2012) Assembly of a new growth cone after axotomy: the precursor to axon regeneration. Nature reviews Neuroscience 13:183-193.

Bray D, Thomas C, Shaw G (1978) Growth cone formation in cultures of sensory neurons. Proceedings of the National Academy of Sciences of the United States of America 75:5226-5229.

Bregman BS, Kunkel-Bagden E, Schnell L, Dai HN, Gao D, Schwab ME (1995) Recovery from spinal cord injury mediated by antibodies to neurite growth inhibitors. Nature 378:498-501.

Brieher W (2013) Mechanisms of actin disassembly. Molecular biology of the cell 24:2299-2302.

Brown J, Bridgman PC (2003) Role of myosin II in axon outgrowth. The journal of histochemistry and cytochemistry : official journal of the Histochemistry Society 51:421-428.

Bubb MR, Spector I, Bershadsky AD, Korn ED (1995) Swinholide A is a microfilament disrupting marine toxin that stabilizes actin dimers and severs actin filaments. The Journal of biological chemistry 270:3463-3466.

Buck KB, Zheng JQ (2002) Growth cone turning induced by direct local modification of microtubule dynamics. The Journal of neuroscience : the official journal of the Society for Neuroscience 22:9358-9367.

Burgoyne RD, Norman KM (1986) Alpha-tubulin is not detyrosylated during axonal transport. Brain research 381:113-120.

Burnette DT, Ji L, Schaefer AW, Medeiros NA, Danuser G, Forscher P (2008) Myosin II activity facilitates microtubule bundling in the neuronal growth cone neck. Developmental cell 15:163-169.

Cafferty WB, Gardiner NJ, Das P, Qiu J, McMahon SB, Thompson SW (2004) Conditioning injury-induced spinal axon regeneration fails in interleukin-6 knock-out mice. The Journal of neuroscience : the official journal of the Society for Neuroscience 24:4432-4443.

Cafferty WB, Gardiner NJ, Gavazzi I, Powell J, McMahon SB, Heath JK, Munson J, Cohen J, Thompson SW (2001) Leukemia inhibitory factor determines the growth status of injured adult sensory neurons. The Journal of neuroscience : the official journal of the Society for Neuroscience 21:7161-7170.

Cai D, Deng K, Mellado W, Lee J, Ratan RR, Filbin MT (2002) Arginase I and polyamines act downstream from cyclic AMP in overcoming inhibition of axonal growth MAG and myelin in vitro. Neuron 35:711-719.

Cambray-Deakin MA, Burgoyne RD (1987) Posttranslational modifications of alpha-tubulin: acetylated and detyrosinated forms in axons of rat cerebellum. The Journal of cell biology 104:1569-1574.

Cambray-Deakin MA, Robson SJ, Burgoyne RD (1988) Colocalisation of acetylated microtubules, glial filaments, and mitochondria in astrocytes in vitro. Cell motility and the cytoskeleton 10:438-449.

Cao Z, Gao Y, Bryson JB, Hou J, Chaudhry N, Siddiq M, Martinez J, Spencer T, Carmel J, Hart RB, Filbin MT (2006) The cytokine interleukin-6 is sufficient but not necessary to mimic the peripheral conditioning lesion effect on axonal growth. The Journal of neuroscience : the official journal of the Society for Neuroscience 26:5565-5573.

Carlier MF, Laurent V, Santolini J, Melki R, Didry D, Xia GX, Hong Y, Chua NH, Pantaloni D (1997) Actin depolymerizing factor (ADF/cofilin) enhances the

rate of filament turnover: implication in actin-based motility. The Journal of cell biology 136:1307-1322.

Cassimeris L, Safer D, Nachmias VT, Zigmond SH (1992) Thymosin beta 4 sequesters the majority of G-actin in resting human polymorphonuclear leukocytes. The Journal of cell biology 119:1261-1270.

Chazotte B (2011) Labeling mitochondria with rhodamine 123. Cold Spring Harbor protocols 2011:892-894.

Chen Y, Tang Y, Vogel LC, Devivo MJ (2013) Causes of spinal cord injury. Topics in spinal cord injury rehabilitation 19:1-8.

Cho Y, Sloutsky R, Naegle KM, Cavalli V (2013) Injury-induced HDAC5 nuclear export is essential for axon regeneration. Cell 155:894-908.

Cohan CS, Welnhofer EA, Zhao L, Matsumura F, Yamashiro S (2001) Role of the actin bundling protein fascin in growth cone morphogenesis: localization in filopodia and lamellipodia. Cell motility and the cytoskeleton 48:109-120.

Coles CH, Bradke F (2015) Coordinating neuronal actin-microtubule dynamics. Current biology : CB 25:R677-691.

Conde C, Caceres A (2009) Microtubule assembly, organization and dynamics in axons and dendrites. Nature reviews Neuroscience 10:319-332.

Cooper JA (1987) Effects of cytochalasin and phalloidin on actin. The Journal of cell biology 105:1473-1478.

David S, Aguayo AJ (1981) Axonal elongation into peripheral nervous system "bridges" after central nervous system injury in adult rats. Science 214:931-933.

Deglincerti A, Jaffrey SR (2012) Insights into the roles of local translation from the axonal transcriptome. Open biology 2:120079.

Deng K, He H, Qiu J, Lorber B, Bryson JB, Filbin MT (2009) Increased synthesis of spermidine as a result of upregulation of arginase I promotes axonal regeneration in culture and in vivo. The Journal of neuroscience : the official journal of the Society for Neuroscience 29:9545-9552.

Dent EW, Gertler FB (2003) Cytoskeletal dynamics and transport in growth cone motility and axon guidance. Neuron 40:209-227.

Dent EW, Gupton SL, Gertler FB (2011) The growth cone cytoskeleton in axon outgrowth and guidance. Cold Spring Harbor perspectives in biology 3.

Dent EW, Tang F, Kalil K (2003) Axon guidance by growth cones and branches: common cytoskeletal and signaling mechanisms. The Neuroscientist : a review journal bringing neurobiology, neurology and psychiatry 9:343-353.

Di Giovanni S, De Biase A, Yakovlev A, Finn T, Beers J, Hoffman EP, Faden AI (2005) In vivo and in vitro characterization of novel neuronal plasticity factors identified following spinal cord injury. The Journal of biological chemistry 280:2084-2091.

Di Giovanni S, Knights CD, Rao M, Yakovlev A, Beers J, Catania J, Avantaggiati ML, Faden AI (2006) The tumor suppressor protein p53 is required for neurite outgrowth and axon regeneration. The EMBO journal 25:4084-4096.

Diaz JF, Andreu JM (1993) Assembly of purified GDP-tubulin into microtubules induced by taxol and taxotere: reversibility, ligand stoichiometry, and competition. Biochemistry 32:2747-2755.

Dietz V, Fouad K (2014) Restoration of sensorimotor functions after spinal cord injury. Brain : a journal of neurology 137:654-667.

Drees F, Gertler FB (2008) Ena/VASP: proteins at the tip of the nervous system. Current opinion in neurobiology 18:53-59.

Drummond DR (2011) Regulation of microtubule dynamics by kinesins. Seminars in cell & developmental biology 22:927-934.

Du J, Frieden C (1998) Kinetic studies on the effect of yeast cofilin on yeast actin polymerization. Biochemistry 37:13276-13284.

Edwards DC, Sanders LC, Bokoch GM, Gill GN (1999) Activation of LIM-kinase by Pak1 couples Rac/Cdc42 GTPase signalling to actin cytoskeletal dynamics. Nature cell biology 1:253-259.

Elam WA, Kang H, De la Cruz EM (2013) Biophysics of actin filament severing by cofilin. FEBS letters 587:1215-1219.

Endo M, Ohashi K, Mizuno K (2007) LIM kinase and slingshot are critical for neurite extension. The Journal of biological chemistry 282:13692-13702.

Endo M, Ohashi K, Sasaki Y, Goshima Y, Niwa R, Uemura T, Mizuno K (2003) Control of growth cone motility and morphology by LIM kinase and Slingshot via phosphorylation and dephosphorylation of cofilin. The Journal of neuroscience : the official journal of the Society for Neuroscience 23:2527-2537.

Enes J, Langwieser N, Ruschel J, Carballosa-Gonzalez MM, Klug A, Traut MH, Ylera B, Tahirovic S, Hofmann F, Stein V, Moosmang S, Hentall ID, Bradke F (2010) Electrical activity suppresses axon growth through Ca(v)1.2 channels in adult primary sensory neurons. Current biology : CB 20:1154-1164.

Ernst MD (2004) Permutation Methods: A Basis for Exact Inference. Statistical Science 19:676-685.

Erturk A, Hellal F, Enes J, Bradke F (2007) Disorganized microtubules underlie the formation of retraction bulbs and the failure of axonal regeneration. The Journal of neuroscience : the official journal of the Society for Neuroscience 27:9169-9180.

Evans L, Mitchison T, Kirschner M (1985) Influence of the centrosome on the structure of nucleated microtubules. The Journal of cell biology 100:1185-1191.

Fagarasanu A, Rachubinski RA (2007) Orchestrating organelle inheritance in Saccharomyces cerevisiae. Current opinion in microbiology 10:528-538.

Fagoe ND, Attwell CL, Kouwenhoven D, Verhaagen J, Mason MR (2015) Overexpression of ATF3 or the combination of ATF3, c-Jun, STAT3 and Smad1 promotes regeneration of the central axon branch of sensory neurons but without synergistic effects. Human molecular genetics 24:6788-6800.

Filbin MT (2003) Myelin-associated inhibitors of axonal regeneration in the adult mammalian CNS. Nature reviews Neuroscience 4:703-713.

Fisher RA (1935) The design of experiments. Oliver and Boyd, Edinburgh.

Flanagan MD, Lin S (1980) Cytochalasins block actin filament elongation by binding to high affinity sites associated with F-actin. The Journal of biological chemistry 255:835-838.

Flynn K, Pak C, Bamburg J (2007) Regulation of Growth Cone Initiation and Actin Dynamics by ADF/Cofilin. In: Intracellular Mechanisms for Neuritogenesis (de Curtis, I., ed), pp 25-56: Springer US.

Flynn KC (2008) The role of Cdc42, ADF/cofilin, Myosin II and during teh establishmnet of neuronal polarity (Dissertation). ProQuest.

Flynn KC (2013) The cytoskeleton and neurite initiation. Bioarchitecture 3:86-109.

Flynn KC, Hellal F, Neukirchen D, Jacob S, Tahirovic S, Dupraz S, Stern S, Garvalov BK, Gurniak C, Shaw AE, Meyn L, Wedlich-Soldner R, Bamburg JR, Small JV, Witke W, Bradke F (2012) ADF/cofilin-mediated actin retrograde flow directs neurite formation in the developing brain. Neuron 76:1091-1107.

Forscher P, Smith SJ (1988) Actions of cytochalasins on the organization of actin filaments and microtubules in a neuronal growth cone. The Journal of cell biology 107:1505-1516.

Gao Y, Deng K, Hou J, Bryson JB, Barco A, Nikulina E, Spencer T, Mellado W, Kandel ER, Filbin MT (2004) Activated CREB is sufficient to overcome inhibitors in myelin and promote spinal axon regeneration in vivo. Neuron 44:609-621.

Garvalov BK, Flynn KC, Neukirchen D, Meyn L, Teusch N, Wu X, Brakebusch C, Bamburg JR, Bradke F (2007) Cdc42 regulates cofilin during the establishment of neuronal polarity. The Journal of neuroscience : the official journal of the Society for Neuroscience 27:13117-13129.

Gaze RM (1970) The Formation of Nerve Connections. London and New York: Academic Press Pp. viii + 288.

Gehler S, Shaw AE, Sarmiere PD, Bamburg JR, Letourneau PC (2004) Brain-derived neurotrophic factor regulation of retinal growth cone filopodial dynamics is mediated through actin depolymerizing factor/cofilin. The Journal of neuroscience : the official journal of the Society for Neuroscience 24:10741-10749.

Ghosh-Roy A, Wu Z, Goncharov A, Jin Y, Chisholm AD (2010) Calcium and cyclic AMP promote axonal regeneration in Caenorhabditis elegans and require DLK-1 kinase. The Journal of neuroscience : the official journal of the Society for Neuroscience 30:3175-3183.

Giannakakou P, Sackett D, Fojo T (2000) Tubulin/microtubules: still a promising target for new chemotherapeutic agents. Journal of the National Cancer Institute 92:182-183.

Goddette DW, Frieden C (1986) The kinetics of cytochalasin D binding to monomeric actin. The Journal of biological chemistry 261:15970-15973.

Gohla A, Birkenfeld J, Bokoch GM (2005) Chronophin, a novel HAD-type serine protein phosphatase, regulates cofilin-dependent actin dynamics. Nature cell biology 7:21-29.

Goldberg DJ, Burmeister DW (1986) Stages in axon formation: observations of growth of Aplysia axons in culture using video-enhanced contrast-differential interference contrast microscopy. The Journal of cell biology 103:1921-1931.

Goldberg JL (2003) How does an axon grow? Genes & development 17:941-958.

Goldberg JL, Espinosa JS, Xu Y, Davidson N, Kovacs GT, Barres BA (2002) Retinal ganglion cells do not extend axons by default: promotion by neurotrophic signaling and electrical activity. Neuron 33:689-702.

Goldstein LS, Yang Z (2000) Microtubule-based transport systems in neurons: the roles of kinesins and dyneins. Annual review of neuroscience 23:39-71.

Gomis-Ruth S, Wierenga CJ, Bradke F (2008) Plasticity of polarization: changing dendrites into axons in neurons integrated in neuronal circuits. Current biology : CB 18:992-1000.

Goodhill GJ, Faville RA, Sutherland DJ, Bicknell BA, Thompson AW, Pujic Z, Sun B, Kita EM, Scott EK (2015) The dynamics of growth cone morphology. BMC biology 13:10.

Goold RG, Gordon-Weeks PR (2004) Glycogen synthase kinase 3beta and the regulation of axon growth. Biochemical Society transactions 32:809-811.

GrandPre T, Li S, Strittmatter SM (2002) Nogo-66 receptor antagonist peptide promotes axonal regeneration. Nature 417:547-551.

Gressin L, Guillotin A, Guerin C, Blanchoin L, Michelot A (2015) Architecture dependence of actin filament network disassembly. Current biology : CB 25:1437-1447.

Gurniak CB, Chevessier F, Jokwitz M, Jonsson F, Perlas E, Richter H, Matern G, Boyl PP, Chaponnier C, Furst D, Schroder R, Witke W (2014) Severe protein aggregate myopathy in a knockout mouse model points to an essential role of cofilin2 in sarcomeric actin exchange and muscle maintenance. European journal of cell biology 93:252-266.

Gurniak CB, Perlas E, Witke W (2005) The actin depolymerizing factor n-cofilin is essential for neural tube morphogenesis and neural crest cell migration. Developmental biology 278:231-241.

Habib AA, Marton LS, Allwardt B, Gulcher JR, Mikol DD, Hognason T, Chattopadhyay N, Stefansson K (1998) Expression of the oligodendrocyte-myelin glycoprotein by neurons in the mouse central nervous system. Journal of neurochemistry 70:1704-1711.

Han PJ, Shukla S, Subramanian PS, Hoffman PN (2004) Cyclic AMP elevates tubulin expression without increasing intrinsic axon growth capacity. Experimental neurology 189:293-302.

Hannila SS, Filbin MT (2008) The role of cyclic AMP signaling in promoting axonal regeneration after spinal cord injury. Experimental neurology 209:321-332.

Hanz S, Perlson E, Willis D, Zheng JQ, Massarwa R, Huerta JJ, Koltzenburg M, Kohler M, van-Minnen J, Twiss JL, Fainzilber M (2003) Axoplasmic importins enable retrograde injury signaling in lesioned nerve. Neuron 40:1095-1104.

Haque SA, Hasaka TP, Brooks AD, Lobanov PV, Baas PW (2004) Monastrol, a prototype anti-cancer drug that inhibits a mitotic kinesin, induces rapid bursts of axonal outgrowth from cultured postmitotic neurons. Cell motility and the cytoskeleton 58:10-16.

Harel NY, Strittmatter SM (2006) Can regenerating axons recapitulate developmental guidance during recovery from spinal cord injury? Nature reviews Neuroscience 7:603-616.

Harvey RJ, Morando L, Rasetti R, Strata P (2005) Spontaneous electrical activity and dendritic spine size in mature cerebellar Purkinje cells. The European journal of neuroscience 21:1777-1784.

Hawkins M, Pope B, Maciver SK, Weeds AG (1993) Human actin depolymerizing factor mediates a pH-sensitive destruction of actin filaments. Biochemistry 32:9985-9993.

Hayden SM, Miller PS, Brauweiler A, Bamburg JR (1993) Analysis of the interactions of actin depolymerizing factor with G- and F-actin. Biochemistry 32:9994-10004.

He Z (2010) Intrinsic control of axon regeneration. Journal of biomedical research 24:2-5.

Hellal F, Hurtado A, Ruschel J, Flynn KC, Laskowski CJ, Umlauf M, Kapitein LC, Strikis D, Lemmon V, Bixby J, Hoogenraad CC, Bradke F (2011) Microtubule stabilization reduces scarring and causes axon regeneration after spinal cord injury. Science 331:928-931.

Herrmann H, Bar H, Kreplak L, Strelkov SV, Aebi U (2007) Intermediate filaments: from cell architecture to nanomechanics. Nature reviews Molecular cell biology 8:562-573.

Hess DT, Patterson SI, Smith DS, Skene JH (1993) Neuronal growth cone collapse and inhibition of protein fatty acylation by nitric oxide. Nature 366:562-565.

Hoffman PN (2010) A conditioning lesion induces changes in gene expression and axonal transport that enhance regeneration by increasing the intrinsic growth state of axons. Experimental neurology 223:11-18.

Holzinger A (2009) Jasplakinolide: an actin-specific reagent that promotes actin polymerization. Methods in molecular biology 586:71-87.

Hotulainen P, Paunola E, Vartiainen MK, Lappalainen P (2005) Actin-depolymerizing factor and cofilin-1 play overlapping roles in promoting rapid F-actin depolymerization in mammalian nonmuscle cells. Molecular biology of the cell 16:649-664.

Huang TY, DerMardirossian C, Bokoch GM (2006) Cofilin phosphatases and regulation of actin dynamics. Current opinion in cell biology 18:26-31.

Ikeda S, Cunningham LA, Boggess D, Hawes N, Hobson CD, Sundberg JP, Naggert JK, Smith RS, Nishina PM (2003) Aberrant actin cytoskeleton leads to accelerated proliferation of corneal epithelial cells in mice deficient for

destrin (actin depolymerizing factor). Human molecular genetics 12:1029-1037.

Ishikawa R, Kohama K (2007) Actin-binding proteins in nerve cell growth cones. Journal of pharmacological sciences 105:6-11.

Janke C, Bulinski JC (2011) Post-translational regulation of the microtubule cytoskeleton: mechanisms and functions. Nature reviews Molecular cell biology 12:773-786.

Janke C, Kneussel M (2010) Tubulin post-translational modifications: encoding functions on the neuronal microtubule cytoskeleton. Trends in neurosciences 33:362-372.

Jensen JRDW, M.; Bamburg, J.R. (1993) Reversible DMSO-induced translocation of actin and actin polymerizing factor from growth cones to nuclei of cultured hippocampal neurons. Soc Neurosci Abstract 19:64.

Jones SL, Selzer ME, Gallo G (2006) Developmental regulation of sensory axon regeneration in the absence of growth cones. Journal of neurobiology 66:1630-1645.

Jung H, Holt CE (2011) Local translation of mRNAs in neural development. Wiley interdisciplinary reviews RNA 2:153-165.

Kerschensteiner M, Schwab ME, Lichtman JW, Misgeld T (2005) In vivo imaging of axonal degeneration and regeneration in the injured spinal cord. Nature medicine 11:572-577.

Kreis TE (1987) Microtubules containing detyrosinated tubulin are less dynamic. The EMBO journal 6:2597-2606.

Kremneva E, Makkonen MH, Skwarek-Maruszewska A, Gateva G, Michelot A, Dominguez R, Lappalainen P (2014) Cofilin-2 controls actin filament length in muscle sarcomeres. Developmental cell 31:215-226.

Kuhn TB, Meberg PJ, Brown MD, Bernstein BW, Minamide LS, Jensen JR, Okada K, Soda EA, Bamburg JR (2000) Regulating actin dynamics in neuronal growth cones by ADF/cofilin and rho family GTPases. Journal of neurobiology 44:126-144.

Laskowski CJ (2008) Intracellular mechanisms underlying enhanced axonal growth in conditioned primary sensory neurons. Master of science thesis.

Laskowski CJ, Bradke F (2013) In vivo imaging: a dynamic imaging approach to study spinal cord regeneration. Experimental neurology 242:11-17.

Lee AC, Suter DM (2008) Quantitative analysis of microtubule dynamics during adhesion-mediated growth cone guidance. Developmental neurobiology 68:1363-1377.

Lee JK, Zheng B (2012) Role of myelin-associated inhibitors in axonal repair after spinal cord injury. Experimental neurology 235:33-42.

Letourneau PC (2009) Actin in axons: stable scaffolds and dynamic filaments. Results and problems in cell differentiation 48:65-90.

Letourneau PC, Shattuck TA (1989) Distribution and possible interactions of actin-associated proteins and cell adhesion molecules of nerve growth cones. Development 105:505-519.

Letourneau PC, Shattuck TA, Ressler AH (1986) Branching of sensory and sympathetic neurites in vitro is inhibited by treatment with taxol. The Journal of neuroscience : the official journal of the Society for Neuroscience 6:1912-1917.

Letourneau PC, Shattuck TA, Ressler AH (1987) "Pull" and "push" in neurite elongation: observations on the effects of different concentrations of cytochalasin B and taxol. Cell motility and the cytoskeleton 8:193-209.

Levy DE, Darnell JE, Jr. (2002) Stats: transcriptional control and biological impact. Nature reviews Molecular cell biology 3:651-662.

Liedtke W, Edelmann W, Bieri PL, Chiu FC, Cowan NJ, Kucherlapati R, Raine CS (1996) GFAP is necessary for the integrity of CNS white matter architecture and long-term maintenance of myelination. Neuron 17:607-615.

Lieleg O, Schmoller KM, Claessens MM, Bausch AR (2009) Cytoskeletal polymer networks: viscoelastic properties are determined by the microscopic interaction potential of cross-links. Biophysical journal 96:4725-4732.

Lin CH, Forscher P (1995) Growth cone advance is inversely proportional to retrograde F-actin flow. Neuron 14:763-771.

Liu K, Tedeschi A, Park KK, He Z (2011) Neuronal intrinsic mechanisms of axon regeneration. Annual review of neuroscience 34:131-152.

Liu L, McBride KM, Reich NC (2005) STAT3 nuclear import is independent of tyrosine phosphorylation and mediated by importin-alpha3. Proceedings of the National Academy of Sciences of the United States of America 102:8150-8155.

Loverde JR, Pfister BJ (2015) Developmental axon stretch stimulates neuron growth while maintaining normal electrical activity, intracellular calcium flux, and somatic morphology. Frontiers in cellular neuroscience 9:308.

Lowery LA, Van Vactor D (2009) The trip of the tip: understanding the growth cone machinery. Nature reviews Molecular cell biology 10:332-343.

Luo L (2000) Rho GTPases in neuronal morphogenesis. Nature reviews Neuroscience 1:173-180.

Lurie DI, Selzer ME (1991) Axonal regeneration in the adult lamprey spinal cord. The Journal of comparative neurology 306:409-416.

Lv L, Han X, Sun Y, Wang X, Dong Q (2012) Valproic acid improves locomotion in vivo after SCI and axonal growth of neurons in vitro. Experimental neurology 233:783-790.

Ma TC, Willis DE (2015) What makes a RAG regeneration associated? Frontiers in molecular neuroscience 8:43.

Mandelkow E, Mandelkow EM (1995) Microtubules and microtubule-associated proteins. Current opinion in cell biology 7:72-81.

Mandolesi G, Madeddu F, Bozzi Y, Maffei L, Ratto GM (2004) Acute physiological response of mammalian central neurons to axotomy: ionic regulation and electrical activity. FASEB journal : official publication of the Federation of American Societies for Experimental Biology 18:1934-1936.

Mar FM, Bonni A, Sousa MM (2014) Cell intrinsic control of axon regeneration. EMBO reports 15:254-263.

Marsh L, Letourneau PC (1984) Growth of neurites without filopodial or lamellipodial activity in the presence of cytochalasin B. The Journal of cell biology 99:2041-2047.

Martin-Villalba A, Winter C, Brecht S, Buschmann T, Zimmermann M, Herdegen T (1998) Rapid and long-lasting suppression of the ATF-2 transcription factor is a common response to neuronal injury. Brain research Molecular brain research 62:158-166.

McGough A, Pope B, Chiu W, Weeds A (1997) Cofilin changes the twist of F-actin: implications for actin filament dynamics and cellular function. The Journal of cell biology 138:771-781.

McKerracher L, David S, Jackson DL, Kottis V, Dunn RJ, Braun PE (1994) Identification of myelin-associated glycoprotein as a major myelin-derived inhibitor of neurite growth. Neuron 13:805-811.

McQuarrie IG, Grafstein B, Gershon MD (1977) Axonal regeneration in the rat sciatic nerve: effect of a conditioning lesion and of dbcAMP. Brain research 132:443-453.

Meberg PJ (2000) Signal-regulated ADF/cofilin activity and growth cone motility. Molecular neurobiology 21:97-107.

Meberg PJ, Bamburg JR (2000) Increase in neurite outgrowth mediated by overexpression of actin depolymerizing factor. The Journal of neuroscience : the official journal of the Society for Neuroscience 20:2459-2469.

Medeiros NA, Burnette DT, Forscher P (2006) Myosin II functions in actin-bundle turnover in neuronal growth cones. Nature cell biology 8:215-226.

Michelot A, Berro J, Guerin C, Boujemaa-Paterski R, Staiger CJ, Martiel JL, Blanchoin L (2007) Actin-filament stochastic dynamics mediated by ADF/cofilin. Current biology : CB 17:825-833.

Miller RHS, J. (2006) Textbook of Neural Repair and Rehabilitation. 1:397-398.

Mitchison T, Kirschner M (1984) Dynamic instability of microtubule growth. Nature 312:237-242.

Mitchison T, Kirschner M (1988) Cytoskeletal dynamics and nerve growth. Neuron 1:761-772.

Mohney RP, Siegel RE, Zigmond RE (1994) Galanin and vasoactive intestinal peptide messenger RNAs increase following axotomy of adult sympathetic neurons. Journal of neurobiology 25:108-118.

Moore DL, Blackmore MG, Hu Y, Kaestner KH, Bixby JL, Lemmon VP, Goldberg JL (2009) KLF family members regulate intrinsic axon regeneration ability. Science 326:298-301.

Moriyama K, Yahara I (1999) Two activities of cofilin, severing and accelerating directional depolymerization of actin filaments, are affected differentially by mutations around the actin-binding helix. The EMBO journal 18:6752-6761.

Moriyama K, Yahara I (2002) The actin-severing activity of cofilin is exerted by the interplay of three distinct sites on cofilin and essential for cell viability. The Biochemical journal 365:147-155.

Morris RL, Hollenbeck PJ (1993) The regulation of bidirectional mitochondrial transport is coordinated with axonal outgrowth. Journal of cell science 104 (Pt 3):917-927.

Mullins RD, Heuser JA, Pollard TD (1998) The interaction of Arp2/3 complex with actin: nucleation, high affinity pointed end capping, and formation of branching networks of filaments. Proceedings of the National Academy of Sciences of the United States of America 95:6181-6186.

Nadkarni AV, Brieher WM (2014) Aip1 destabilizes cofilin-saturated actin filaments by severing and accelerating monomer dissociation from ends. Current biology : CB 24:2749-2757.

Nakashima K, Sato N, Nakagaki T, Abe H, Ono S, Obinata T (2005) Two mouse cofilin isoforms, muscle-type (MCF) and non-muscle type (NMCF), interact with F-actin with different efficiencies. Journal of biochemistry 138:519-526.

Neumann S, Bradke F, Tessier-Lavigne M, Basbaum AI (2002) Regeneration of sensory axons within the injured spinal cord induced by intraganglionic cAMP elevation. Neuron 34:885-893.

Neumann S, Woolf CJ (1999) Regeneration of dorsal column fibers into and beyond the lesion site following adult spinal cord injury. Neuron 23:83-91.

Ng J, Luo L (2004) Rho GTPases regulate axon growth through convergent and divergent signaling pathways. Neuron 44:779-793.

Nikulina E, Tidwell JL, Dai HN, Bregman BS, Filbin MT (2004) The phosphodiesterase inhibitor rolipram delivered after a spinal cord lesion promotes axonal regeneration and functional recovery. Proceedings of the National Academy of Sciences of the United States of America 101:8786-8790.

Niwa R, Nagata-Ohashi K, Takeichi M, Mizuno K, Uemura T (2002) Control of actin reorganization by Slingshot, a family of phosphatases that dephosphorylate ADF/cofilin. Cell 108:233-246.

Normoyle KP, Brieher WM (2012) Cyclase-associated protein (CAP) acts directly on F-actin to accelerate cofilin-mediated actin severing across the range of physiological pH. The Journal of biological chemistry 287:35722-35732.

Ohashi K, Nagata K, Maekawa M, Ishizaki T, Narumiya S, Mizuno K (2000) Rho-associated kinase ROCK activates LIM-kinase 1 by phosphorylation at threonine 508 within the activation loop. The Journal of biological chemistry 275:3577-3582.

Ono S (2007) Mechanism of depolymerization and severing of actin filaments and its significance in cytoskeletal dynamics. International review of cytology 258:1-82.

Ono S, Minami N, Abe H, Obinata T (1994) Characterization of a novel cofilin isoform that is predominantly expressed in mammalian skeletal muscle. The Journal of biological chemistry 269:15280-15286.

Pak CW, Flynn KC, Bamburg JR (2008) Actin-binding proteins take the reins in growth cones. Nature reviews Neuroscience 9:136-147.

Pan YA, Misgeld T, Lichtman JW, Sanes JR (2003) Effects of neurotoxic and neuroprotective agents on peripheral nerve regeneration assayed by time-lapse imaging in vivo. The Journal of neuroscience : the official journal of the Society for Neuroscience 23:11479-11488.

Park KK, Liu K, Hu Y, Kanter JL, He Z (2010) PTEN/mTOR and axon regeneration. Experimental neurology 223:45-50.

Park KK, Liu K, Hu Y, Smith PD, Wang C, Cai B, Xu B, Connolly L, Kramvis I, Sahin M, He Z (2008) Promoting axon regeneration in the adult CNS by modulation of the PTEN/mTOR pathway. Science 322:963-966.

Pavlov D, Muhlrad A, Cooper J, Wear M, Reisler E (2007) Actin filament severing by cofilin. Journal of molecular biology 365:1350-1358.

Phillips WT, Kiratli BJ, Sarkarati M, Weraarchakul G, Myers J, Franklin BA, Parkash I, Froelicher V (1998) Effect of spinal cord injury on the heart and cardiovascular fitness. Current problems in cardiology 23:641-716.

Piperno G, LeDizet M, Chang XJ (1987) Microtubules containing acetylated alpha-tubulin in mammalian cells in culture. The Journal of cell biology 104:289-302.

Pollard TD, Cooper JA (2009) Actin, a central player in cell shape and movement. Science 326:1208-1212.

Prinjha R, Moore SE, Vinson M, Blake S, Morrow R, Christie G, Michalovich D, Simmons DL, Walsh FS (2000) Inhibitor of neurite outgrowth in humans. Nature 403:383-384.

Pruyne D, Evangelista M, Yang C, Bi E, Zigmond S, Bretscher A, Boone C (2002) Role of formins in actin assembly: nucleation and barbed-end association. Science 297:612-615.

Pruyne D, Legesse-Miller A, Gao L, Dong Y, Bretscher A (2004) Mechanisms of polarized growth and organelle segregation in yeast. Annual review of cell and developmental biology 20:559-591.

Qiu J, Cafferty WB, McMahon SB, Thompson SW (2005) Conditioning injury-induced spinal axon regeneration requires signal transducer and activator of transcription 3 activation. The Journal of neuroscience : the official journal of the Society for Neuroscience 25:1645-1653.

Qiu J, Cai D, Dai H, McAtee M, Hoffman PN, Bregman BS, Filbin MT (2002) Spinal axon regeneration induced by elevation of cyclic AMP. Neuron 34:895-903.

Quinlan ME, Heuser JE, Kerkhoff E, Mullins RD (2005) Drosophila Spire is an actin nucleation factor. Nature 433:382-388.

Raivich G, Bohatschek M, Da Costa C, Iwata O, Galiano M, Hristova M, Nateri AS, Makwana M, Riera-Sans L, Wolfer DP, Lipp HP, Aguzzi A, Wagner EF,

Behrens A (2004) The AP-1 transcription factor c-Jun is required for efficient axonal regeneration. Neuron 43:57-67.

Ramer MS, Priestley JV, McMahon SB (2000) Functional regeneration of sensory axons into the adult spinal cord. Nature 403:312-316.

Ramesh V (2004) Merlin and the ERM proteins in Schwann cells, neurons and growth cones. Nature reviews Neuroscience 5:462-470.

Ramon y Cajal S (1928) Degeneration and regeneration of the nervous system. Translated by RM May, edited by J deFelipe and EG Jones (New York: Oxford University Press), 1991.

Raper J, Mason C (2010) Cellular strategies of axonal pathfinding. Cold Spring Harbor perspectives in biology 2:a001933.

Redmond L, Kashani AH, Ghosh A (2002) Calcium regulation of dendritic growth via CaM kinase IV and CREB-mediated transcription. Neuron 34:999-1010.

Reier PJ, Lane MA, Hall ED, Teng YD, Howland DR (2012) Translational spinal cord injury research: preclinical guidelines and challenges. Handbook of clinical neurology 109:411-433.

Richardson PM, Issa VM (1984) Peripheral injury enhances central regeneration of primary sensory neurones. Nature 309:791-793.

Richardson PM, McGuinness UM, Aguayo AJ (1980) Axons from CNS neurons regenerate into PNS grafts. Nature 284:264-265.

Richardson PM, Miao T, Wu D, Zhang Y, Yeh J, Bo X (2009) Responses of the nerve cell body to axotomy. Neurosurgery 65:A74-79.

Riedl J, Crevenna AH, Kessenbrock K, Yu JH, Neukirchen D, Bista M, Bradke F, Jenne D, Holak TA, Werb Z, Sixt M, Wedlich-Soldner R (2008) Lifeact: a versatile marker to visualize F-actin. Nature methods 5:605-607.

Robson SJ, Burgoyne RD (1989) Differential localisation of tyrosinated, detyrosinated, and acetylated alpha-tubulins in neurites and growth cones of dorsal root ganglion neurons. Cell motility and the cytoskeleton 12:273-282.

Rosenblatt J, Agnew BJ, Abe H, Bamburg JR, Mitchison TJ (1997) Xenopus actin depolymerizing factor/cofilin (XAC) is responsible for the turnover of actin filaments in Listeria monocytogenes tails. The Journal of cell biology 136:1323-1332.

Rossignol S, Schwab M, Schwartz M, Fehlings MG (2007) Spinal cord injury: time to move? The Journal of neuroscience : the official journal of the Society for Neuroscience 27:11782-11792.

Rothermel M, Brunert D, Zabawa C, Diaz-Quesada M, Wachowiak M (2013) Transgene expression in target-defined neuron populations mediated by retrograde infection with adeno-associated viral vectors. The Journal of neuroscience : the official journal of the Society for Neuroscience 33:15195-15206.

Ruschel J, Hellal F, Flynn KC, Dupraz S, Elliott DA, Tedeschi A, Bates M, Sliwinski C, Brook G, Dobrindt K, Peitz M, Brustle O, Norenberg MD, Blesch A, Weidner N, Bunge MB, Bixby JL, Bradke F (2015) Axonal regeneration. Systemic

administration of epothilone B promotes axon regeneration after spinal cord injury. Science 348:347-352.

Sabry JH, O'Connor TP, Evans L, Toroian-Raymond A, Kirschner M, Bentley D (1991) Microtubule behavior during guidance of pioneer neuron growth cones in situ. The Journal of cell biology 115:381-395.

Saijilafu, Hur EM, Zhou FQ (2011) Genetic dissection of axon regeneration via in vivo electroporation of adult mouse sensory neurons. Nature communications 2:543.

Sanders MC, Goldstein AL, Wang YL (1992) Thymosin beta 4 (Fx peptide) is a potent regulator of actin polymerization in living cells. Proceedings of the National Academy of Sciences of the United States of America 89:4678-4682.

Sasaki Y, Hayashi K, Shirao T, Ishikawa R, Kohama K (1996) Inhibition by drebrin of the actin-bundling activity of brain fascin, a protein localized in filopodia of growth cones. Journal of neurochemistry 66:980-988.

Schaefer AW, Kabir N, Forscher P (2002) Filopodia and actin arcs guide the assembly and transport of two populations of microtubules with unique dynamic parameters in neuronal growth cones. The Journal of cell biology 158:139-152.

Schaefer AW, Schoonderwoert VT, Ji L, Mederios N, Danuser G, Forscher P (2008) Coordination of actin filament and microtubule dynamics during neurite outgrowth. Developmental cell 15:146-162.

Schevzov G, Curthoys NM, Gunning PW, Fath T (2012) Functional diversity of actin cytoskeleton in neurons and its regulation by tropomyosin. International review of cell and molecular biology 298:33-94.

Schiff PB, Fant J, Horwitz SB (1979) Promotion of microtubule assembly in vitro by taxol. Nature 277:665-667.

Schnell L, Schwab ME (1990) Axonal regeneration in the rat spinal cord produced by an antibody against myelin-associated neurite growth inhibitors. Nature 343:269-272.

Schulze E, Kirschner M (1987) Dynamic and stable populations of microtubules in cells. The Journal of cell biology 104:277-288.

Schwaiger FW, Hager G, Schmitt AB, Horvat A, Hager G, Streif R, Spitzer C, Gamal S, Breuer S, Brook GA, Nacimiento W, Kreutzberg GW (2000) Peripheral but not central axotomy induces changes in Janus kinases (JAK) and signal transducers and activators of transcription (STAT). The European journal of neuroscience 12:1165-1176.

Scott RW, Olson MF (2007) LIM kinases: function, regulation and association with human disease. Journal of molecular medicine 85:555-568.

Seijffers R, Mills CD, Woolf CJ (2007) ATF3 increases the intrinsic growth state of DRG neurons to enhance peripheral nerve regeneration. The Journal of neuroscience : the official journal of the Society for Neuroscience 27:7911-7920.

Sept D, McCammon JA (2001) Thermodynamics and kinetics of actin filament nucleation. Biophysical journal 81:667-674.

Shewan D, Dwivedy A, Anderson R, Holt CE (2002) Age-related changes underlie switch in netrin-1 responsiveness as growth cones advance along visual pathway. Nature neuroscience 5:955-962.

Shin JE, Cho Y, Beirowski B, Milbrandt J, Cavalli V, DiAntonio A (2012) Dual leucine zipper kinase is required for retrograde injury signaling and axonal regeneration. Neuron 74:1015-1022.

Silver J, Miller JH (2004) Regeneration beyond the glial scar. Nature reviews Neuroscience 5:146-156.

Skene JH (1989) Axonal growth-associated proteins. Annual review of neuroscience 12:127-156.

Smith CL (1994) Cytoskeletal movements and substrate interactions during initiation of neurite outgrowth by sympathetic neurons in vitro. The Journal of neuroscience : the official journal of the Society for Neuroscience 14:384-398.

Smith DS, Skene JH (1997) A transcription-dependent switch controls competence of adult neurons for distinct modes of axon growth. The Journal of neuroscience : the official journal of the Society for Neuroscience 17:646-658.

Snider WD, Zhou FQ, Zhong J, Markus A (2002) Signaling the pathway to regeneration. Neuron 35:13-16.

Song G, Ouyang G, Bao S (2005) The activation of Akt/PKB signaling pathway and cell survival. Journal of cellular and molecular medicine 9:59-71.

Song H, Poo M (2001) The cell biology of neuronal navigation. Nature cell biology 3:E81-88.

Stiess M, Bradke F (2011) Neuronal polarization: the cytoskeleton leads the way. Developmental neurobiology 71:430-444.

Suarez C, Roland J, Boujemaa-Paterski R, Kang H, McCullough BR, Reymann AC, Guerin C, Martiel JL, De la Cruz EM, Blanchoin L (2011) Cofilin tunes the nucleotide state of actin filaments and severs at bare and decorated segment boundaries. Current biology : CB 21:862-868.

Sun F, He Z (2010) Neuronal intrinsic barriers for axon regeneration in the adult CNS. Current opinion in neurobiology 20:510-518.

Tanaka E, Ho T, Kirschner MW (1995) The role of microtubule dynamics in growth cone motility and axonal growth. The Journal of cell biology 128:139-155.

Tanaka E, Sabry J (1995) Making the connection: cytoskeletal rearrangements during growth cone guidance. Cell 83:171-176.

Tedeschi A (2011) Tuning the orchestra: transcriptional pathways controlling axon regeneration. Frontiers in molecular neuroscience 4:60.

Tedeschi A, He Z (2010) Axon regeneration: electrical silencing is a condition for regrowth. Current biology : CB 20:R713-714.

Thuret S, Moon LD, Gage FH (2006) Therapeutic interventions after spinal cord injury. Nature reviews Neuroscience 7:628-643.

Tojima T (2012) Intracellular signaling and membrane trafficking control bidirectional growth cone guidance. Neuroscience research 73:269-274.

Tojima T, Hines JH, Henley JR, Kamiguchi H (2011) Second messengers and membrane trafficking direct and organize growth cone steering. Nature reviews Neuroscience 12:191-203.

Tom VJ, Steinmetz MP, Miller JH, Doller CM, Silver J (2004) Studies on the development and behavior of the dystrophic growth cone, the hallmark of regeneration failure, in an in vitro model of the glial scar and after spinal cord injury. The Journal of neuroscience : the official journal of the Society for Neuroscience 24:6531-6539.

Toshima J, Toshima JY, Amano T, Yang N, Narumiya S, Mizuno K (2001a) Cofilin phosphorylation by protein kinase testicular protein kinase 1 and its role in integrin-mediated actin reorganization and focal adhesion formation. Molecular biology of the cell 12:1131-1145.

Toshima J, Toshima JY, Takeuchi K, Mori R, Mizuno K (2001b) Cofilin phosphorylation and actin reorganization activities of testicular protein kinase 2 and its predominant expression in testicular Sertoli cells. The Journal of biological chemistry 276:31449-31458.

Toshima JY, Toshima J, Watanabe T, Mizuno K (2001c) Binding of 14-3-3beta regulates the kinase activity and subcellular localization of testicular protein kinase 1. The Journal of biological chemistry 276:43471-43481.

Tsujino H, Kondo E, Fukuoka T, Dai Y, Tokunaga A, Miki K, Yonenobu K, Ochi T, Noguchi K (2000) Activating transcription factor 3 (ATF3) induction by axotomy in sensory and motoneurons: A novel neuronal marker of nerve injury. Molecular and cellular neurosciences 15:170-182.

Udina E, Furey M, Busch S, Silver J, Gordon T, Fouad K (2008) Electrical stimulation of intact peripheral sensory axons in rats promotes outgrowth of their central projections. Experimental neurology 210:238-247.

Van Troys M, Huyck L, Leyman S, Dhaese S, Vandekerkhove J, Ampe C (2008) Ins and outs of ADF/cofilin activity and regulation. European journal of cell biology 87:649-667.

Vartiainen MK, Mustonen T, Mattila PK, Ojala PJ, Thesleff I, Partanen J, Lappalainen P (2002) The three mouse actin-depolymerizing factor/cofilins evolved to fulfill cell-type-specific requirements for actin dynamics. Molecular biology of the cell 13:183-194.

Villar MJ, Cortes R, Theodorsson E, Wiesenfeld-Hallin Z, Schalling M, Fahrenkrug J, Emson PC, Hokfelt T (1989) Neuropeptide expression in rat dorsal root ganglion cells and spinal cord after peripheral nerve injury with special reference to galanin. Neuroscience 33:587-604.

Vitriol EA, Zheng JQ (2012) Growth cone travel in space and time: the cellular ensemble of cytoskeleton, adhesion, and membrane. Neuron 73:1068-1081.

Wade RH (2009) On and around microtubules: an overview. Molecular biotechnology 43:177-191.

Wang Y, Shibasaki F, Mizuno K (2005) Calcium signal-induced cofilin dephosphorylation is mediated by Slingshot via calcineurin. The Journal of biological chemistry 280:12683-12689.

Wanner M, Lang DM, Bandtlow CE, Schwab ME, Bastmeyer M, Stuermer CA (1995) Reevaluation of the growth-permissive substrate properties of goldfish optic nerve myelin and myelin proteins. The Journal of neuroscience : the official journal of the Society for Neuroscience 15:7500-7508.

Webster DR, Gundersen GG, Bulinski JC, Borisy GG (1987) Differential turnover of tyrosinated and detyrosinated microtubules. Proceedings of the National Academy of Sciences of the United States of America 84:9040-9044.

Westermann S, Weber K (2003) Post-translational modifications regulate microtubule function. Nature reviews Molecular cell biology 4:938-947.

Wiggan O, Bernstein BW, Bamburg JR (2005) A phosphatase for cofilin to be HAD. Nature cell biology 7:8-9.

Wills Z, Marr L, Zinn K, Goodman CS, Van Vactor D (1999) Profilin and the Abl tyrosine kinase are required for motor axon outgrowth in the Drosophila embryo. Neuron 22:291-299.

Witte H, Bradke F (2008) The role of the cytoskeleton during neuronal polarization. Current opinion in neurobiology 18:479-487.

Witte H, Neukirchen D, Bradke F (2008) Microtubule stabilization specifies initial neuronal polarization. The Journal of cell biology 180:619-632.

Wu Z, Ghosh-Roy A, Yanik MF, Zhang JZ, Jin Y, Chisholm AD (2007) Caenorhabditis elegans neuronal regeneration is influenced by life stage, ephrin signaling, and synaptic branching. Proceedings of the National Academy of Sciences of the United States of America 104:15132-15137.

Wylie SR, Chantler PD (2001) Separate but linked functions of conventional myosins modulate adhesion and neurite outgrowth. Nature cell biology 3:88-92.

Wyndaele M, Wyndaele JJ (2006) Incidence, prevalence and epidemiology of spinal cord injury: what learns a worldwide literature survey? Spinal cord 44:523-529.

Xiao HS, Huang QH, Zhang FX, Bao L, Lu YJ, Guo C, Yang L, Huang WJ, Fu G, Xu SH, Cheng XP, Yan Q, Zhu ZD, Zhang X, Chen Z, Han ZG, Zhang X (2002) Identification of gene expression profile of dorsal root ganglion in the rat peripheral axotomy model of neuropathic pain. Proceedings of the National Academy of Sciences of the United States of America 99:8360-8365.

Xu XM, Guenard V, Kleitman N, Bunge MB (1995) Axonal regeneration into Schwann cell-seeded guidance channels grafted into transected adult rat spinal cord. The Journal of comparative neurology 351:145-160.

Yamada KM, Spooner BS, Wessells NK (1970) Axon growth: roles of microfilaments and microtubules. Proceedings of the National Academy of Sciences of the United States of America 66:1206-1212.

Yang P, Yang Z (2012) Enhancing intrinsic growth capacity promotes adult CNS regeneration. Journal of the neurological sciences 312:1-6.

Ylera B, Bradke F (2007) Stimulating Intrinsic Growth Potential in Mammalian Neurons, Chapter 3. Model Organisms in Spinal Cord Regeneration Editors: Catherina G Becker and Thomas Becker.

Ylera B, Erturk A, Hellal F, Nadrigny F, Hurtado A, Tahirovic S, Oudega M, Kirchhoff F, Bradke F (2009) Chronically CNS-injured adult sensory neurons gain regenerative competence upon a lesion of their peripheral axon. Current biology : CB 19:930-936.

Zakharenko S, Popov S (1998) Dynamics of axonal microtubules regulate the topology of new membrane insertion into the growing neurites. The Journal of cell biology 143:1077-1086.

Zou H, Ho C, Wong K, Tessier-Lavigne M (2009) Axotomy-induced Smad1 activation promotes axonal growth in adult sensory neurons. The Journal of neuroscience : the official journal of the Society for Neuroscience 29:7116-7123.

PERSONAL CONTRIBUTIONS

The following persons have contributed significantly to the acquisition and/or quantification of data for my PhD project:

Dr. Andrea Tedeschi:	*In vivo* regeneration studies (Figures 3.17 B and C, 3.21 A-F, 3.29 A-C and 3.30 A-C)
Dr. Kevin C. Flynn:	Image acquisition and quantification of actin dynamics (Figure 3.11)
Dr. Sebastian Dupraz:	Biochemical analyses (Figures 3.13 B-F, 3.15 D-F and 3.18 A)
Telma E. da Silva Santos:	Image acquisition and quantification of actin dynamics (Figures 3.12 D-G, 3.16 A-D, 3.19 A-F and 3.23 A-D)
Marianne Braun:	Preparation of DRG samples for electron microscopy and image acquisition (Figures 3.7, 3.8, 3.9 and 3.10)

ACKNOWLEDGEMENTS

First of all, I would like to thank my supervisor Prof. Dr. Frank Bradke for giving me the opportunity to work on a very fascinating PhD project in his laboratory. I am grateful for the trust and patience, the enthusiasm and the scientific support throughout the duration of my PhD.

I am deeply indebted to Dr. Andrea Tedeschi, Dr. Kevin Flynn, Dr. Sebastian Dupraz and Telma da Silva Santos for the enormous support in planning, implementing and quantifying data for my PhD project. Without you it would not have been possible! I am very grateful to Dr. Charlotte Coles and Dr. Kevin Flynn for critically reading my thesis and giving helpful suggestions. Furthermore, I am very grateful to Liane Meyn, Kerstin Weisheit and Jessica Gonyer for excellent and tireless support with neuronal cultures, plasmid maxi-preps, genotyping, animal care and surgeries. A special hug goes to Dr. Dorothee Neukirchen and Dr. Sina Stern who besides being fantastic colleagues have become great friends!

Finally, I wholeheartedly thank every single member of the Bradke lab - present and past - for making the last years such a wonderful and motivating experience! You certainly made this saying come true:

"IF YOU WANT TO GO FAST, GO ALONE;
IF YOU WANT TO GO FAR, GO TOGETHER!"
(African proverb)

Thank you for having walked this road with me!

Das größte Dankeschön gilt jedoch meiner Familie, insbesondere meinen Eltern, meiner Schwester, Beam und Rotraut. Ihr habt immer an mich geglaubt, mich motiviert und in Momenten aufgebaut, wenn mir die Puste auszugehen schien. Danke für all eure Liebe und den Rückhalt in den letzten Jahren.

Besonders bei dir, Beam, möchte ich mich bedanken, dass du mich auf diesem Weg unterstützt hast, mir nach der Geburt unserer zwei Mädels zu Hause den Rücken freigehalten hast und während aller Höhen und Tiefen für mich da warst.

PUBLICATIONS

Laskowski CJ, Tedeschi A, Dupraz S, da Silva Santos TE, Flynn KC, Gurniak CB, Witke W, and Bradke F. **Conditioning Drives Axon Regeneration by Cofilin Mediated Actin Turnover.** (manuscript in preparation)

Tedeschi A, Dupraz S, Laskowski CJ, Xue J, Ulas T, Beyer M, Schultze JL, and Frank Bradke. **Transcriptome analysis identifies the calcium channel subunit Alpha2delta2 as a key regulator of axon regeneration**. (resubmitted)

Puttagunta R, Tedeschi A, Sória MG, Hervera A, Lindner R, Rathore KI, Gaub P, Joshi Y, Nguyen T, Schmandke A, Laskowski CJ, Boutillier AL, Bradke F, and Di Giovanni S. **PCAF-Dependent Epigenetic Changes Promote Axonal Regeneration in the Central Nervous System**. Nat Commun. 2014, Apr 1;5:3527.

Laskowski CJ, and Bradke F. **Review: In vivo Imaging: A Dynamic Imaging Approach To Study Spinal Cord Regeneration.** Exp Neurol. 2013 Apr; 242:11-7. Epub 2012 Jul 24.

Hellal F, Hurtado A, Ruschel J, Flynn KC, Laskowski CJ, Umlauf M, Kapitein LC, Strikis D, Lemmon V, Bixby J, Hoogenraad CC, and Bradke F. **Microtubule Stabilization Reduces Scarring and Causes Axon Regeneration After Spinal Cord Injury.** Science 2011, Feb 18;331(6019):928-31. Epub 2011 Jan 27.